Geometry of weak measurements and its application to optical interferometry(Dissertation_全文)

AUTHOR(S):

Tamate, Shuhei

Geometry of weak measurements and its application to optical interferometry

Shuhei Tamate

Contents

Chapter 1

Introduction

1.1 Background

An ensemble of systems is an essential concept in quantum mechanical experiments. A quantum state describes the statistical properties of an identically prepared ensemble. In a standard experiment, an ensemble is prepared by a projective measurement before an experiment. This selection of the ensemble can be called the pre-selection. The state of the pre-selected ensemble is represented as a state vector $|\psi_{\rm i}\rangle$. We can predict the results of measurements on this ensemble by calculating the evolution of the state vector.

In 1964, Aharonov, Bergmann, and Lebowitz [1] found that a quantum ensemble can also be selected after an experiment by measuring the final state of the system. The selection of an ensemble after an experiment is called the post-selection. In their study, they consider the pre- and post- selected ensemble in a time symmetric manner, and proposed a method to analyze the statistical properties of this ensemble. The state of the pre- and post-selected ensemble is described by *two-state* [2], that is, a pair of the pre-selected state $|\psi_{\rm i}\rangle$ and the post-selected state $|\psi_{\rm f}\rangle$. The formulation of quantum mechanics based on pre- and post-selected ensembles is now known as the two-state vector formalism [3].

Weak measurements were introduced by Aharonov, Albert, and Vaidman [4] to measure the expectation value of an observable for a pre- and post-selected ensemble. The weak measurement is simply a measurement whose interaction is so weak that the measured system is hardly disturbed. The word *weak measurements*, however, often refers to *weak measurements on a pre- and post-selected ensemble*. Although a single weak measurement gives little information about the ensemble, sufficiently large number of measurements gives us enough information to determine the expectation value of an observable. The expectation value obtained via weak

measurements is called the weak value. The weak value of an observable $\hat{A}$ is defined by

$$\langle \hat{A} \rangle_{\mathrm{w}} := \frac{\langle \psi_{\mathrm{f}} | \hat{A} | \psi_{\mathrm{i}} \rangle}{\langle \psi_{\mathrm{f}} | \psi_{\mathrm{i}} \rangle}. \tag{1.1}$$

The weak value states how a pre- and post-selected ensemble affects the other systems (or probes) via weak interactions. The form of the weak value is similar to that of the ordinary expectation value. However, unlike the expectation value for pre-selected-only ensembles, the weak value can lie outside the range of eigenvalues.

The pre- and post-selected ensemble is known to exhibit various weird phenomena such as Hardy's paradox [5, 6] and quantum N-box problem [7]. Interestingly, weak values often show strange values (outside the range of eigenvalues) in those paradoxical systems. The weak value thus could capture the quantum nature emerging in pre- and post-selected ensembles. The weak measurement has played important role as a experimental method to analyze quantum paradoxes [8, 9, 10]. There are some quantitative studies about the relationship between the strangeness of weak values and manifestation of the quantum natures such as the violation of Leggett-Garg inequality [11, 12, 13] and spontaneous pair production [14].

Another interesting property of the weak value is that the weak value can be unboundedly large for nearly orthogonal pre- and post-selections. This means that a particular pre- and post-selected ensemble has the potential to affect the other systems even thorough weak interactions. Hosten and Kwiat regarded the pre- and post-selection as the amplification technique to measure weak interactions. In 2008, using weak measurements, they measured the spin-Hall effect of light, which is caused by the weak spin-orbit interaction of light [15].

In their stand point, the pre- and post-selected ensemble is no longer the target of measurements. What actually measured is the strength of interaction. We can use the pre- and post-selected ensemble to detect the feeble effects caused by weak interactions between the "measured" system and the probe system. The amplification scheme using pre- and post-selection is now known as the weak-value amplification.

After the first observation of spin-Hall effect of light via weak measurements, the weak-value amplification has been applied to various precision measurements. For example, beam deflection measurements [16, 17, 18], frequency measurements [19], measurements of the plasmonic spin Hall effect [20], measurements of optical activities [21, 22], and measurements of temperature [23].

On the fundamental side, there have also been significant progress toward the investigation of the properties of pre- and post-selected ensembles. Many relationships between weak values and fundamental concepts in quantum mechanics have been found. For example, it was shown that the wavefunction of a quantum parti-

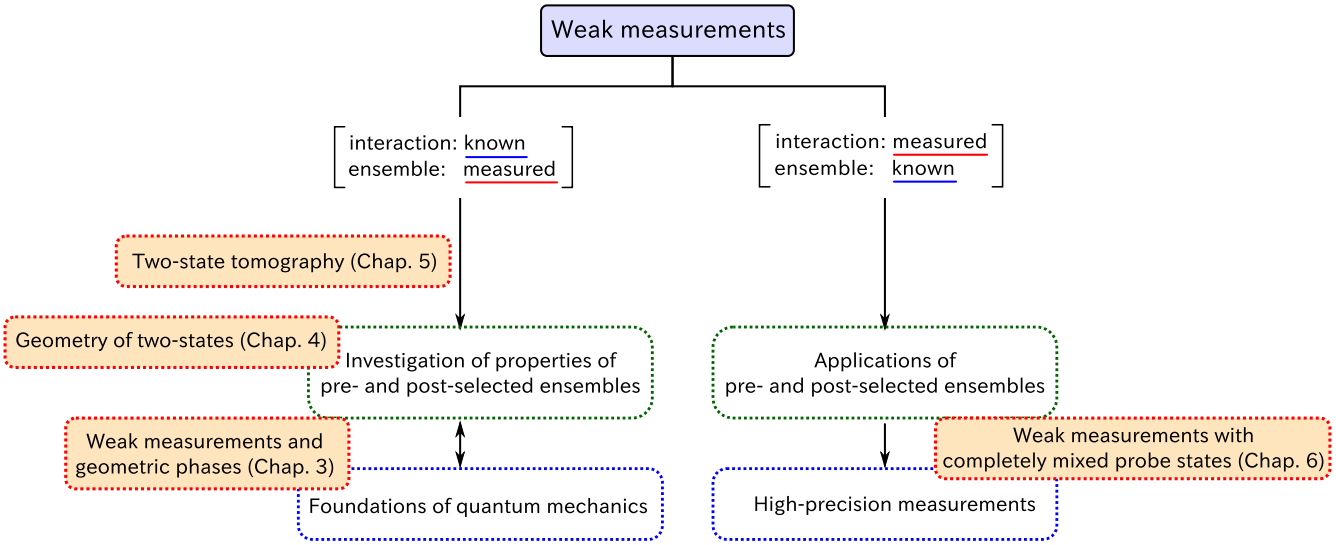

Figure 1.1: Directions of research on weak measurements.

cle can be viewed as one of the weak values [24]. Since weak values can be directly measured via weak measurements, finding the relationship between weak values and any other concepts gives the operational meanings of those concepts. Using weak measurements, the direct observation of the quantum wavefunction [24], observation of the average trajectories of single photons [25], and the verification of Ozawa's uncertainty relation [26] have been realized.

1.2 Objective and outline of this thesis

Weak measurements have mainly two directions of research. The overview of the research directions is shown in Fig. 1.1. Figure 1.1 also shows the relationships between the research directions and our studies.

The first direction is toward the investigation the properties of pre- and post-selected ensemble. Thereby, it is aimed at revealing the foundations of quantum mechanics. This direction of research is motivated by the seminal work of Aharonov and co-workers.

The second direction is toward the application of the pre- and post-selection as an amplification scheme. To use the weak-value amplification, we could improve the precision of various measurements. This direction is initiated by Hosten and Kwiat.

The main aim of this thesis is to construct the geometric treatment of pre- and post-selected ensembles, and thereby to develop the new optical interferometry using weak measurements.

In this thesis, we begin with introducing the relationship between the weak measurement and the geometric phase in Chap. 3. On the basis of this relationship, we construct the geometric picture to treat the properties of pre- and post-selected ensembles in Chap. 4. Chapter 5 shows how to measure the state of a pre- and post-selected ensemble completely using a weak spin-exchange interaction. We also describe geometrically that how the information about a pre and post-selected ensemble transferred to the probe system via weak measurements. Finally, in Chap. 6, we demonstrate a new optical interferometry based on weak measurements. By using this method, we demonstrate that the polarization rotation can be measured with unpolarized light.

In the following, we briefly describe the content of each chapter.

Chapter 2: Fundamentals

We introduce the fundamental formalism and notations of quantum mechanics. The state description of quantum systems and mathematical foundations of quantum measurement are presented. After that, we introduce the two-state vector formalism, which is a method to treat the pre- and post-selected ensembles in quantum mechanics. Weak measurements are introduced to measure the expectation value of the pre- and post-selected ensemble. We also describe the basics of linear optics used in later chapters.

Chapter 3: Weak measurements and geometric phases

We consider the interference effect occurred in weak measurements. We introduce an interferometer for a particle with internal degree of freedom, and investigate the interference effect caused by post-selection. It is turned out that the geometric phase plays an important role in weak measurements. We present the relationship between anomalously large weak values and the singularity of geometric phases.

Chapter 4: Geometry of two-states

The Bloch sphere representation for two-state vector formalism is developed in this chapter. This representation enable us to visualize the relationship between two-state operators and weak values. The strange weak values are investigated from the geometric point of view. We also present how to maximize the weak value of an observable under the fixed success probability of post-selection. This problem is important for the weak-value amplification.

Chapter 5: Two-state vector tomography via spin-exchange interaction

The properties of a pre- and post-selected ensemble are completely described by two-state vectors. We explain how we can measure the two-state vector using weak measurements via spin-exchange interaction. This procedure serves as a tomography of the two-state vector. An optical experiment that demonstrates tomography of the two-state vector is also proposed.

Chapter 6: Weak measurements with completely mixed probe states

We consider the advantage of weak measurements as a method for precision measurements. The noise tolerance of weak measurements is revealed based on geometric consideration. To demonstrate the weak measurements with noisy probe states, we perform the weak measurements with completely mixed states in an optical system. The polarization rotation is measured experimentally via weak measurement with unpolarized light.

Chapter 2

Fundamentals

This chapter provides the fundamental formalism and notations of quantum mechanics. The formalism introduced in this chapter is mainly based on the treatments used in the field of quantum information and quantum computation [27]. We also present the basics of the two-state vector formalism. After that, we describe the mathematical treatment of weak measurements. Finally, we introduce the basics of linear optics, which is needed to implement quantum measurements in optical systems.

2.1 Fundamentals of quantum mechanics

2.1.1 Quantum states and observables

A state of a quantum system is described by a *ket* vector $|\psi\rangle$ in a complex Hilbert space $\mathcal{H}$. The dual space of $\mathcal{H}$ is denoted by $\mathcal{H}^*$ and its element $\langle\phi| \in \mathcal{H}^*$ is called a *bra* vector. The dual inner product of a ket $|\psi\rangle$ and a bra $\langle\phi|$ is denoted by $\langle\phi|\psi\rangle$.

Manipulation of quantum states is described by using linear operators acting on $\mathcal{H}$. A linear operator on $\mathcal{H}$ is denoted by a letter with a hat, such as $\hat{A}$. An operator $\hat{A}$ maps a ket vector $|\psi\rangle$ to another ket vector $\hat{A}|\psi\rangle$. The operator $\hat{A}$ can also be viewed as an operator acting on a bra vector $\langle\phi| \in \mathcal{H}^*$ from the right-hand side. The operator $\hat{A}$ maps a bra vector to another bra vector $\langle\phi|\hat{A}$ to satisfy the following rule:

$$(\langle\phi|\hat{A})|\psi\rangle = \langle\phi|(\hat{A}|\psi\rangle). \tag{2.1}$$

A ket operator $|\psi\rangle$ has a one-to-one corresponding bra vector $\langle\psi|$, which is represented by using the same letter ψ. The transformation between a ket and the corresponding bra vector is denoted by a dagger $\dagger$, i.e., $|\psi\rangle^\dagger = \langle\psi|$ and $\langle\psi|^\dagger = |\psi\rangle$.

A mapped ket vector $\hat{A}|\psi\rangle$ also has a corresponding bra vector; we denote this bra vector as $\langle\psi|\hat{A}^\dagger$. The operation maps $\hat{A}$ to $\hat{A}^\dagger$ is called the Hermitian conjugation.

A state $|\psi\rangle$ can describe only statistical properties of a quantum system. A physical observable is represented by an Hermitian operator $\hat{A}$ and its expectation value $\langle\hat{A}\rangle$ can be calculated by the following rule,

$$\langle\hat{A}\rangle = \frac{\langle\psi|\hat{A}|\psi\rangle}{\langle\psi|\psi\rangle}. \tag{2.2}$$

A ket vector is often normalized so that $\langle\psi|\psi\rangle = 1$. In such a case, Eq. (2.2) is reduced to

$$\langle\hat{A}\rangle = \langle\psi|\hat{A}|\psi\rangle. \tag{2.3}$$

We define a density operator $\hat{\rho}$ corresponding to a state $|\psi\rangle$ as

$$\hat{\rho} = |\psi\rangle\langle\psi|, \tag{2.4}$$

The expectation value can be written as

$$\langle\hat{A}\rangle = \frac{\mathrm{tr}(\hat{\rho}\hat{A})}{\mathrm{tr}\hat{\rho}}. \tag{2.5}$$

A density operator is also often normalized so that $\mathrm{tr}\hat{\rho} = 1$. For a normalized density operator,

$$\langle\hat{A}\rangle = \mathrm{tr}(\hat{\rho}\hat{A}). \tag{2.6}$$

A density operator can also describe the mixture of states. The mixture of states $|\psi_k\rangle$ with probabilities p_k is represented as

$$\hat{\rho} = \sum_k p_k|\psi_k\rangle\langle\psi_k|, \tag{2.7}$$

where $|\psi_k\rangle$ are assumed to be normalized. In general, a density operator is a positive operator. A physical state has a one-to-one correspondence to a normalized density operator.

If a density operator is a rank-1 operator, the state represented by the density operator is called a pure state; otherwise, the state is called a mixed state.

2.1.2 Time evolution of quantum states

The time evolution of a closed quantum state is described by a unitary operator $\hat{U}$. A unitary operator is an operator that satisfies $\hat{U}\hat{U}^\dagger = \hat{U}^\dagger\hat{U} = \hat{I}$, where $\hat{I}$ is the identity operator. A ket vector $|\psi\rangle$ is mapped to $\hat{U}|\psi\rangle$ after the time evolution. A density operator $\hat{\rho}$ evolves into $\hat{U}\hat{\rho}\hat{U}^\dagger$.

Every unitary operator is generated by an Hermitian operator $\hat{G}$ as

$$\hat{U} = \exp(-\mathrm{i}\theta\hat{G}), \tag{2.8}$$

where θ is a real parameter. The operator $\hat{G}$ is called the generator of evolution. When a unitary operator is parameterized by the time t, the generator is conventionally written as $\hat{H}/\hbar$, where $\hat{H}$ is an Hermitian operator and $\hbar$ is Planck's constant h divided by 2π. In this case, a unitary operator is expressed as

$$\hat{U}(t) = \exp\left(-\mathrm{i}t\frac{\hat{H}}{\hbar}\right). \tag{2.9}$$

The operator $\hat{H}$ is called the Hamiltonian.

2.1.3 Qubits

A quantum system associated with a two-dimensional Hilbert space is called a *qubit* in the field of quantum information. For example, the spin of a spin-1/2 particle or the polarization of a photon is regarded as a qubit. The basis states are conventionally denoted by $|0\rangle$ and $|1\rangle$. This is an analogous to a classical bit.

An arbitrary state $|\psi\rangle$ of a qubit can be expressed as a linear combination of $|0\rangle$ and $|1\rangle$ as

$$|\psi\rangle = c_0|0\rangle + c_1|1\rangle, \tag{2.10}$$

where c_0 and c_1 are complex numbers satisfying $|c_0|^2 + |c_1|^2 = 1$.

The set of all Hermitian operators on a qubit forms a real vector space with the scalar product $\mathrm{tr}(\hat{A}\hat{B})$. One of the orthogonal basis in this vector space is the set of the following four operators:

$$\hat{I} = |0\rangle\langle 0| + |1\rangle\langle 1|, \tag{2.11}$$

$$\hat{\sigma}_x = |0\rangle\langle 1| + |1\rangle\langle 0|, \tag{2.12}$$

$$\hat{\sigma}_y = -\mathrm{i}|0\rangle\langle 1| + \mathrm{i}|1\rangle\langle 0|, \tag{2.13}$$

$$\hat{\sigma}_z = |0\rangle\langle 0| - |1\rangle\langle 1|. \tag{2.14}$$

The operator $\hat{I}$ is the identity operator. The operators $\hat{\sigma}_x$, $\hat{\sigma}_y$, and $\hat{\sigma}_z$ are called the Pauli operators. We also use $\hat{X}$, $\hat{Y}$, and $\hat{Z}$ to represent the Pauli operators $\hat{\sigma}_x$, $\hat{\sigma}_y$, and $\hat{\sigma}_z$, respectively. The vector operator composed of the Pauli operators is denoted by $\hat{\boldsymbol{\sigma}} := (\hat{\sigma}_x, \hat{\sigma}_y, \hat{\sigma}_z)^{\mathrm{T}}$. There is the useful formula for calculating the product of the two Pauli operators:

$$(\boldsymbol{a}\cdot\hat{\boldsymbol{\sigma}})(\boldsymbol{b}\cdot\hat{\boldsymbol{\sigma}}) = (\boldsymbol{a}\cdot\boldsymbol{b})\hat{I} + \mathrm{i}(\boldsymbol{a}\times\boldsymbol{b})\cdot\hat{\boldsymbol{\sigma}}. \tag{2.15}$$

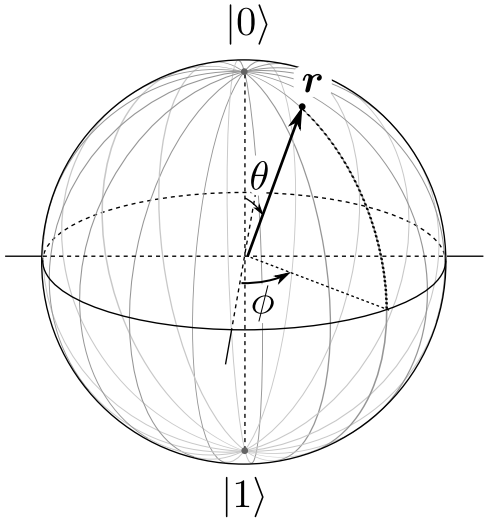

Figure 2.1: Bloch sphere representation of a state in a qubit system.

Using the Pauli operators, we can decompose a density operator as

$$\hat{\rho} = \frac{1}{2}(\hat{I} + \boldsymbol{r} \cdot \hat{\boldsymbol{\sigma}}), \tag{2.16}$$

where $\boldsymbol{r}$ is a real vector in $\mathbb{R}^3$. The vector $\boldsymbol{r}$ is called the Bloch vector and is represented as a point in a unit ball, which is called the Bloch ball. The Bloch vector corresponding to a pure state is represented on a unit sphere, which is called the Bloch sphere.

There is a useful parameterization of a pure state as

$$|\psi\rangle = \mathrm{e}^{\mathrm{i}\gamma} \left[\cos(\theta/2)|0\rangle + \mathrm{e}^{\mathrm{i}\phi} \sin(\theta/2)|1\rangle\right]. \tag{2.17}$$

In this parameterization, θ and ϕ correspond to the polar and azimuthal angles of the vector $\boldsymbol{r}$ corresponding to $\hat{\rho} = |\psi\rangle\langle\psi|$ as shown in Fig. 2.1. The parameter γ is an overall phase factor irrelevant to the Bloch sphere representation.

Every observable of a qubit can be represented as $x\hat{I} + y(\boldsymbol{n} \cdot \hat{\boldsymbol{\sigma}})$, where x and y are real number, and $\boldsymbol{n}$ is a unit vector. Since the identity operator carries no information about the state of the qubit, the important part of the observable is $y\boldsymbol{n} \cdot \hat{\boldsymbol{\sigma}}$. The spectral decomposition of the operator $\boldsymbol{n} \cdot \hat{\boldsymbol{\sigma}}$ takes the following form:

$$\boldsymbol{n} \cdot \hat{\boldsymbol{\sigma}} = \frac{1}{2}(\hat{I} + \boldsymbol{n} \cdot \hat{\boldsymbol{\sigma}}) - \frac{1}{2}(\hat{I} - \boldsymbol{n} \cdot \hat{\boldsymbol{\sigma}}). \tag{2.18}$$

Therefore, the state represented by the Bloch vectors $\boldsymbol{n}$ and $-\boldsymbol{n}$ are the two eigenstates of the operator $\boldsymbol{n} \cdot \hat{\boldsymbol{\sigma}}$ with eigenvalues 1 and -1, respectively. For the observable $x\hat{I} + y(\boldsymbol{n} \cdot \hat{\boldsymbol{\sigma}})$, the eigenstate is also represented by the Bloch vectors $\boldsymbol{n}$ and $-\boldsymbol{n}$. The eigenvalues are $x + y$ and $x - y$, respectively.

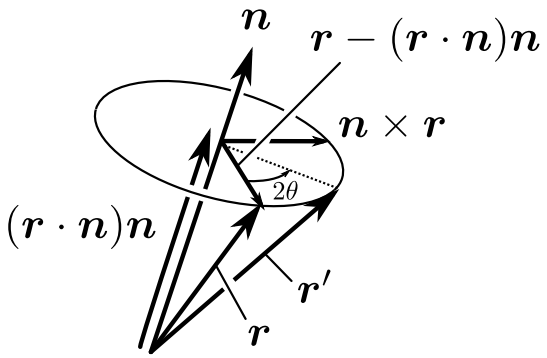

Figure 2.2: Rotation of the Bloch vector.

Finally, we consider the unitary evolution of a qubit. Ignoring an unimportant overall phase factor, Every unitary operator on a qubit can be generated by the generator that has a form of $\boldsymbol{n}\cdot\hat{\boldsymbol{\sigma}}$. The unitary operator generated by $\boldsymbol{n}\cdot\hat{\boldsymbol{\sigma}}$ is written explicitly as

$$\begin{aligned}\hat{U} &= \exp(-\mathrm{i}\theta\boldsymbol{n}\cdot\hat{\boldsymbol{\sigma}}) \\ &= \mathrm{e}^{-\mathrm{i}\theta}\frac{1}{2}(\hat{I}+\boldsymbol{n}\cdot\hat{\boldsymbol{\sigma}}) + \mathrm{e}^{\mathrm{i}\theta}\frac{1}{2}(\hat{I}-\boldsymbol{n}\cdot\hat{\boldsymbol{\sigma}}) \\ &= \cos\theta\hat{I} - \mathrm{i}\sin\theta\,\boldsymbol{n}\cdot\hat{\boldsymbol{\sigma}}. \end{aligned} \tag{2.19}$$

The evolution of the density operator $\hat{\rho} = (\hat{I}+\boldsymbol{r}\cdot\hat{\boldsymbol{\sigma}})/2$ is

$$\hat{U}\hat{\rho}\hat{U}^{\dagger} = \frac{1}{2}(\hat{I}+\boldsymbol{r}'\cdot\hat{\boldsymbol{\sigma}}), \tag{2.20}$$

where $\boldsymbol{r}'$ is given by

$$\boldsymbol{r}' = (\boldsymbol{r}\cdot\boldsymbol{n})\boldsymbol{n} + \cos(2\theta)[\boldsymbol{r}-(\boldsymbol{r}\cdot\boldsymbol{n})\boldsymbol{n}] + \sin(2\theta)(\boldsymbol{n}\times\boldsymbol{r}). \tag{2.21}$$

Figure 2.2 shows that the vector $\boldsymbol{r}'$ can be produced by rotating the vector $\boldsymbol{r}$ about the axis $\boldsymbol{n}$ by the angle 2θ. Therefore, every unitary evolution is represented as a rotation of the Bloch vector.

2.1.4 Composite systems

We consider the composite system whose components are two distinct physical systems. Suppose these two system have corresponding Hilbert spaces denoted by $\mathcal{H}$ and $\mathcal{K}$, respectively. The state space of the composite physical system is represented by the tensor product of the spaces $\mathcal{H}$ and $\mathcal{K}$, i.e., $\mathcal{H}\otimes\mathcal{K}$. If the state of the system $\mathcal{H}$ is $|\psi\rangle$ and the state of the system $\mathcal{K}$ is $|\phi\rangle$, the state of the composite system is

represented by $|\psi\rangle \otimes |\phi\rangle$. We abbreviate this notation to be $|\psi\rangle|\phi\rangle$ when there is no confusion. An operator $\hat{A}$ on the first system $\mathcal{H}$ is replaced by $\hat{A} \otimes \hat{I}$ when treating the composite system. Similarly, an operator $\hat{B}$ on the second system $\mathcal{K}$ is replaced by $\hat{I} \otimes \hat{B}$.

2.1.5 Quantum operations

A quantum operation or a quantum channel is a process which changes the state of a quantum system. A quantum operation is represented by a linear map $\mathcal{E}$ on the vector space $\mathcal{L}(\mathcal{H})$, which is composed of all linear operations on $\mathcal{H}$. The transformation of a density operator is written as

$$\hat{\rho}' = \mathcal{E}(\hat{\rho}). \tag{2.22}$$

A linear map $\mathcal{E}$ is said to be positive if $\mathcal{E}(\hat{\rho})$ is a positive operator for any positive operator $\hat{\rho}$. Since the output of a quantum operation must be another density operator, any quantum operation $\mathcal{E}$ must be positive. Furthermore, a linear map $\mathcal{E}$ is said to be completely positive if $\mathcal{E} \otimes \mathcal{I}$ is positive. Here, $\mathcal{I}$ is the identity map on an ancillary system. Since a quantum operation may be applied on only a part of a composite system, any quantum operation must be completely positive. A quantum operation must also be trace-preserving, $\mathrm{tr}\mathcal{E}(\hat{\rho}) = \mathrm{tr}\hat{\rho}$. Owing to Choi's theorem [28, 27], any quantum operation $\mathcal{E}$ can be represented as the following form

$$\mathcal{E}(\hat{\rho}) = \sum_n \hat{E}_n \hat{\rho} \hat{E}_n^\dagger, \tag{2.23}$$

where $\hat{E}_n$ are operators on $\mathcal{H}$. From the condition of trace-preserving, $\hat{E}_n$ must satisfy $\sum_n \hat{E}_n^\dagger \hat{E}_n = \hat{I}$, which is called the completeness relation. The right-hand side of Eq. (2.23) is called the Kraus representation [29].

2.1.6 Quantum measurements

A quantum measurement is described by a set of operators $\{\hat{M}_n\}$, where the subscript n denotes the result of the measurement. The probability of obtaining the result n is

$$p(n) = \mathrm{tr}(\hat{\rho} \hat{M}_n^\dagger \hat{M}_n), \tag{2.24}$$

and the state after obtaining the result n is

$$\hat{\rho}_n = \frac{\hat{M}_n \hat{\rho} \hat{M}_n^\dagger}{\mathrm{tr}(\hat{\rho} \hat{M}_n^\dagger \hat{M}_n)}. \tag{2.25}$$

Measurement operators must satisfy the completeness relation,

$$\sum_n \hat{M}_n^\dagger \hat{M}_n = \hat{I}. \tag{2.26}$$

This condition corresponds to the fact that the sum of probabilities of all outcomes must be 1.

A projection operator $\hat{P}$ is the Hermitian operator satisfying $\hat{P}^2 = \hat{P}$. When a measurement is described by a set of projection operators $\{\hat{P}_n\}$, the measurement is called a projective measurement.

Suppose we are interested only in the measurement results but in the state after the measurement. In such a case, the positive operators $\hat{E}_n := \hat{M}_n^\dagger \hat{M}_n$ are enough to describe the measurement. The set of positive operators $\{\hat{E}_n\}$ satisfies the completeness relation

$$\sum_n \hat{E}_n = \hat{I}. \tag{2.27}$$

A set of operators satisfying this completeness relation is called the positive-operator-valued measure (POVM). Using the POVM, the probability of obtaining result n is given by

$$p(n) = \mathrm{tr}(\hat{\rho}\hat{E}_n). \tag{2.28}$$

2.1.7 Indirect measurement model

We show that any measurement can be decomposed into two processes: (i) a coupling with an ancillary system and (ii) a projective measurement on the ancillary system. We call the ancillary system for an indirect measurement as the probe system. We can thus perform any measurement indirectly by coupling a probe and measuring it.

To perform a measurement described by $\{\hat{M}_n\}$ indirectly, we consider the following map

$$|\psi\rangle|0\rangle \quad \to \quad \sum_n \hat{M}_n|\psi\rangle|n\rangle, \tag{2.29}$$

where $|0\rangle$ is an initial state of the probe. The states $|n\rangle$ are orthonormal basis states of the probe. It is known that there exists a unitary operation $\hat{U}$ on the composite system realizing this map [27],

$$\hat{U}|\psi\rangle|0\rangle = \sum_n \hat{M}_n|\psi\rangle|n\rangle. \tag{2.30}$$

Subsequently, we measure the probe system with projection operators $\hat{P}_n = |n\rangle\langle n|$.

Let $\hat{\rho} = |\psi\rangle\langle\psi|$. We obtain the result n with probability

$$p(n) = \mathrm{tr}\left(\sum_{k,l} \hat{M}_k \hat{\rho} \hat{M}_l^\dagger \otimes |k\rangle\langle l| (\hat{I} \otimes \hat{P}_n)\right) = \mathrm{tr}(\hat{M}_n^\dagger \hat{\rho} \hat{M}_n). \tag{2.31}$$

The state after obtaining the result n is

$$\begin{aligned}\hat{\rho}_n &= (\hat{I} \otimes \hat{P}_n)\left(\sum_{k,l} \hat{M}_k \hat{\rho} \hat{M}_l^\dagger \otimes |k\rangle\langle l|\right)(\hat{I} \otimes \hat{P}_n) \Big/ p(n) \\ &= \frac{\hat{M}_n \hat{\rho} \hat{M}_n^\dagger}{\mathrm{tr}(\hat{\rho} \hat{M}_n^\dagger \hat{M}_n)} \otimes |n\rangle\langle n|. \end{aligned} \tag{2.32}$$

This result is the same as using the measurement operators $\{\hat{M}_n\}$.

2.1.8 von Neumann measurement

The fundamental model of the indirect measurement is first proposed by von Neumann in his book focusing on mathematical foundations of quantum mechanics [30]. He considered how the value of an observable $\hat{A}$ can be measured indirectly.

We assume that the measured system is described by a finite-dimensional Hilbert space and the probe is a particle in one dimension. The position of the particle corresponds to the meter of a measuring device. We consider the following impulsive interaction Hamiltonian at time t_0:

$$\hat{H}_\mathrm{I}(t) = x_0 \delta(t - t_0) \hat{A} \otimes \hat{p}, \tag{2.33}$$

where x_0 represents a unit of the probe shift and $\hat{p}$ is the momentum operator of the particle. The evolution operator $\hat{U}$ is given by

$$\hat{U} = \exp\left(-\mathrm{i}\frac{x_0}{\hbar} \hat{A} \otimes \hat{p}\right). \tag{2.34}$$

Expanding $\hat{A}$ in the basis in which $\hat{A}$ is diagonal,

$$\hat{A} = \sum_a a |a\rangle\langle a|. \tag{2.35}$$

The evolution operator $\hat{U}$ can be expressed as

$$\hat{U} = \sum_a |a\rangle\langle a| \otimes \mathrm{e}^{-\mathrm{i}(a x_0/\hbar)\hat{p}}. \tag{2.36}$$

Note that $\mathrm{e}^{-\mathrm{i}(a x_0/\hbar)\hat{p}}$ is the translation operator for a spatial displacement of $a x_0$,

$$\mathrm{e}^{-\mathrm{i}(a x_0/\hbar)\hat{p}} |x\rangle = |x + a x_0\rangle, \tag{2.37}$$

where $|x\rangle$ is an eigenstate of the position operator $\hat{x}$. Assume that the initial state of system $|\psi\rangle$ and that of probe $|\phi\rangle$ are given by

$$|\psi\rangle = \sum_a \psi(a)|a\rangle, \tag{2.38}$$

$$|\phi\rangle = \int \mathrm{d}x\, \phi(x)|x\rangle. \tag{2.39}$$

Then the state $|\Psi\rangle$ of the whole system after the interaction is

$$|\Psi\rangle = \sum_a \psi(a)|a\rangle \otimes \left(\int \mathrm{d}x\, \phi(x - ax_0)|x\rangle \right). \tag{2.40}$$

The probe state is shifted in proportion to each eigenvalue of $\hat{A}$. Denote the probe state shifted in proportion to a as

$$|\phi_a\rangle := \int \mathrm{d}x\, \phi(x - ax_0)|x\rangle, \tag{2.41}$$

then

$$|\Psi\rangle = \sum_a \psi(a)|a\rangle|\phi_a\rangle. \tag{2.42}$$

If the probe wavepacket is enough narrow to resolve the eigenvalues of $\hat{A}$, i.e., $|\langle\phi_a|\phi_{a'}\rangle| \ll 1$ for $a \neq a'$, we obtain the result a with probability $|\psi(a)|^2$ by measuring the position of the probe. This result is equivalent to the measurement of $\hat{A}$.

2.2 Two-state vector formalism

The two-state vector formalism is a description of quantum mechanics based on pre- and post-selected ensembles [3, 7]. In standard quantum mechanical experiments, we perform a projective measurement to choose an initial state of an ensemble. After that, we observe statistical properties of the ensemble by repeating measurements. In two-state vector formalism, we also select the final state of the ensemble. The initial and final measurements to select the ensemble are called pre- and post-selection, respectively. The properties of the ensemble are described by a pair of pre- and post-selected state vectors.

We define the two-state operator [2, 31] describing pre- and post-selected ensemble as

$$\hat{W} := |\psi_\mathrm{i}\rangle\langle\psi_\mathrm{f}|, \tag{2.43}$$

where $|\psi_{\rm i}\rangle$ and $|\psi_{\rm f}\rangle$ is pre- and post-selected states, respectively. We also use the normalized version of the two-state operator defined by

$$\hat{W} := \frac{|\psi_{\rm i}\rangle\langle\psi_{\rm f}|}{\langle\psi_{\rm f}|\psi_{\rm i}\rangle}, \tag{2.44}$$

which is a gauge invariant operator.

2.2.1 Measurements on pre- and post-selected ensembles

We show that the probability of obtaining the result n for the measurement $\{\hat{M}_n\}$ conditioned on initial and final states is given by the formula [32],

$$p(n|\psi_{\rm f},\psi_{\rm i}) = \frac{\left|{\rm tr}(\hat{W}\hat{M}_n)\right|^2}{\sum_n \left|{\rm tr}(\hat{W}\hat{M}_n)\right|^2}, \tag{2.45}$$

where both of normalized and unnormalized two-state operator $\hat{W}$ are acceptable. Therefore, the two-state operator $\hat{W}$ completely describe the statistical properties of a pre- and post-selected ensemble.

The formula (2.45) is derived by using Bayes' theorem and the standard formulation of quantum mechanics. Bayes' theorem yields

$$p(n|\psi_{\rm f},\psi_{\rm i}) = \frac{p(\psi_{\rm f}|n,\psi_{\rm i})p(n|\psi_{\rm i})}{\sum_n p(\psi_{\rm f}|n,\psi_{\rm i})p(n|\psi_{\rm i})}. \tag{2.46}$$

From Eq. (2.24) and Eq. (2.25), the probability of obtaining the result n is given by

$$p(n|\psi_{\rm i}) = \langle\psi_{\rm i}|\hat{M}_n^\dagger\hat{M}_n|\psi_{\rm i}\rangle. \tag{2.47}$$

and the conditional state when obtaining the result n is

$$\hat{\rho}_n = \frac{\hat{M}_n|\psi_{\rm i}\rangle\langle\psi_{\rm i}|\hat{M}_n^\dagger}{p(n|\psi_{\rm i})}. \tag{2.48}$$

Hence,

$$p(\psi_{\rm f}|n,\psi_{\rm i}) = \langle\psi_{\rm f}|\hat{\rho}_n|\psi_{\rm f}\rangle = \frac{\left|\langle\psi_{\rm f}|\hat{M}_n|\psi_{\rm i}\rangle\right|^2}{p(n|\psi_{\rm i})}. \tag{2.49}$$

Rewriting Eq. (2.49), we obtain

$$p(\psi_{\rm f}|n,\psi_{\rm i})p(n|\psi_{\rm i}) = \left|\langle\psi_{\rm f}|\hat{M}_n|\psi_{\rm i}\rangle\right|^2. \tag{2.50}$$

Substituting this in Eq. (2.46), we obtain Eq. (2.45).

When the measurement is a projective measurement, i.e, $\hat{M}_n = \hat{P}_n$, Eq. (2.45) is reduced to

$$p(n|\psi_{\rm f},\psi_{\rm i}) = \frac{\left|\langle\psi_{\rm f}|\hat{P}_n|\psi_{\rm i}\rangle\right|^2}{\sum_n \left|\langle\psi_{\rm f}|\hat{P}_n|\psi_{\rm i}\rangle\right|^2}. \tag{2.51}$$

Equation (2.51) was first derived by Aharonov, Bergmann and Lebowitz (ABL) and is known as the ABL formula.

2.2.2 Incomplete pre- and post-selections

We consider the case when the pre- and post-selections are incomplete. In such a case pre- and post-selected states are denoted by density operators $\hat{\rho}_{\rm i}$ and $\hat{\rho}_{\rm f}$. The procedure of the pre-selection in the state $\hat{\rho}_{\rm i}$ seems to be no ambiguity; however, that of the post-selection in the state $\hat{\rho}_{\rm f}$ is somewhat ambiguous. We explain this procedure in detail.

The incomplete measurement is described by a POVM $\{\hat{E}_m\}$. We assume that the POVM $\{\hat{E}_m\}$ includes the operator $\hat{\rho}_{\rm f}$. For simplicity, we set $\hat{E}_1 = \hat{\rho}_{\rm f}$.[1] The post-selection in the state $\hat{\rho}_{\rm f}$ is achieved by performing the measurement $\{\hat{E}_m\}$ and choosing the ensemble corresponding to the result $m = 1$.

Next, we derive the formula corresponding to Eq. (2.45) for incomplete pre- and post-selections. When we prepare the state $\hat{\rho}_{\rm i}$, The probability obtaining the result n for measurement $\{\hat{M}_n\}$ is given by

$$p(n|\rho_{\rm i}) = {\rm tr}(\hat{\rho}_{\rm i}\hat{M}_n^\dagger\hat{M}_n), \tag{2.52}$$

and the conditional state when obtaining the result n is

$$\hat{\rho}_n = \frac{\hat{M}_n\hat{\rho}_{\rm i}\hat{M}_n^\dagger}{p(n|\rho_{\rm i})}. \tag{2.53}$$

From Eq. (2.28), the success probability of post-selection for given $\hat{\rho}_{\rm i}$ and n is

$$p(\rho_{\rm f}|n,\rho_{\rm i}) = {\rm tr}(\hat{\rho}_n\hat{\rho}_{\rm f}) = \frac{{\rm tr}(\hat{M}_n\hat{\rho}_{\rm i}\hat{M}_n^\dagger\hat{\rho}_{\rm f})}{p(n|\rho_{\rm i})}. \tag{2.54}$$

Finally, Bayes' theorem (2.46) gives

$$p(n|\rho_{\rm f},\rho_{\rm i}) = \frac{{\rm tr}(\hat{\rho}_{\rm f}\hat{M}_n\hat{\rho}_{\rm i}\hat{M}_n^\dagger)}{\sum_n {\rm tr}(\hat{\rho}_{\rm f}\hat{M}_n\hat{\rho}_{\rm i}\hat{M}_n^\dagger)}. \tag{2.55}$$

[1] Assuming $\hat{E}_1 = C\hat{\rho}_{\rm f}$ for a positive constant number C gives the same result in the following discussion.

Note that the pair of pre- and post-selected states is no longer described by a single operator $\hat{W}$ when pre- and post-selection are incomplete.

2.3 Weak measurements

In this section, we first introduce the direct measurement model for weak measurements. Thereby, we explain how the results of weak measurements can be described by using the two-state operator.

After that, we describe indirect measurement models of weak measurements. Weak measurements were first proposed by Aharonov, Albert and Vaidman (AAV) as an indirect measurement model for pre- and post-selected ensembles [4]. By using the AAV model, the weak value of an observable is introduced as the counterpart of the ordinary expectation value of an observable.

We also describe weak measurements with a qubit probe. Considering the qubit probe, we can visualize the evolution of the probe in weak measurements on the Bloch sphere.

Finally, we describe how the signal-to-noise ratio of measurements is improved by using pre- and post-selected ensembles. This is the underlying principle of the weak-value amplification.

2.3.1 Direct measurement model

In Sec. 2.2, we have observed that complete pre- and post-selected ensembles can be described by the single operator $\hat{W}$, while incomplete pre- and post-selected ensembles cannot be described by the single operator. We show that, however, the results of *weak* measurements can be described by a single operator $\hat{W}$ defined by

$$\hat{W} := \frac{\hat{\rho}_{\mathrm{i}}\hat{\rho}_{\mathrm{f}}}{\mathrm{tr}(\hat{\rho}_{\mathrm{i}}\hat{\rho}_{\mathrm{f}})}, \tag{2.56}$$

even if pre- and post-selections are incomplete. The definition (2.56) is equivalent to Eq. (2.44) when pre- and post-selections are complete.

We first describe the definition of weak measurements. Weak measurements are the measurements that hardly disturb the measured system, instead they give little information on the system. The measurement operator of a weak measurement is defined as the following form:

$$\hat{M}_n = \sqrt{w_n}\left(\hat{I} + \frac{\epsilon}{2}\hat{N}_n\right) + O(\epsilon^2), \tag{2.57}$$

where w_n are real numbers and $\epsilon||\hat{N}_n|| \ll 1$ for all n. The parameter ϵ represents the strength of the measurement. From the completeness relation (2.26), w_n and

$\hat{N}_n$ must satisfy the following relations:

$$\sum_n w_n = 1, \tag{2.58}$$

$$\sum_n w_n(\hat{N}_n + \hat{N}_n^\dagger) = O(\epsilon). \tag{2.59}$$

We next show that the results of weak measurements can be described by the single operator $\hat{W}$ given in Eq. (2.56). It will be shown by calculating Eq. (2.55) for the case of weak measurements. From Eq.(2.57), we obtain

$$\begin{aligned}\mathrm{tr}(\hat{\rho}_\mathrm{f}\hat{M}_n\hat{\rho}_\mathrm{i}\hat{M}_n^\dagger) &= w_n\left[\mathrm{tr}(\hat{\rho}_\mathrm{f}\hat{\rho}_\mathrm{i}) + \frac{\epsilon}{2}\mathrm{tr}(\hat{\rho}_\mathrm{f}\hat{N}_n\hat{\rho}_\mathrm{i}) + \frac{\epsilon}{2}\mathrm{tr}(\hat{\rho}_\mathrm{i}\hat{N}_n^\dagger\hat{\rho}_\mathrm{f})\right] + O(\epsilon^2) \\ &= w_n\mathrm{tr}(\hat{\rho}_\mathrm{f}\hat{\rho}_\mathrm{i})[1 + \epsilon\,\mathrm{Re}\,\mathrm{tr}(\hat{W}\hat{N}_n)] + O(\epsilon^2).\end{aligned} \tag{2.60}$$

Substituting this to Eq. (2.55) gives

$$p(n|\rho_\mathrm{f},\rho_\mathrm{i}) = w_n\left\{1 + \epsilon\,\mathrm{Re}\,\mathrm{tr}\left[\hat{W}\left(\hat{N}_n - \sum_m w_m\hat{N}_m\right)\right]\right\} + O(\epsilon^2). \tag{2.61}$$

This shows that we can calculate the probability distribution of weak measurements by using the single operator $\hat{W}$ given in Eq. (2.56).

If $\hat{N}_n$ are Hermitian operators, $\sum_n w_n\hat{N}_n = O(\epsilon)$ follows Eq. (2.59). Hence,

$$\begin{aligned}p(\rho_\mathrm{f}|\rho_\mathrm{i}) &= \sum_n \mathrm{tr}(\hat{\rho}_\mathrm{f}\hat{M}_n\hat{\rho}_\mathrm{i}\hat{M}_n^\dagger) \\ &= \mathrm{tr}(\hat{\rho}_\mathrm{f}\hat{\rho}_\mathrm{i}) + O(\epsilon^2).\end{aligned} \tag{2.62}$$

This means that the success probability of post-selection is disturbed only the second order to the measurement strength ϵ. In this case, $p(n|\rho_\mathrm{f},\rho_\mathrm{i})$ takes a simple form as

$$p(n|\rho_\mathrm{f},\rho_\mathrm{i}) = w_n[1 + \epsilon\,\mathrm{Re}\,\mathrm{tr}(\hat{W}\hat{N}_n)] + O(\epsilon^2). \tag{2.63}$$

2.3.2 AAV weak measurement

We describe one of the indirect measurement models of weak measurements, which was introduced by Aharonov, Albert, and Vaidman (AAV) [4]. This model can be used to measure the ordinary expectation value of an observable for a pre-selected-only ensemble. By applying the same measurement to pre- and post-selected ensemble, we obtain the counterpart of expectation value of an observable for pre- and post-selected ensemble, which is called the weak value of the observable.

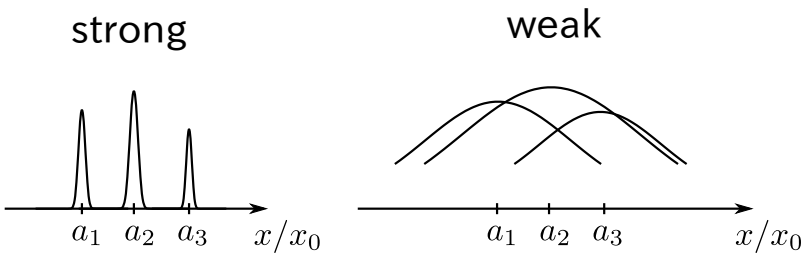

Figure 2.3: Comparison between strong and weak measurements. The wavepacket of the probe state for strong measurements is sufficiently sharp to distinguish each eigenvalue of an observable. That for weak measurements is too broad to distinguish each eigenvalue; however, we can extract the expectation value of the observable by repeating measurements.

Pre-selected-only ensembles

We reconsider the indirect measurement model described in Sec. 2.1.8. The only difference is that the interaction is assumed to be too weak to distinguish each eigenvalue of a measured observable $\hat{A}$. In other words, the probe wavepacket is enough wider than the displacement induced by the measurement interaction, as shown in Fig. 2.3. In this case, we cannot obtain the probability distribution of eigenvalues of $\hat{A}$. However, we can extract the expectation value $\langle\hat{A}\rangle$ from the average displacement of the probe wavepacket by repeating measurements. In the following, we show this fact.

Tracing out the measured system in Eq. (2.42), we obtain the probe state after the interaction as

$$\hat{\rho}_{\rm f} = \sum_a p(a)|\phi_a\rangle\langle\phi_a|, \tag{2.64}$$

where $p(a) := |\psi(a)|^2$. We denote the initial position of the probe as $\langle\hat{x}\rangle_{\rm i} := \langle\phi|\hat{x}|\phi\rangle$. The subscript i represents that the average is taken for the initial probe state. We also use the subscript f to represent the average for the final probe state. We introduce the operator measuring the displacement of the probe from the initial position as $\delta_{\rm i}\hat{x} := \hat{x} - \langle\hat{x}\rangle_{\rm i}$. The expectation value of the probe shift is calculated as

$$\begin{aligned}\langle\delta_{\rm i}\hat{x}\rangle_{\rm f} &= \sum_a p(a)[\langle\phi_a|\hat{x}|\phi_a\rangle - \langle\hat{x}\rangle_{\rm i}] \\ &= \sum_a p(a)\cdot a x_0 \\ &= \langle\hat{A}\rangle x_0.\end{aligned} \tag{2.65}$$

Therefore, we can extract the expectation value of the observable $\hat{A}$ from the average displacement.

Pre- and post-selected ensembles

We consider the case when the indirect measurements are performed on a pre- and post-selected ensemble. The following calculation is based on Jozsa's paper [33].

Recalling that measurement interaction is given by Eq. (2.34), the unnormalized probe state after the post-selection is

$$\begin{aligned}|\phi_{\rm f}\rangle &= \langle\psi_{\rm f}|\hat{U}|\psi_{\rm i}\rangle|\phi\rangle \\ &= \langle\psi_{\rm f}|\exp\left(-{\rm i}\frac{x_0}{\hbar}\hat{A}\otimes\hat{p}\right)|\psi_{\rm i}\rangle|\phi\rangle \\ &\simeq \langle\psi_{\rm f}|\psi_{\rm i}\rangle\left(1-{\rm i}\frac{x_0}{\hbar}\langle\hat{A}\rangle_{\rm w}\hat{p}\right)|\phi\rangle, \end{aligned} \tag{2.66}$$

where we define the weak value of the observable $\hat{A}$ as

$$\langle\hat{A}\rangle_{\rm w} := \frac{\langle\psi_{\rm f}|\hat{A}|\psi_{\rm i}\rangle}{\langle\psi_{\rm f}|\psi_{\rm i}\rangle}. \tag{2.67}$$

In the third line of Eq. (2.66), we neglected the higher order term in x_0 since we assumed that the interaction is sufficiently weak. However, the condition to justify the approximation is somewhat complicated, because the momentum operator $\hat{p}$ is not bounded. Thus the condition must depend on the initial state of the probe. The simple condition for the approximation is given by [34]

$$||\hat{A}||\frac{x_0\Delta p}{\hbar} \ll 1. \tag{2.68}$$

where Δp is the standard deviation of the momentum operator for the initial probe state. For more sophisticated analyses, see Ref. [34] and [35].

We denote the expectation value of an observable $\hat{M}$ for the initial and final probe state as

$$\langle\hat{M}\rangle_{\rm i} := \frac{\langle\phi|\hat{M}|\phi\rangle}{\langle\phi|\phi\rangle}, \tag{2.69}$$

$$\langle\hat{M}\rangle_{\rm f} := \frac{\langle\phi_{\rm f}|\hat{M}|\phi_{\rm f}\rangle}{\langle\phi_{\rm f}|\phi_{\rm f}\rangle}. \tag{2.70}$$

The unnormalized readout for the measurement of $\hat{M}$ is

$$\langle\phi_{\rm f}|\hat{M}|\phi_{\rm f}\rangle \simeq \mathcal{P}({\rm f}|{\rm i})\left(\langle\hat{M}\rangle_{\rm i} + \frac{x_0}{\hbar}\,{\rm Re}\langle\hat{A}\rangle_{\rm w}\langle-{\rm i}[\hat{M},\hat{p}]\rangle_{\rm i} + \frac{x_0}{\hbar}\,{\rm Im}\langle\hat{A}\rangle_{\rm w}\langle\{\hat{M},\hat{p}\}\rangle_{\rm i}\right), \tag{2.71}$$

where $[\hat{A},\hat{B}] := \hat{A}\hat{B}-\hat{B}\hat{A}$ and $\{\hat{A},\hat{B}\} := \hat{A}\hat{B}+\hat{B}\hat{A}$ for observables $\hat{A}$ and $\hat{B}$. We also defined $\mathcal{P}({\rm f}|{\rm i}) := |\langle\psi_{\rm f}|\psi_{\rm i}\rangle|^2$, which is the success probability of post-selection

without measurement disturbance. Setting $\hat{M} = \hat{I}$ in Eq. (2.71) gives the success probability of the post-selection as

$$\langle \phi_{\rm f} | \phi_{\rm f} \rangle \simeq \mathcal{P}({\rm f}|{\rm i}) \left(1 + 2\frac{x_0}{\hbar} \, {\rm Im} \langle \hat{A} \rangle_{\rm w} \langle \hat{p} \rangle_{\rm i} \right). \tag{2.72}$$

Define the shift operator for an observable $\hat{M}$ as $\delta_{\rm i}\hat{M} := \hat{M} - \langle \hat{M} \rangle_{\rm i}$. Then the average shift of the observable $\hat{M}$ is

$$\langle \delta_{\rm i} \hat{M} \rangle_{\rm f} \simeq \frac{x_0}{\hbar} \, {\rm Re} \langle \hat{A} \rangle_{\rm w} \langle -{\rm i}[\hat{M}, \hat{p}] \rangle_{\rm i} + \frac{x_0}{\hbar} \, {\rm Im} \langle \hat{A} \rangle_{\rm w} \langle \{ \delta_{\rm i} \hat{M}, \delta_{\rm i} \hat{p} \} \rangle_{\rm i}. \tag{2.73}$$

Suppose we take the observable $\hat{M} = \hat{x}$ in the same way as weak measurements for pre-selected-only ensembles. The average shift of the position is

$$\langle \delta_{\rm i} \hat{x} \rangle_{\rm f} = x_0 \, {\rm Re} \langle \hat{A} \rangle_{\rm w} + x_0 \, {\rm Im} \langle \hat{A} \rangle_{\rm w} \frac{\langle \{ \delta_{\rm i} \hat{x}, \delta_{\rm i} \hat{p} \} \rangle_{\rm i}}{\hbar}. \tag{2.74}$$

Note that the term $\langle \{ \delta_{\rm i} \hat{x}, \delta_{\rm i} \hat{p} \} \rangle_{\rm i}$ represents the correlation between the position and momentum. Choosing the initial probe state such that the position and momentum have no correlation, we obtain the real part of the weak value

$$\langle \delta_{\rm i} \hat{x} \rangle_{\rm f} = x_0 \, {\rm Re} \langle \hat{A} \rangle_{\rm w}. \tag{2.75}$$

Note that the sufficient condition for no correlation between the position and momentum is that the initial probe wavefunction is real, as shown in Appendix A.1. The real part of the weak value works as the expectation value for a pre- and post-selected ensemble.

In the case of pre- and post-selected ensembles, the momentum $\hat{p}$ of the probe is also shifted by the weak interaction. The average shift of the momentum is

$$\langle \delta_{\rm i} \hat{p} \rangle_{\rm f} = 2\frac{x_0}{\hbar} \langle (\delta_{\rm i} \hat{p})^2 \rangle_{\rm i} \, {\rm Im} \langle \hat{A} \rangle_{\rm w}. \tag{2.76}$$

Thus the imaginary part of the weak value contribute to the momentum shift of the probe. In contrast to the position shift, the momentum shift depends on the state of the probe.

2.3.3 Weak measurements with a qubit probe

We describe the weak measurements with a qubit probe. Considering the qubit probe, we can illustrate the evolution of the probe intuitively on the Bloch sphere.

Suppose the measurement interaction to be the following unitary operator,

$$\hat{U}(\theta) = \exp\left(-{\rm i}\theta \hat{A} \otimes \hat{Z} \right), \tag{2.77}$$

where $\hat{A}$ is a measured observable and $\hat{Z}$ is the Pauli Z operator; the θ represents the strength of measurements.

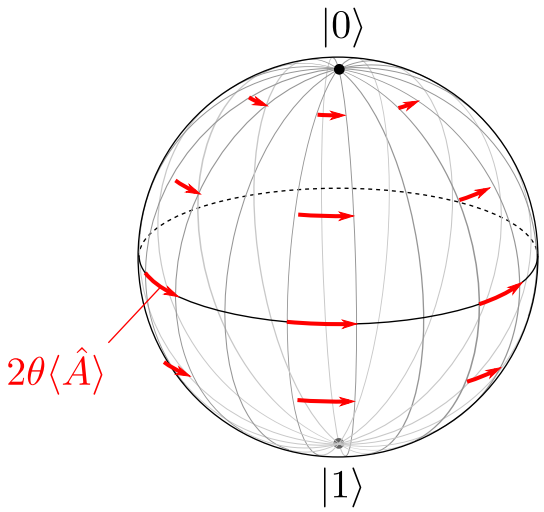

Figure 2.4: Evolution of the qubit probe for a pre-selected-only ensemble.

Pre-selected-only ensembles

Denote the initial state of the measured system as $|\psi_\mathrm{i}\rangle$. Let $\hat{\rho}_\mathrm{i}$ be the initial state of the probe. The probe state $\hat{\rho}_\mathrm{f}$ after the unitary evolution is given by

$$\hat{\rho}_\mathrm{f}(\theta) = \mathrm{tr}_\mathrm{S}[\hat{U}(\theta)(|\psi_\mathrm{i}\rangle\langle\psi_\mathrm{i}| \otimes \hat{\rho}_\mathrm{i})\hat{U}(\theta)^\dagger], \tag{2.78}$$

where tr_S is the partial trace over the measured system. Assuming that the interaction is weak, i.e., $\theta||\hat{A}|| \ll 1$, we obtain

$$\hat{\rho}_\mathrm{f} = \hat{\rho}_\mathrm{i} - \mathrm{i}\theta\langle\hat{A}\rangle[\hat{Z}, \hat{\rho}_\mathrm{i}] + O(\theta^2) \tag{2.79}$$

$$= \mathrm{e}^{-\mathrm{i}\theta\langle\hat{A}\rangle\hat{Z}}\rho_\mathrm{i}\mathrm{e}^{\mathrm{i}\theta\langle\hat{A}\rangle\hat{Z}} + O(\theta^2). \tag{2.80}$$

This indicates that the probe state is rotated about the Z axis by the angle $2\theta\langle\hat{A}\rangle$, as shown in Fig. 2.4

To extract the expectation value of $\hat{A}$, we prepare the initial state in $(|0\rangle + |1\rangle)/\sqrt{2}$, which is the $+1$ eigenstate of the Pauli X operator. We then measure the Pauli Y operator.

$$\begin{aligned}\mathrm{tr}(\hat{\rho}_\mathrm{f}\hat{Y}) &= \mathrm{tr}(\hat{\rho}_\mathrm{i}\hat{Y}) - \mathrm{i}\theta\langle\hat{A}\rangle\mathrm{tr}(\hat{\rho}_\mathrm{i}[\hat{Y}, \hat{Z}]) + O(\theta^2) \\ &= 2\theta\langle\hat{A}\rangle + O(\theta^2).\end{aligned} \tag{2.81}$$

Pre- and post-selected ensembles

When the system state is pre- and post-selected, the unnormalized evolution operator $\hat{V}(\theta)$ is given by

$$\begin{aligned}\hat{V}(\theta) &= \langle\psi_{\rm f}|\hat{U}(\theta)|\psi_{\rm i}\rangle \\ &= \langle\psi_{\rm f}|\psi_{\rm i}\rangle(\hat{I} - {\rm i}\theta\langle\hat{A}\rangle_{\rm w}\hat{Z}) + O(\theta^2) \\ &= \langle\psi_{\rm f}|\psi_{\rm i}\rangle \exp(-{\rm i}\theta\langle\hat{A}\rangle_{\rm w}\hat{Z}) + O(\theta^2). \end{aligned} \tag{2.82}$$

Note that the operator $\exp(-{\rm i}\theta\langle\hat{A}\rangle_{\rm w}\hat{Z})$ is not a unitary operator since the weak value $\langle\hat{A}\rangle_{\rm w}$ is generally a complex number. The operator $\exp(-{\rm i}\theta\langle\hat{A}\rangle_{\rm w}\hat{Z})$ can be decomposed into the unitary and non-unitary parts as

$$\exp(-{\rm i}\theta\langle\hat{A}\rangle_{\rm w}\hat{Z}) = \exp(-{\rm i}\theta\,{\rm Re}\langle\hat{A}\rangle_{\rm w}\hat{Z})\exp(\theta\,{\rm Im}\langle\hat{A}\rangle_{\rm w}\hat{Z}). \tag{2.83}$$

The real and imaginary parts of the weak value induce the unitary and non-unitary evolution, respectively.

The unitary part $\exp(-{\rm i}\theta\,{\rm Re}\langle\hat{A}\rangle_{\rm w}\hat{Z})$ rotates the state about the Z axis by the angle $2\theta\langle\hat{A}\rangle_{\rm w}$.

We consider the evolution induced by the non-unitary part $\exp(\theta\,{\rm Im}\langle\hat{A}\rangle_{\rm w}\hat{Z})$. For simplicity, we assume that $\theta\,{\rm Im}\langle\hat{A}\rangle_{\rm w} > 0$. The non-unitary operator $\exp(\theta\,{\rm Im}\langle\hat{A}\rangle_{\rm w}\hat{Z})$ amplifies the amplitude of the state $|0\rangle$ relative to the state $|1\rangle$:

$$\exp(\theta\,{\rm Im}\langle\hat{A}\rangle_{\rm w}\hat{Z})|0\rangle = {\rm e}^{\theta\,{\rm Im}\langle\hat{A}\rangle_{\rm w}}|0\rangle, \tag{2.84}$$

$$\exp(\theta\,{\rm Im}\langle\hat{A}\rangle_{\rm w}\hat{Z})|1\rangle = {\rm e}^{-\theta\,{\rm Im}\langle\hat{A}\rangle_{\rm w}}|1\rangle. \tag{2.85}$$

Therefore, all probe states are shifted toward the north pole on the Bloch sphere.

The evolution of the qubit probe is summarized in Fig 2.5.

Next, we calculate the average shift of the probe. The unnormalized final state of the probe is given by

$$\begin{aligned}\hat{\rho}_{\rm f} &= \hat{V}(\theta)\hat{\rho}_{\rm i}\hat{V}(\theta)^\dagger \\ &= \mathcal{P}({\rm f}|{\rm i})\left[\hat{\rho}_{\rm i} - {\rm i}\theta\,{\rm Re}\langle\hat{A}\rangle_{\rm w}[\hat{Z},\hat{\rho}_{\rm i}] + \theta\,{\rm Im}\langle\hat{A}\rangle_{\rm w}\{\hat{Z},\hat{\rho}_{\rm i}\}\right] + O(\theta^2). \end{aligned} \tag{2.86}$$

where $\mathcal{P}({\rm f}|{\rm i}) := |\langle\psi_{\rm f}|\psi_{\rm i}\rangle|^2$. We denote the expectation value of a probe observable $\hat{M}$ for the initial and final probe states as

$$\begin{aligned}\langle\hat{M}\rangle_{\rm i} &:= \frac{{\rm tr}(\hat{\rho}_{\rm i}\hat{M})}{{\rm tr}\hat{\rho}_{\rm i}}, \\ \langle\hat{M}\rangle_{\rm f} &:= \frac{{\rm tr}(\hat{\rho}_{\rm f}\hat{M})}{{\rm tr}\hat{\rho}_{\rm f}}. \end{aligned} \tag{2.87}$$

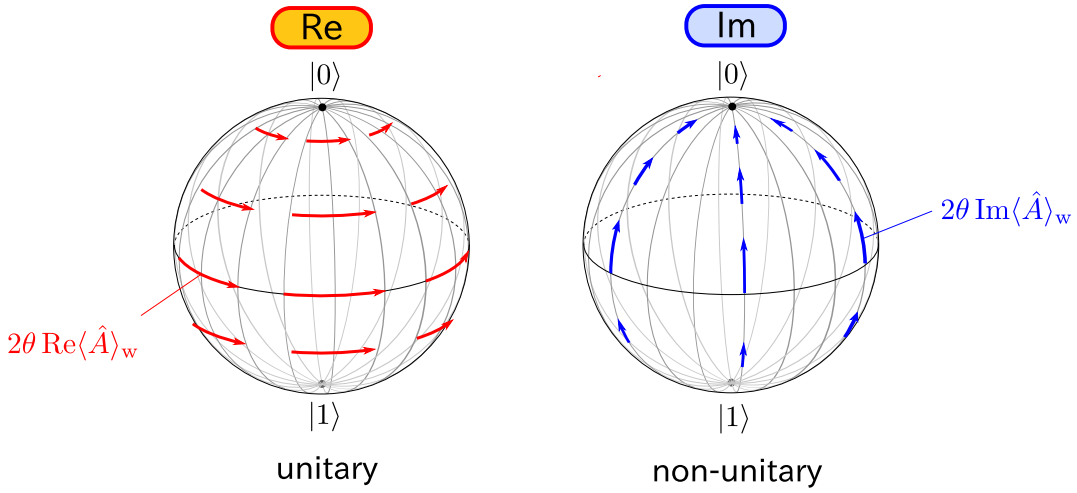

Figure 2.5: Evolution of the qubit probe for a pre- and post-selected ensemble. Left and right figures represent the evolution induced by the real and imaginary parts of the weak value, respectively. The unitary part of the evolution rotates the state about the Z axis. The non-unitary part shifts the state toward the north pole.

We also introduce the operator $\delta_\mathrm{i}\hat{M} := \hat{M} - \langle\hat{M}\rangle_\mathrm{i}$, which represents the shift of the observable from the initial value. The expectation value of $\delta_\mathrm{i}\hat{M}$ is calculated as

$$\langle\delta_\mathrm{i}\hat{M}\rangle_\mathrm{f} = \theta\,\mathrm{Re}\langle\hat{A}\rangle_\mathrm{w}\langle -\mathrm{i}[\hat{M},\hat{Z}]\rangle_\mathrm{i} + \theta\,\mathrm{Im}\langle\hat{A}\rangle_\mathrm{w}\langle\{\delta_\mathrm{i}\hat{M},\delta_\mathrm{i}\hat{Z}\}\rangle_\mathrm{i} + O(\theta^2). \tag{2.88}$$

Suppose the initial probe state to be $|\psi_\mathrm{i}\rangle = (|0\rangle + |1\rangle)/\sqrt{2}$; this state is toward the X direction. Figure 2.5 shows that if we measure the Pauli Y operator we can obtain the real part of the weak value. On the other hand, if we measure the Pauli Z operator we can obtain the imaginary part of the weak value. In fact, for $\hat{M} = \hat{Y}, \hat{Z}$, Eq. (2.88) reduces to

$$\langle\delta_\mathrm{i}\hat{Y}\rangle_\mathrm{f} = \langle\hat{Y}\rangle_\mathrm{f} = 2\theta\,\mathrm{Re}\langle\hat{A}\rangle_\mathrm{w} + O(\theta^2), \tag{2.89}$$

$$\langle\delta_\mathrm{i}\hat{Z}\rangle_\mathrm{f} = \langle\hat{Z}\rangle_\mathrm{f} = 2\theta\,\mathrm{Im}\langle\hat{A}\rangle_\mathrm{w} + O(\theta^2). \tag{2.90}$$

2.3.4 Weak-value amplification

As shown in Sec. 2.3.2 and 2.3.3, the average shift of the probe is proportional to the interaction strength and the weak value. If the interaction strength is known, we can extract the weak value of an observable. Conversely, if the weak value is known, we can estimate the interaction strength by performing weak measurements. This point of view leads to high precision measurement using pre- and post-selected ensembles.

Since the weak value can be unboundedly large, the average shift of the probe can be amplified by using the post-selection. This amplification technique is known as the weak-value amplification.

Although the post-selection causes the large shift of the probe, it also reduces the number of success measurements. As a results, the precision of the measurement is almost the same as the case of no post-selection when there is no noise.

However, the post-selection is known to improve the signal-to-noise ratio (SNR) against some kinds of noises such as systematic noise [36] and correlated noise [37]. Roughly speaking, the post-selection concentrates the signal of the measurement in a few trials; this concentration of the signal enables us to defeat some kinds of noise.

In the following, we describe which type of noise can be defeated by using post-selection.

In the case of no post-selection, the probe shift is proportional to the expectation value of a measured observable $\hat{A}$. To maximize the probe shift, the initial state of the measured system should be the eigenstate with respect to the largest absolute value of the eigenvalues. Let $a_{\max}$ and $a_{\min}$ be the maximum and minimum eigenvalues of $\hat{A}$, respectively. The maximum probe shift is represented as θa_{M}, where $a_{\mathrm{M}} := \max\{|a_{\max}|, |a_{\min}|\}$ and θ is the interaction strength to be measured. Repeating the measurement N times, the measured signal S_{i} is given by

$$S_{\mathrm{i}} = N\theta a_{\mathrm{M}}. \tag{2.91}$$

With pots-selection, on the other hand, the probe shift is proportional to the weak value of an observable $\hat{A}$. As shown in Appendix. A.2, when we fix the success probability $\mathcal{P}(\mathrm{f}|\mathrm{i})$ of the post-selection, the maximum modulus of the weak value satisfies

$$\max_{\mathcal{P}(\mathrm{f}|\mathrm{i}):\ \mathrm{const.}} |\langle \hat{A} \rangle_{\mathrm{w}}| \geq \frac{\Delta a}{2\sqrt{\mathcal{P}(\mathrm{f}|\mathrm{i})}}, \tag{2.92}$$

where $\Delta a := a_{\max} - a_{\min}$. When we perform the measurement N times, the post-selection succeeds $N\mathcal{P}(\mathrm{f}|\mathrm{i})$ times on average. Therefore, the measured signal $S_{\mathrm{f,i}}$ for N trials satisfies

$$S_{\mathrm{f,i}} \geq N\mathcal{P}(\mathrm{f}|\mathrm{i}) \cdot \theta \frac{\Delta a}{2\sqrt{\mathcal{P}(\mathrm{f}|\mathrm{i})}} = N\sqrt{\mathcal{P}(\mathrm{f}|\mathrm{i})}\,\theta \frac{\Delta a}{2}. \tag{2.93}$$

To evaluate the SNR of the measurements, we assume that the dominant noise is proportional N^{α}, where N is the number of success trials. The parameter α depends on the kind of noise. For example, the systematic noise corresponds to $\alpha = 1$, and the shot noise corresponds to $\alpha = 1/2$. We introduce the proportional constant k, then noise is represented as kN^{α}.

	Without post-selection	With post-selection
Signal	N	$\sqrt{\mathcal{P}(\mathrm{f}\|\mathrm{i})}N$
Noise	N^{α}	$[\mathcal{P}(\mathrm{f}\|\mathrm{i})N]^{\alpha}$
SNR	$N^{1-\alpha}$	$\mathcal{P}(\mathrm{f}\|\mathrm{i})^{1/2-\alpha}N^{1-\alpha}$

Table 2.1: S/N comparison between standard measurements and weak measurements. Unimportant constant factors are omitted.

We denote the SNRs of the weak measurements with and without post-selection as $\mathrm{SNR}_{\mathrm{f,i}}$ and $\mathrm{SNR}_{\mathrm{i}}$, respectively.

The SNR of the weak measurements without post-selection is simply

$$\begin{aligned}\mathrm{SNR}_{\mathrm{i}} &= \frac{S_{\mathrm{i}}}{kN^{\alpha}} \\ &= \theta k^{-1} a_{\mathrm{M}} N^{1-\alpha}. \end{aligned} \tag{2.94}$$

With post-selection, the number of success trials reduces to $\mathcal{P}(\mathrm{f}|\mathrm{i})N$. Thus the noise is also reduced to $k[\mathcal{P}(\mathrm{f}|\mathrm{i})N]^{\alpha}$. The SNR of the weak measurement with post-selection is

$$\begin{aligned}\mathrm{SNR}_{\mathrm{f,i}} &= \frac{S_{\mathrm{f,i}}}{k[\mathcal{P}(\mathrm{f}|\mathrm{i})N]^{\alpha}} \\ &\geq \theta k^{-1} \frac{\Delta a}{2} \mathcal{P}(\mathrm{f}|\mathrm{i})^{1/2-\alpha} N^{1-\alpha}. \end{aligned} \tag{2.95}$$

Note that $\Delta a/2$ and a_{M} have the same order of magnitude, unless $\hat{A}$ is almost equal to a constant times the identity operator.

The comparison between weak measurements with and without post-selection is shown in Table. 2.1. In Table. 2.1, we omit the unimportant constant factors. If dominant noise corresponds to $\alpha > 1/2$, weak measurements with post-selection have a net gain of SNR by the factor $\mathcal{P}(\mathrm{f}|\mathrm{i})^{1/2-\alpha}$. Thus, for example, systematic noise ($\alpha = 1$) can be reduced by using pot-selection. However, since the shot noise corresponds to $\alpha = 1/2$, there is no improvement of an ultimate limit of SNR.

2.4 Photonic qubits and linear optics

To implement weak measurements in optical systems, we use the two degree of freedom of a photon, its path and polarization. In this section, we describe the way to represent a qubit by using the path or polarization of a photon. We also present the quantum mechanical treatments of linear optical elements.

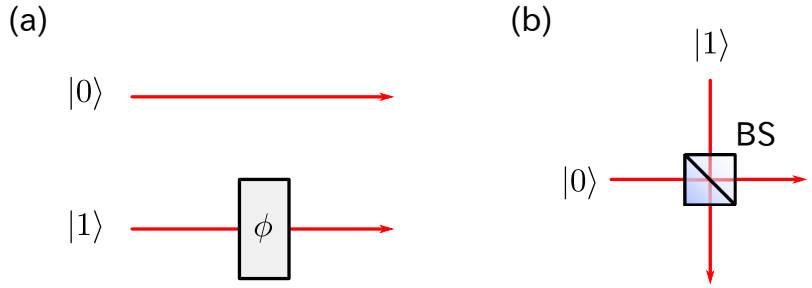

Figure 2.6: Optical elements: (a) Phase shifter; (b) Beam splitter. A red arrow represents each optical mode.

2.4.1 Path qubits

We describe the way to represent a qubit by using two spatial modes, or two paths. The state of two spatial modes can be represented by using the bracket notation like

$$|m, n\rangle. \tag{2.96}$$

In this notation, the first number m represents the number of photons in the first mode and the second number n represents the number of photons in the second mode. Now, we assume that there is only one photon in those two modes. The photon must exist in either the first mode or in the second modes. Thus, there are two possible states $|1, 0\rangle$ or $|0, 1\rangle$. We assign the states $|0\rangle$ and $|1\rangle$ of a qubit to these two states:

$$|0\rangle := |1, 0\rangle, \tag{2.97}$$
$$|1\rangle := |0, 1\rangle. \tag{2.98}$$

This representation of a qubit by the two possible paths of a photon is known as the dual-rail representation [38]. We call the qubit represented by the two paths of photon as a *path qubit*.

We consider how the optical elements act on the state of a path qubit. We describe the actions of two optical elements: a phase shifter and a beam splitter.

Figure 2.6 (a) represents a phase shifter with a retardation angle ϕ. The phase shifter causes the phase delay of an angle ϕ for one of the two paths. The unitary operation $\hat{U}_{\mathrm{P}}(\phi)$ of the phase shifter on a path qubit is represented in the $\{|0\rangle, |1\rangle\}$ basis as follows:

$$\hat{U}_{\mathrm{P}}(\phi) \doteq \begin{pmatrix} 1 & 0 \\ 0 & \mathrm{e}^{\mathrm{i}\phi} \end{pmatrix}. \tag{2.99}$$

The phase shifter can be implemented by varying the optical path length.

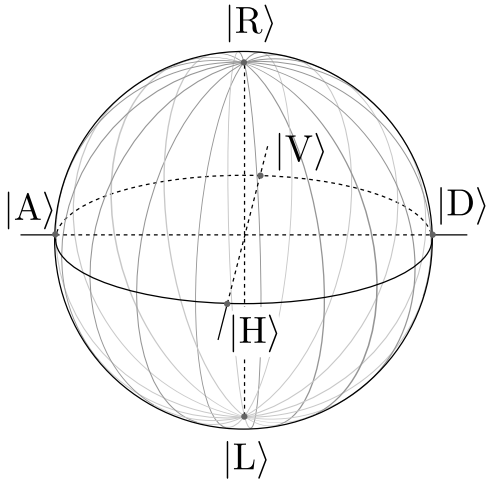

Figure 2.7: States of a polarization qubit on the Bloch sphere.

The second fundamental element is a beam splitter as shown in Fig. 2.6 (b). The action of the beam splitter is represented by

$$\hat{U}_{\mathrm{BS}} \doteq \frac{1}{\sqrt{2}} \begin{pmatrix} 1 & 1 \\ 1 & -1 \end{pmatrix}. \tag{2.100}$$

The photon incident from one of the two paths is transformed to an equally weighted superposition state of two paths.

The path state can be measured by setting a photo detector on each path.

2.4.2 Polarization qubits

The second representation of a qubit by a photon uses its polarization degree of freedom. We call this type of qubit as a *polarization qubit*. We denote the horizontal and vertical polarization as $|\mathrm{H}\rangle$ and $|\mathrm{V}\rangle$. Using $|\mathrm{H}\rangle$ and $|\mathrm{V}\rangle$, the diagonal and anti-diagonal polarization, $|\mathrm{D}\rangle$ and $|\mathrm{A}\rangle$, are written as

$$|\mathrm{D}\rangle = \frac{1}{\sqrt{2}}(|\mathrm{H}\rangle + |\mathrm{V}\rangle), \tag{2.101}$$

$$|\mathrm{A}\rangle = \frac{1}{\sqrt{2}}(|\mathrm{H}\rangle - |\mathrm{V}\rangle). \tag{2.102}$$

The right and left circular polarization, $|\mathrm{R}\rangle$ and $|\mathrm{L}\rangle$, are written as

$$|\mathrm{R}\rangle = \frac{1}{\sqrt{2}}(|\mathrm{H}\rangle + \mathrm{i}|\mathrm{V}\rangle), \tag{2.103}$$

$$|\mathrm{L}\rangle = \frac{1}{\sqrt{2}}(|\mathrm{H}\rangle - \mathrm{i}|\mathrm{V}\rangle). \tag{2.104}$$

We identify $|\mathrm{R}\rangle$ and $|\mathrm{L}\rangle$ of polarization with $|0\rangle$ and $|1\rangle$ of a qubit:

$$|0\rangle := |\mathrm{R}\rangle, \tag{2.105}$$
$$|1\rangle := |\mathrm{L}\rangle. \tag{2.106}$$

The each state of polarization is depicted on the Bloch sphere as shown in Fig. 2.7. The Bloch sphere for the polarization qubit is also called as the Poincaré sphere.

A wave plate is one of the basic optical elements acting on the polarization qubit. A wave plate is made of birefringent crystal such as quartz crystal. As shown in Fig. 2.8 (a), a wave plate has two axes called the fast and slow axes; these axes correspond to two eigen axes of the birefringent crystal. The fast axis has a smaller refractive index than the slow axis. The polarization along the fast axis feels the retardation of phase by an angle ϕ relative to the polarization along the slow axis. We consider the action of the wave plate whose fast axis rotated by an angle θ from the horizontal axis as shown in Fig. 2.8 (a). The action of the wave plate is represented as a rotation on the Bloch sphere as shown in Fig. 2.8 (b). The rotation axis is written by the vector $\boldsymbol{n}(\theta) := \cos(2\theta)\boldsymbol{e}_x + \sin(2\theta)\boldsymbol{e}_y$, where $\boldsymbol{e}_x$ and $\boldsymbol{e}_y$ represent the unit vectors along x and y directions. The unitary operator representing the action of the wave plate is written as

$$\begin{aligned}\hat{U}_{\mathrm{WP}}(\theta,\phi) &= \mathrm{e}^{\mathrm{i}\phi/2}\frac{1}{2}(\hat{I} + \boldsymbol{n}(\theta)\cdot\hat{\boldsymbol{\sigma}}) + \mathrm{e}^{-\mathrm{i}\phi/2}\frac{1}{2}(\hat{I} - \boldsymbol{n}(\theta)\cdot\hat{\boldsymbol{\sigma}}) \\ &= \cos(\phi/2)\,\hat{I} + \mathrm{i}\sin(\phi/2)(\cos(2\theta)\,\hat{\sigma}_x + \sin(2\theta)\,\hat{\sigma}_y).\end{aligned} \tag{2.107}$$

The wave plates having retardation angles π and $\pi/2$ are especially called a half-wave plate (HWP) and a quarter-wave plate (QWP), respectively. We denote the unitary operation of a HWP and a QWP as $\hat{U}_{\mathrm{HWP}}(\theta) := \hat{U}_{\mathrm{WP}}(\theta,\pi)$ and $\hat{U}_{\mathrm{QWP}}(\theta) := \hat{U}_{\mathrm{WP}}(\theta,\pi/2)$, respectively.

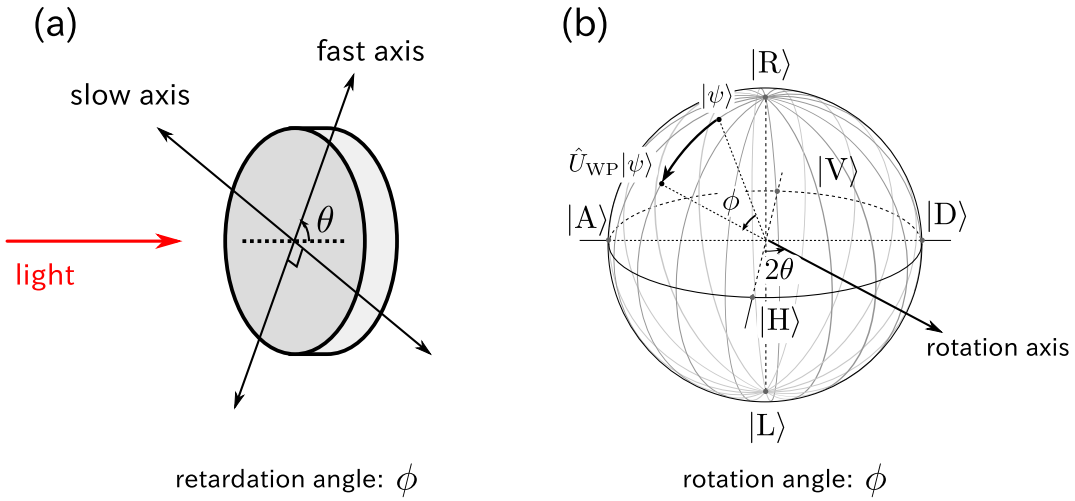

Figure 2.8: (a) Wave plate. The angle of the fast axis from the horizontal axis is represented by θ. (b) Action of the wave plate on the Bloch sphere. A quantum state $|\psi\rangle$ is rotated by the retardation angle ϕ. The rotation axis is tilted by the angle 2θ from the direction of $|\mathrm{H}\rangle$.

Chapter 3

Weak measurements and geometric phases

3.1 Introduction

In this chapter, we further investigate the AAV model of weak measurements introduced in Sec. 2.3.2. The aim of this chapter is to clarify the interference effect occurred in weak measurements for pre- and post-selected ensembles. In weak measurements, the measurement interaction is assumed to be weak, and the wavepackets of the probe remain overlapped. Therefore, the anomalously large shift in proportion to the weak value must be understood as a consequence of the interference induced by the post-selection.

To investigate the interference effect, we consider an interferometer for a particle with an internal degree of freedom. It serves as a framework common to the weak measurement and the quantum eraser [39].

In Sec. 3.2, we show an analogy between the weak measurement and the quantum eraser. In Sec. 3.3, we first investigate the change of interference in a quantum eraser. We demonstrate that the geometric phase [40], particularly the Pancharatnam phase [41], appears as a result of post-selection in the quantum eraser. In Sec. 3.3, we examine the role of the post-selection in weak measurements. We show that the extraordinary displacement of the probe wavepacket in weak measurements is the result of a geometric property of the Pancharatnam phase, which is induced by the post-selection. The weak value can be geometrically understood in terms of the behavior of geodesic arcs on the Bloch sphere.

3.2 Analogy between quantum erasers and weak measurements

Both setups for a quantum eraser and the AAV weak measurements can be regarded as an interferometer for a particle with an internal degree of freedom. Figure 3.1 shows the setups for a quantum eraser and the AAV weak measurements. In the quantum eraser, we consider the double-slit interferometer which has two possible paths. In the AAV weak measurement, on the other hand, a particle takes multiple paths labelled with a continuous variable p, which corresponds to the transverse momentum of the particle. This is only difference between the two setups.

3.3 Pancharatnam phase in quantum erasers

We first consider the effect of post-selection in a quantum eraser as shown in Fig. 3.1 (a).

In a quantum system, there exists a complementary relation between which-path information and visibility of interference [42]. When we can extract the which-path information from the internal state of a particle, the visibility of interference is decreased. The idea of quantum eraser is that one can erase the which-path information by post-selecting the internal state, and then the visibility of interference is recovered.

In this section, we show that the post-selection of the internal state not only results in the recovery of visibility, but also changes the phase of the interference. We focus on the phase shift in the quantum eraser and demonstrate that the phase shift induced by post-selection can be expressed in terms of the Pancharatnam phase.

Assume that the initial state of the path is

$$|\phi_{\mathrm{i}}\rangle = c_1|p_1\rangle + c_2|p_2\rangle, \quad (c_1, c_2 \in \mathbb{C},\ |c_1|^2 + |c_2|^2 = 1) \tag{3.1}$$

where $|p_1\rangle$ and $|p_2\rangle$ correspond to the states of the upper and lower paths, as shown in Fig. 3.1 (a). We introduce the projection operator $\hat{P}(\delta)$ for determining the relative phase of the paths as

$$\hat{P}(\delta) = |\phi(\delta)\rangle\langle\phi(\delta)|, \quad |\phi(\delta)\rangle = \frac{1}{\sqrt{2}}(|p_1\rangle + \mathrm{e}^{\mathrm{i}\delta}|p_2\rangle). \tag{3.2}$$

We can measure the interference pattern by sweeping the parameter δ.

In order to calibrate the interferometer, we first examine the initial interference pattern and determine the phase δ_{i} that maximizes the detection probability. The

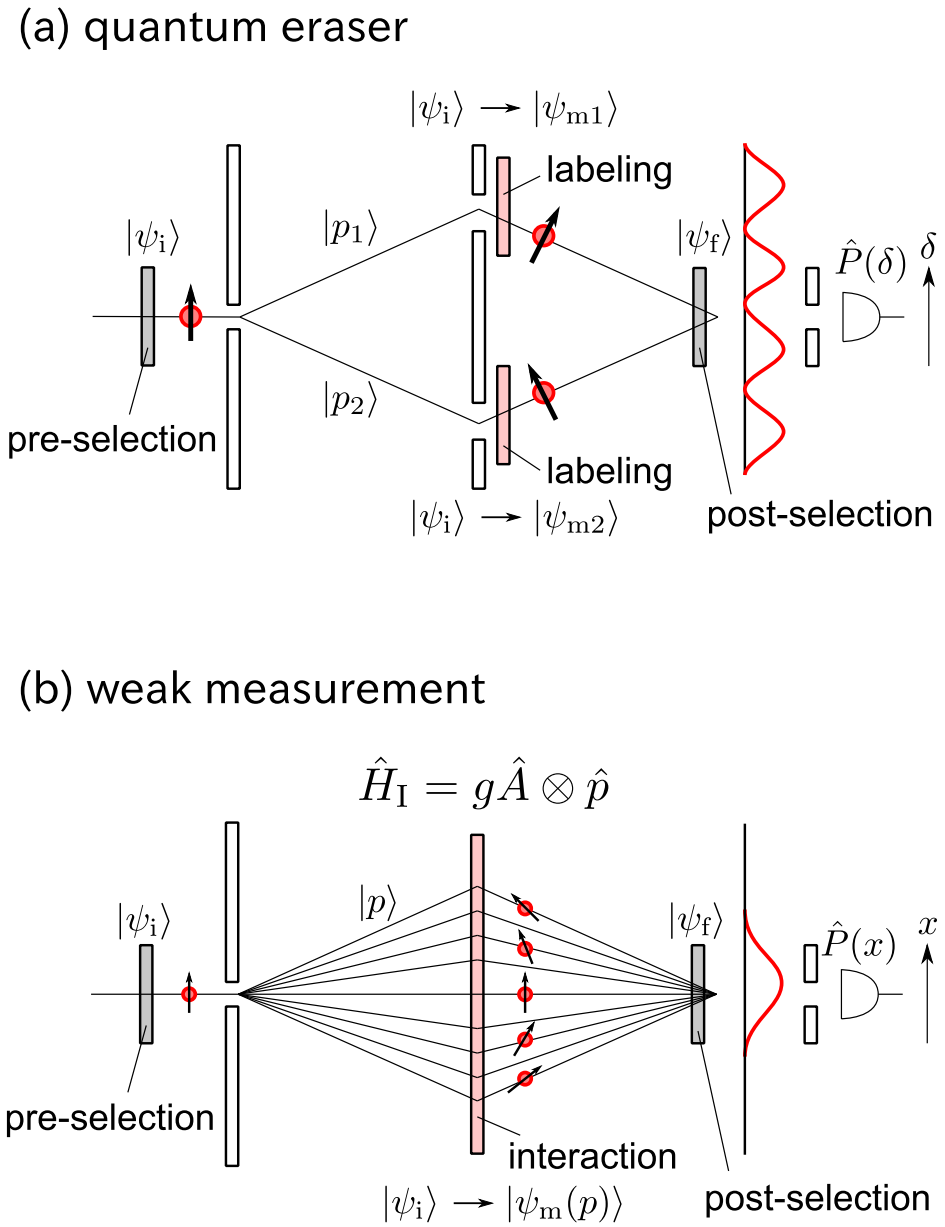

Figure 3.1: (a) Setup for a quantum eraser. We label the paths by utilizing the particle's internal degree of freedom and erase the which-path information by post-selecting the internal state. (b) Setup for weak measurements. We label the momentum eigenstates by the Hamiltonian $\hat{H}_\mathrm{I} = g\hat{A} \otimes \hat{p}$ and post-select the internal state.

detection probability is given by

$$\mathrm{tr}(|\phi_{\mathrm{i}}\rangle\langle\phi_{\mathrm{i}}|\hat{P}(\delta)) = \frac{1}{2}\left[1 + 2\,|c_1^* c_2|\cos(-\delta + \arg(c_1^* c_2))\right]. \tag{3.3}$$

In this case, the phase δ_{i} is given by

$$\delta_{\mathrm{i}} = \arg(c_1^* c_2), \tag{3.4}$$

which provides the origin of the phase, and the choice of the origin depends on our calibration of the interferometer.

Secondly, we consider the internal degree of freedom and assume that its initial state is $|\psi_{\mathrm{i}}\rangle$. The initial state of the composite system can be expressed as

$$|\Psi_{\mathrm{i}}\rangle = |\psi_{\mathrm{i}}\rangle \otimes (c_1|p_1\rangle + c_2|p_2\rangle). \tag{3.5}$$

In order to label the particle according to the paths, we let the initial state $|\psi_{\mathrm{i}}\rangle$ evolve into the states $|\psi_{\mathrm{m}1}\rangle$ and $|\psi_{\mathrm{m}2}\rangle$ corresponding to the paths $|p_1\rangle$ and $|p_2\rangle$, respectively. We assume that $\langle\psi_{\mathrm{m}1}|\psi_{\mathrm{m}2}\rangle \neq 0$. This condition means that we cannot completely distinguish the paths. Then the state of the composite system can be expressed as the non-maximally entangled state,

$$|\Psi_{\mathrm{m}}\rangle = c_1|\psi_{\mathrm{m}1}\rangle|p_1\rangle + c_2|\psi_{\mathrm{m}2}\rangle|p_2\rangle. \tag{3.6}$$

The interference pattern is found to be

$$\mathrm{tr}(|\Psi_{\mathrm{m}}\rangle\langle\Psi_{\mathrm{m}}|\hat{P}(\delta)) = \frac{1}{2}\left[1 + 2\,|c_1^* c_2|\,|\langle\psi_{\mathrm{m}1}|\psi_{\mathrm{m}2}\rangle|\cos(-\delta + \delta_{\mathrm{i}} + \arg\langle\psi_{\mathrm{m}1}|\psi_{\mathrm{m}2}\rangle)\right]. \tag{3.7}$$

The phase δ_{m} that gives the maximum detection probability is

$$\delta_{\mathrm{m}} = \delta_{\mathrm{i}} + \arg\langle\psi_{\mathrm{m}1}|\psi_{\mathrm{m}2}\rangle. \tag{3.8}$$

Thus the phase shift $\delta^{(1)}$ due to the labeling is

$$\delta^{(1)} = \delta_{\mathrm{m}} - \delta_{\mathrm{i}} = \arg\langle\psi_{\mathrm{m}1}|\psi_{\mathrm{m}2}\rangle. \tag{3.9}$$

This implies that we can measure the intrinsic phase difference between the internal states $|\psi_{\mathrm{m}1}\rangle$ and $|\psi_{\mathrm{m}2}\rangle$ as the phase shift $\delta^{(1)}$. The definition of the relative phase between two different states as $\arg\langle\psi_{\mathrm{m}1}|\psi_{\mathrm{m}2}\rangle$ was proposed by Pancharatnam [41]. When $\arg\langle\psi_{\mathrm{m}1}|\psi_{\mathrm{m}2}\rangle = 0$ is satisfied, $|\psi_{\mathrm{m}1}\rangle$ and $|\psi_{\mathrm{m}2}\rangle$ are known to be 'in phase.'

Next, we examine the phase shift that is induced by post-selection in the quantum eraser. After the post-selection of the internal state in $|\psi_{\mathrm{f}}\rangle$, the state of the composite system is given by

$$\begin{aligned} |\Psi_{\mathrm{f}}\rangle &= |\psi_{\mathrm{f}}\rangle\langle\psi_{\mathrm{f}}||\Psi_{\mathrm{m}}\rangle \\ &= |\psi_{\mathrm{f}}\rangle \otimes (c_1\langle\psi_{\mathrm{f}}|\psi_{\mathrm{m}1}\rangle|p_1\rangle + c_2\langle\psi_{\mathrm{f}}|\psi_{\mathrm{m}2}\rangle|p_2\rangle). \end{aligned} \tag{3.10}$$

The detection probability is

$$\begin{aligned}\mathrm{tr}(|\Psi_\mathrm{f}\rangle\langle\Psi_\mathrm{f}|\hat{P}(\delta)) = |c_1|^2\,|\langle\psi_\mathrm{f}|\psi_\mathrm{m1}\rangle|^2 + |c_2|^2\,|\langle\psi_\mathrm{f}|\psi_\mathrm{m2}\rangle|^2 \\ + 2\,|c_1^* c_2|\,|\langle\psi_\mathrm{m1}|\psi_\mathrm{f}\rangle\langle\psi_\mathrm{f}|\psi_\mathrm{m2}\rangle|\cos(-\delta+\delta_\mathrm{i}+\arg\langle\psi_\mathrm{m1}|\psi_\mathrm{f}\rangle\langle\psi_\mathrm{f}|\psi_\mathrm{m2}\rangle).\end{aligned} \tag{3.11}$$

Then constructive interference occurs at

$$\delta_\mathrm{f} = \delta_\mathrm{i} + \arg\langle\psi_\mathrm{m1}|\psi_\mathrm{f}\rangle\langle\psi_\mathrm{f}|\psi_\mathrm{m2}\rangle. \tag{3.12}$$

The phase shift $\delta^{(2)}$ that is induced by the post-selection is calculated as

$$\delta^{(2)} = \delta_\mathrm{f} - \delta_\mathrm{m} = \arg\langle\psi_\mathrm{m1}|\psi_\mathrm{f}\rangle\langle\psi_\mathrm{f}|\psi_\mathrm{m2}\rangle\langle\psi_\mathrm{m2}|\psi_\mathrm{m1}\rangle. \tag{3.13}$$

This phase shift is gauge invariant; that is, it is independent of the phase factor of each state. In fact, the right hand side of Eq. (3.13) represents the geometric phase, particularly the so-called Pancharatnam phase for the three states $|\psi_\mathrm{m1}\rangle$, $|\psi_\mathrm{m2}\rangle$ and $|\psi_\mathrm{f}\rangle$ [43, 44].

Assuming that the particle has two internal states such as for polarization or spin 1/2, the Pancharatnam phase is known to be related to the solid angle Ω (see Fig. 3.2) of the geodesic triangle on the Bloch sphere by the following relation:

$$\arg\langle\psi_\mathrm{m1}|\psi_\mathrm{f}\rangle\langle\psi_\mathrm{f}|\psi_\mathrm{m2}\rangle\langle\psi_\mathrm{m2}|\psi_\mathrm{m1}\rangle = -\frac{\Omega}{2}. \tag{3.14}$$

Figure 3.2 shows the relation between Eqs. (3.8) and (3.12), each of which corresponds to interferometry *without* and *with* post-selection, respectively. In both procedures, the initial state $|\psi_\mathrm{i}\rangle$ evolves into $|\psi_\mathrm{m1}\rangle$ and $|\psi_\mathrm{m2}\rangle$ according to the corresponding paths, and the phase difference between the two states is obtained by measuring the interference pattern. Without post-selection, we directly compare the phases between the two states $|\psi_\mathrm{m1}\rangle$ and $|\psi_\mathrm{m2}\rangle$. However, with post-selection, we compare the phases indirectly via the post-selected state $|\psi_\mathrm{f}\rangle$. The difference between δ_m and δ_f is attributed to the Pancharatnam phase (3.14) and it can be obtained as the phase shift $\delta^{(2)} = \delta_\mathrm{f} - \delta_\mathrm{m}$. The Pancharatnam phase for three states has been experimentally measured using setups similar to that shown in Fig. 3.1 (a) [45, 46].

It should be noted that the phases δ_i, δ_m and δ_f by themselves depend on our calibration of the interferometer. On the contrast, the phase shifts $\delta^{(1)} = \delta_\mathrm{m} - \delta_\mathrm{i}$ and $\delta^{(2)} = \delta_\mathrm{f} - \delta_\mathrm{m}$ are independent of the initial path state, and provide the phase information about the internal states. The phase shift $\delta^{(1)}$ represents the intrinsic phase difference between the two intermediate states $|\psi_\mathrm{m1}\rangle$ and $|\psi_\mathrm{m2}\rangle$. The phase shift $\delta^{(2)}$ represents the Pancharatnam phase among the three states $|\psi_\mathrm{m1}\rangle$, $|\psi_\mathrm{m2}\rangle$ and $|\psi_\mathrm{f}\rangle$, and critically depends on the choice of the post-selected state $|\psi_\mathrm{f}\rangle$.

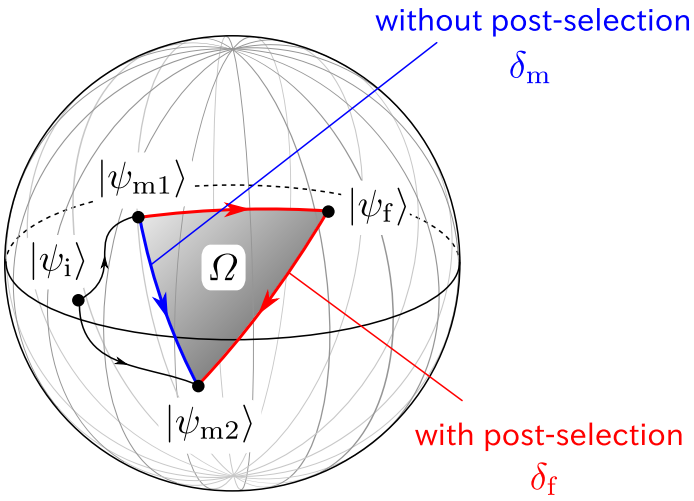

Figure 3.2: Pancharatnam phase on the Bloch sphere. The initial state $|\psi_{\mathrm{i}}\rangle$ evolves into $|\psi_{\mathrm{m1}}\rangle$ and $|\psi_{\mathrm{m2}}\rangle$. We compare the phases between them with or without post-selection in $|\psi_{\mathrm{f}}\rangle$. The geodesic triangle formed by $|\psi_{\mathrm{m1}}\rangle$, $|\psi_{\mathrm{m2}}\rangle$, and $|\psi_{\mathrm{f}}\rangle$ (shaded area) represents the Pancharatnam phase that results from the post-selection.

3.4 Reinterpretation of weak measurements

3.4.1 The Pancharatnam-phase-induced displacement

In this section, we describe how the Pancharatnam phase contributes to the displacement of probe wavepackets in weak measurements by applying the analogy introduced in Sec. 3.2.

Figure 3.1 (b) shows the setup for the weak measurement. The interferometer has multiple paths labeled with a continuous variable p, which is the transverse momentum of the particle. In the context of the weak measurement, the internal state of the particle corresponds to the measured system state, and the transverse (the x-direction) wavepacket corresponds to the probe state. We assume the initial probe state to be a real-valued function centered at $p = 0$ in the transverse momentum space. Since we measure the position of the particle in weak measurements, the detection operator $\hat{P}(x)$ is given by

$$\hat{P}(x) = |x\rangle\langle x|, \quad |x\rangle = \frac{1}{\sqrt{2\pi\hbar}} \int_{\mathbb{R}} \mathrm{e}^{-\mathrm{i}xp/\hbar} |p\rangle \mathrm{d}p, \tag{3.15}$$

where $|x\rangle$ is the transverse position eigenstate and $|p\rangle$ is the transverse momentum eigenstate. The transverse position x in Eq. (3.15) determines the phase gradient in the transverse momentum space and plays the same role as the phase difference δ in Eq. (3.2). While we obtain the phase difference between the two paths by measuring

the constructive interference points in the quantum eraser, we obtain the phase gradient in the momentum space by measuring the center of the wavepacket in weak measurements. In the quantum eraser, the initial calibration of the interferometer is required. Similarly, the prior determination of the center of the wavepacket is required in weak measurements.

In an analogous way to the quantum eraser, we analyze the phase change in the weak measurement. The interaction between the measured and probe system can be regarded as a labeling process. We label each momentum eigenstate under the interaction Hamiltonian $\hat{H}_{\rm I} = g\hat{A} \otimes \hat{p}$, where g is the coupling constant, $\hat{A}$ is a measured observable, and $\hat{p}$ is the transverse momentum operator. After the interaction for a time period τ, $|\psi_{\rm i}\rangle$ evolves into $|\psi_{\rm m}(p)\rangle = {\rm e}^{-{\rm i}G p\hat{A}/\hbar}|\psi_{\rm i}\rangle$ according to the path $|p\rangle$, where $G = g\tau$. This process leads to the phase difference $\Theta^{(1)}(p)$ between the momentum eigenstates $|p=0\rangle$ and $|p\rangle$:

$$\begin{aligned}\Theta^{(1)}(p) &= \arg\langle\psi_{\rm m}(0)|\psi_{\rm m}(p)\rangle \\ &= \arg\langle\psi_{\rm i}|{\rm e}^{-{\rm i}Gp\hat{A}/\hbar}|\psi_{\rm i}\rangle \\ &\sim -\frac{G\langle\hat{A}\rangle}{\hbar}p. \end{aligned} \tag{3.16}$$

We retained only the first order term in p. The phase change $\Theta^{(1)}(p)$ can be regarded as the dynamical phase [40], which is proportional to the energy of the particle. In fact, $\Theta^{(1)}$ is expressed as

$$\Theta^{(1)}(p) \sim -\frac{\langle\psi_{\rm i}|\langle p|\hat{H}_{\rm I}|\psi_{\rm i}\rangle|p\rangle\tau}{\hbar} = -\frac{G\langle\hat{A}\rangle}{\hbar}p. \tag{3.17}$$

The p-dependent phase shift changes the constructive interference point and is measured as the displacement of the wavepacket. The displacement $\Delta x^{(1)}$ due to the labeling is given by

$$\Delta x^{(1)} = -\hbar\left.\frac{{\rm d}\Theta^{(1)}}{{\rm d}p}\right|_{p=0} = G\langle\hat{A}\rangle. \tag{3.18}$$

Thus, we can obtain the expectation value of the observable $\hat{A}$.

We next consider the effect of the post-selection. As shown in Eq. (3.13), when we post-select the internal state in $|\psi_{\rm f}\rangle$, the Pancharatnam phase $\Theta^{(2)}(p)$ appears as an additional phase shift:

$$\begin{aligned}\Theta^{(2)}(p) &= \arg\langle\psi_{\rm m}(0)|\psi_{\rm f}\rangle\langle\psi_{\rm f}|\psi_{\rm m}(p)\rangle\langle\psi_{\rm m}(p)|\psi_{\rm m}(0)\rangle \\ &= \arg\left[\langle\psi_{\rm i}|\psi_{\rm f}\rangle\langle\psi_{\rm f}|{\rm e}^{-{\rm i}Gp\hat{A}/\hbar}|\psi_{\rm i}\rangle\langle\psi_{\rm i}|{\rm e}^{{\rm i}Gp\hat{A}/\hbar}|\psi_{\rm i}\rangle\right] \\ &\sim -\frac{G({\rm Re}\langle\hat{A}\rangle_{\rm w} - \langle\hat{A}\rangle)}{\hbar}p. \end{aligned} \tag{3.19}$$

Hence, the displacement $\Delta x^{(2)}$ caused by the post-selection is

$$\Delta x^{(2)} = -\hbar \left.\frac{\mathrm{d}\Theta^{(2)}}{\mathrm{d}p}\right|_{p=0} = G(\mathrm{Re}\langle\hat{A}\rangle_{\mathrm{w}} - \langle\hat{A}\rangle). \tag{3.20}$$

After all, the displacement Δx for the whole process of the weak measurement is the sum of $\Delta x^{(1)}$ and $\Delta x^{(2)}$:

$$\Delta x = \Delta x^{(1)} + \Delta x^{(2)} = G\,\mathrm{Re}\langle\hat{A}\rangle_{\mathrm{w}}. \tag{3.21}$$

Consequently, the displacement Δx is obtained as the real part of the weak value $\langle\hat{A}\rangle_{\mathrm{w}}$. The counterintuitive effects in weak measurements such as the unbounded weak value can be attributed to the Pancharatnam-phase-induced displacement $\Delta x^{(2)}$, as will be shown in Sec. 3.4.2.

3.4.2 Phase jump in the Pancharatnam phase

In weak measurements, the smaller the inner product of $|\psi_{\mathrm{i}}\rangle$ and $|\psi_{\mathrm{f}}\rangle$, the larger is the displacement Δx. This effect is closely related to the phase jump in the Pancharatnam phase that is caused by the geometrical singularity of geodesics on the Bloch sphere [45, 46, 47].

As an example, we consider a two-state system as a measured system. The initial state $|\psi_{\mathrm{i}}\rangle$, the post-selected state $|\psi_{\mathrm{f}}\rangle$, and the observable $\hat{A}$ are assumed as follows:

$$|\psi_{\mathrm{i}}\rangle = |0\rangle, \tag{3.22}$$
$$|\psi_{\mathrm{f}}\rangle = \sin\theta|0\rangle + \cos\theta|1\rangle, \tag{3.23}$$
$$\hat{A} = \hat{X}, \tag{3.24}$$

where $|0\rangle$ and $|1\rangle$ are basis states of the measured system, and $\hat{X}$ is the Pauli X operator. The expectation value and the weak value of $\hat{A}$ are

$$\langle\hat{A}\rangle = \langle\psi_{\mathrm{i}}|\hat{A}|\psi_{\mathrm{i}}\rangle = 0, \tag{3.25}$$
$$\langle\hat{A}\rangle_{\mathrm{w}} = \frac{\langle\psi_{\mathrm{f}}|\hat{A}|\psi_{\mathrm{i}}\rangle}{\langle\psi_{\mathrm{f}}|\psi_{\mathrm{i}}\rangle} = \frac{1}{\tan\theta}. \tag{3.26}$$

The system state $|\psi_{\mathrm{m}}(p)\rangle$ that is evolved corresponding to the probe state $|p\rangle$ is given by

$$\begin{aligned}|\psi_{\mathrm{m}}(p)\rangle &= \mathrm{e}^{-\mathrm{i}Gp\hat{A}/\hbar}|\psi_{\mathrm{i}}\rangle \\ &= \cos\varphi|0\rangle - \mathrm{i}\sin\varphi|1\rangle,\end{aligned} \tag{3.27}$$

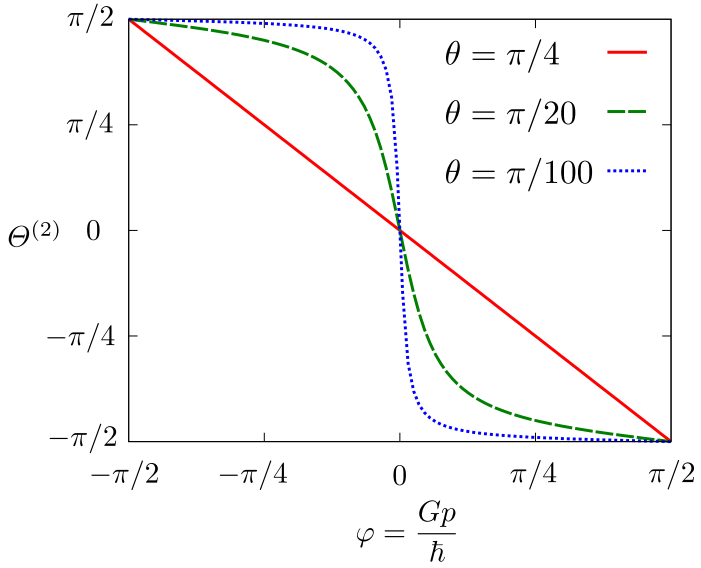

Figure 3.3: Variation of Pancharatnam phase $\Theta^{(2)}$ for several θ. The gradient of the Pancharatnam phase becomes steeper with decreasing θ. Since the Pancharatnam phase obtained around $p = 0$ is limited to π, the region in which the Pancharatnam phase changes linearly becomes smaller for the smaller θ.

where $\varphi(p) := Gp/\hbar$. The additional phase shift induced between the momentum eigenstates $|p = 0\rangle$ and $|p\rangle$ by post-selection is derived as

$$\begin{aligned}\Theta^{(2)}(p) &= \arg\langle\psi_\mathrm{i}|\psi_\mathrm{f}\rangle\langle\psi_\mathrm{f}|\psi_\mathrm{m}(p)\rangle\langle\psi_\mathrm{m}(p)|\psi_\mathrm{i}\rangle \\ &= -\tan^{-1}\left(\frac{\tan\varphi}{\tan\theta}\right). \end{aligned} \tag{3.28}$$

We show the variation in $\Theta^{(2)}$ for several post-selected states in Fig. 3.3. The trend in the phase change can be well understood by considering the geometrical meaning of the Pancharatnam phase. Figure 3.4 shows the variation of the geodesic triangle on the Bloch sphere. The initial state $|\psi_\mathrm{i}\rangle$ corresponds to the north pole $|0\rangle$ and the post-selected state $|\psi_\mathrm{f}\rangle$ occurs near the south pole $|1\rangle$. The solid angle $\Omega(p)$ of the geodesic triangle connecting $|\psi_\mathrm{i}\rangle$, $|\psi_\mathrm{m}(p)\rangle$, and $|\psi_\mathrm{f}\rangle$ is related to the Pancharatnam phase by the relation $\Theta^{(2)}(p) = -\Omega(p)/2$ as shown in Eq. (3.14).

For simplicity, we assume $0 < \theta \ll \pi/4$ and set $|\psi_\mathrm{i}^\perp\rangle = |1\rangle$. We sweep φ for a fixed value of θ. For $\varphi > \theta$, the distance between $|\psi_\mathrm{m}(p)\rangle$ and $|\psi_\mathrm{i}\rangle$ becomes large as compared to that between $|\psi_\mathrm{f}\rangle$ and $|\psi_\mathrm{i}^\perp\rangle$. Therefore, the path of the geodesic arc connecting $|\psi_\mathrm{m}(p)\rangle$ and $|\psi_\mathrm{f}\rangle$ passes close to the path connecting $|\psi_\mathrm{m}(p)\rangle$ and $|\psi_\mathrm{i}^\perp\rangle$. Since, in this example, the geodesic arc connecting $|\psi_\mathrm{m}(p)\rangle$ and $|\psi_\mathrm{i}^\perp\rangle$ is always on the same great circle, the geodesic arc connecting $|\psi_\mathrm{m}(p)\rangle$ and $|\psi_\mathrm{f}\rangle$ remains almost constant. As a result, the variation in the Pancharatnam phase in the range $\varphi > \theta$

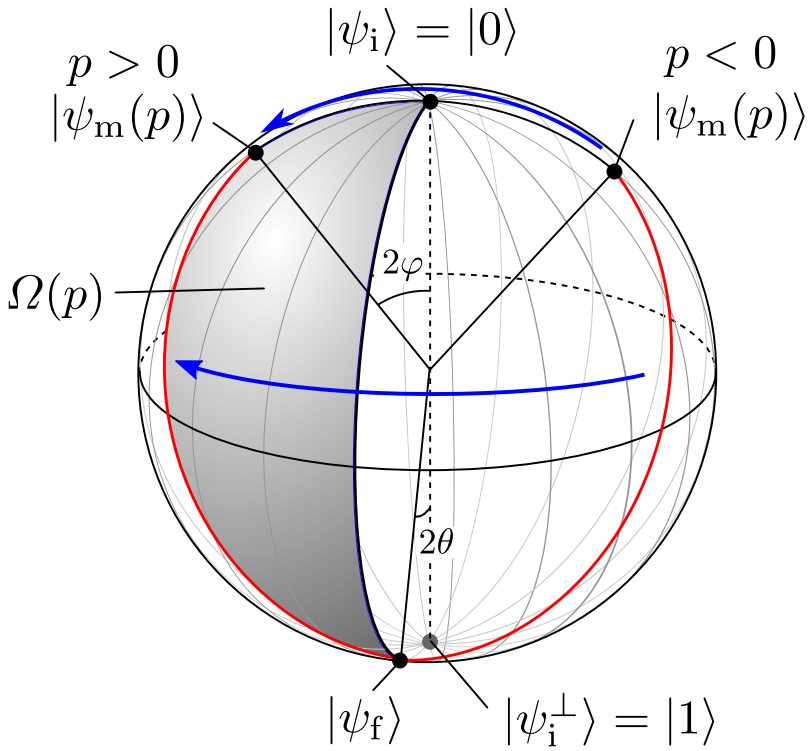

Figure 3.4: Variation of geodesic triangle on the Bloch sphere. The initial internal state $|\psi_\mathrm{i}\rangle$ corresponds to the north pole $|0\rangle$, and the post-selected state $|\psi_\mathrm{f}\rangle$ occurs near the south pole $|1\rangle$. After the interaction, the internal state is rotated clockwise or anti-clockwise into $|\psi_\mathrm{m}(p)\rangle$ according to $p < 0$ or $p > 0$. By the post-selection, the transverse momentum eigenstate $|p\rangle$ acquires the Pancharatnam phase $\Theta^{(2)}(p) = -\Omega(p)/2$. When $|\psi_\mathrm{m}(p)\rangle$ traverses the north pole $|0\rangle$, the geodesic arc connecting $|\psi_\mathrm{m}(p)\rangle$ and $|\psi_\mathrm{f}\rangle$ rapidly sweeps across the surface of the Bloch sphere, and therefore the Pancharatnam phase also changes rapidly around $p = 0$.

is quite small. This is also true in the range $\varphi < -\theta$. For $\varphi < 0$, however, the geodesic arc connecting $|\psi_{\rm m}(p)\rangle$ and $|\psi_{\rm i}^{\perp}\rangle$ goes in the opposite direction around the Bloch sphere, as compared to that in the case of $\varphi > 0$. Thus, the geodesic arc connecting $|\psi_{\rm m}(p)\rangle$ and $|\psi_{\rm f}\rangle$ must change rapidly in the range $-\theta < \varphi < \theta$. This is why the Pancharatnam phase jumps by π around $p = 0$. As shown in Fig. 3.3, the smaller the value of θ, the steeper is the gradient of $\Theta^{(2)}(p)$.

Weak measurements utilize the large gradient of the Pancharatnam phase around $p = 0$. Since $\langle \hat{A} \rangle = 0$ in this example, the real part of the weak value is proportional to the gradient of the Pancharatnam phase:

$$\Delta x = G\,\mathrm{Re}\langle \hat{A} \rangle_{\rm w} = -\hbar \left. \frac{\mathrm{d}\Theta^{(2)}}{\mathrm{d}p} \right|_{p=0}. \tag{3.29}$$

Therefore, when $\langle \psi_{\rm f} | \psi_{\rm i} \rangle \sim \theta$ is small, we can obtain the large displacement.

The Pancharatnam phase varies nonlinearly with p; therefore, in order to maintain the shape of the wavepacket, the momentum distribution of the wavepacket must be contained in the range in which the Pancharatnam phase changes linearly [48]. Let Δp be the standard deviation of the momentum, then the condition under which the Pancharatnam phase varies linearly is given by $\varphi(\Delta p) = G\Delta p/\hbar \ll \theta$, that is,

$$\frac{\Delta p}{\hbar} \ll \frac{\theta}{G} \simeq \frac{\tan\theta}{G} = \frac{1}{G|\,\mathrm{Re}\langle \hat{A} \rangle_{\rm w}|}. \tag{3.30}$$

This condition can be related to the weakness condition mentioned in [35] and [49]. The requirement of the weakness condition comes from the fact that the Pancharatnam phase that is obtained by the phase jump is limited to π, i.e. a quarter of the solid angle of the Bloch sphere. Since the weak value is determined from the gradient of the Pancharatnam phase, in order to obtain a large weak value, we must prepare a probe wavepacket having a small momentum variance so that it can be confined within the linear region.

3.5 Summary

In this chapter, we introduced the interferometer for a particle having an internal degrees of freedom, which is a framework common to the weak measurement and the quantum eraser. We first examined the phase change in the quantum eraser. It turned out that the post-selection in quantum eraser plays a role to change the way of the phase comparison between internal states. As a result, when we post-select the internal state, the Pancharatnam phase appears as an additional phase shift of interference pattern.

Subsequently, we considered the weak measurement in the interferometric framework with relating it to the quantum eraser. We also focused on the phase change in the weak measurement, and demonstrated that the extraordinary displacement in weak measurement is caused by the Pancharatnam phase that is obtained by post-selection. The unbounded weak value is achieved by utilizing the phase jump in the Pancharatnam phase. The weakness condition can be also derived from the nonlinear property of the Pancharatnam phase.

Chapter 4

Geometry of two-states

4.1 Introduction

In Sec. 2.2, we described that the state of the pre- and post-selected ensemble can be expressed by the two-state operator. In this chapter, we present a geometric representation of the two-state operator. We explain how the two-state operator can be depicted on the Bloch sphere.

By using the Bloch sphere representation, we tackle two problems. The first problem is how the negative weak value of the projection operator can be understood geometrically. The second problem is how we can maximize the weak value for fixed success probability. The maximization of the weak value is important when we design the setup for the weak-value amplification.

4.2 Geometry of two-state operators

The two-state operator $\hat{W}$ is defined by

$$\hat{W} = \frac{|\psi_{\rm i}\rangle\langle\psi_{\rm f}|}{\langle\psi_{\rm f}|\psi_{\rm i}\rangle}, \tag{4.1}$$

where $|\psi_{\rm i}\rangle$ and $|\psi_{\rm f}\rangle$ are pre- and post-selected states, respectively. The two-state operator $\hat{W}$ has similar properties to those of the density operator. The trace of the product of the two-state operator $\hat{W}$ and an observable $\hat{A}$ gives the weak value of $\hat{A}$:

$$\langle\hat{A}\rangle_{\rm w} = {\rm tr}(\hat{W}\hat{A}). \tag{4.2}$$

To construct a geometric representation, we first decompose the two-state operator, and then we describe the geometric interpretation of each component.

The two-state operator $\hat{W}$ can be decomposed into Hermitian and anti-Hermitian parts as follows:

$$\hat{W} = \hat{W}^{\mathrm{R}} + \mathrm{i}\hat{W}^{\mathrm{I}}, \tag{4.3}$$

$$\hat{W}^{\mathrm{R}} := \frac{1}{2}(\hat{W} + \hat{W}^{\dagger}), \tag{4.4}$$

$$\hat{W}^{\mathrm{I}} := \frac{1}{2\mathrm{i}}(\hat{W} - \hat{W}^{\dagger}), \tag{4.5}$$

where the operators $\hat{W}^{\mathrm{R}}$ and $\hat{W}^{\mathrm{I}}$ are both Hermitian operators. $\hat{W}^{\mathrm{R}}$ and $\hat{W}^{\mathrm{I}}$ are related to the real and imaginary parts of weak value, respectively:

$$\mathrm{Re}\langle\hat{A}\rangle_{\mathrm{w}} = \mathrm{tr}(\hat{W}^{\mathrm{R}}\hat{A}), \tag{4.6}$$

$$\mathrm{Im}\langle\hat{A}\rangle_{\mathrm{w}} = \mathrm{tr}(\hat{W}^{\mathrm{I}}\hat{A}). \tag{4.7}$$

We also define the following Hermitian operators related to $\hat{W}^{\mathrm{R}}$ as

$$\hat{W}^{\mathrm{R}}_{\mathrm{i}} := \hat{W}^{\mathrm{R}} - \hat{\rho}_{\mathrm{i}}, \tag{4.8}$$

$$\hat{W}^{\mathrm{R}}_{\mathrm{f}} := \hat{W}^{\mathrm{R}} - \hat{\rho}_{\mathrm{f}}, \tag{4.9}$$

where $\hat{\rho}_{\mathrm{i}} = |\psi_{\mathrm{i}}\rangle\langle\psi_{\mathrm{i}}|$ and $\hat{\rho}_{\mathrm{f}} = |\psi_{\mathrm{f}}\rangle\langle\psi_{\mathrm{f}}|$. Then the two-state operator $\hat{W}$ is decomposed into three parts as

$$\hat{W} = \hat{\rho}_{\mathrm{i}} + \hat{W}^{\mathrm{R}}_{\mathrm{i}} + \hat{W}^{\mathrm{I}} \tag{4.10}$$

$$= \hat{\rho}_{\mathrm{f}} + \hat{W}^{\mathrm{R}}_{\mathrm{f}} + \hat{W}^{\mathrm{I}}. \tag{4.11}$$

Next we consider the geometric meaning of each components. We denote the state space composed of all pure state operators as $\mathcal{R}$. For a two-state system, $\mathcal{R}$ is equivalent to the Bloch sphere. The tangent space of $\mathcal{R}$ at $\hat{\rho}$ is denoted as $T\mathcal{R}_{\hat{\rho}}$. As shown in Appendix B.1, the tangent space $T\mathcal{R}_{\hat{\rho}}$ is expressed as

$$T\mathcal{R}_{\hat{\rho}} = \{\hat{B} \,|\, \hat{B}^{\dagger} = \hat{B}, \mathrm{tr}\hat{B} = 0, \{\hat{B}, \hat{\rho}\} = \hat{B}\}. \tag{4.12}$$

It can be confirmed that

$$\hat{W}^{\mathrm{R}}_{\mathrm{i}}, \hat{W}^{\mathrm{I}} \in T\mathcal{R}_{\hat{\rho}_{\mathrm{i}}}, \tag{4.13}$$

$$\hat{W}^{\mathrm{R}}_{\mathrm{f}}, \hat{W}^{\mathrm{I}} \in T\mathcal{R}_{\hat{\rho}_{\mathrm{f}}}. \tag{4.14}$$

There are also the conjugate relations

$$\hat{W}^{\mathrm{R}}_{\mathrm{i}} = \mathrm{i}[\hat{\rho}_{\mathrm{i}}, \hat{W}^{\mathrm{I}}], \tag{4.15}$$

$$\hat{W}^{\mathrm{I}} = -\mathrm{i}[\hat{\rho}_{\mathrm{i}}, \hat{W}^{\mathrm{R}}_{\mathrm{i}}], \tag{4.16}$$

$$\hat{W}^{\mathrm{R}}_{\mathrm{f}} = -\mathrm{i}[\hat{\rho}_{\mathrm{f}}, \hat{W}^{\mathrm{I}}], \tag{4.17}$$

$$\hat{W}^{\mathrm{I}} = \mathrm{i}[\hat{\rho}_{\mathrm{f}}, \hat{W}^{\mathrm{R}}_{\mathrm{f}}]. \tag{4.18}$$

Therefore, $\hat{W}_{\mathrm{i}}^{\mathrm{R}}$ and $\hat{W}^{\mathrm{I}}$ are orthogonal to each other under the trace inner product:

$$\mathrm{tr}(\hat{W}_{\mathrm{i}}^{\mathrm{R}}\hat{W}^{\mathrm{I}}) = 0. \tag{4.19}$$

Furthermore, $\hat{W}_{\mathrm{i}}^{\mathrm{R}}$ and $\hat{W}^{\mathrm{I}}$ have the same length,

$$\begin{aligned}\mathrm{tr}[(\hat{W}_{\mathrm{i}}^{\mathrm{R}})^2] &= \mathrm{tr}(-\mathrm{i}\hat{W}_{\mathrm{i}}^{\mathrm{R}}[\hat{\rho}_{\mathrm{i}}, \hat{W}^{\mathrm{I}}]) \\ &= \mathrm{tr}(\mathrm{i}[\hat{\rho}_{\mathrm{i}}, \hat{W}_{\mathrm{i}}^{\mathrm{R}}]\hat{W}^{\mathrm{I}}) \\ &= \mathrm{tr}[(\hat{W}^{\mathrm{I}})^2]. \end{aligned} \tag{4.20}$$

Similarly,

$$\mathrm{tr}(\hat{W}_{\mathrm{f}}^{\mathrm{R}}\hat{W}^{\mathrm{I}}) = 0, \tag{4.21}$$

$$\mathrm{tr}[(\hat{W}_{\mathrm{f}}^{\mathrm{R}})^2] = \mathrm{tr}[(\hat{W}^{\mathrm{I}})^2]. \tag{4.22}$$

We further show that $\hat{W}_{\mathrm{i}}^{\mathrm{R}}$ is one of the tangent vectors along the geodesic curve from $\hat{\rho}_{\mathrm{i}}$ to $\hat{\rho}_{\mathrm{f}}$. It is known that the geodesic curve from $\hat{\rho}_{\mathrm{i}}$ to $\hat{\rho}_{\mathrm{f}}$ is expressed as follows [44].

$$\hat{\rho}(t) = \frac{|\psi(t)\rangle\langle\psi(t)|}{\langle\psi(t)|\psi(t)\rangle}, \tag{4.23}$$

$$|\psi(t)\rangle = \cos t|\psi_{\mathrm{i}}\rangle + \mathrm{e}^{\mathrm{i}\arg\langle\psi_{\mathrm{f}}|\psi_{\mathrm{i}}\rangle}\sin t|\psi_{\mathrm{f}}\rangle. \tag{4.24}$$

The tangent vector along the geodesic curve from ρ_{i} to ρ_{f} is calculated as

$$\left.\frac{\mathrm{d}}{\mathrm{d}t}\right|_{t=0}\hat{\rho}(t) = 2\,|\langle\psi_{\mathrm{f}}|\psi_{\mathrm{i}}\rangle|\,\hat{W}_{\mathrm{i}}^{\mathrm{R}}. \tag{4.25}$$

Therefore, $\hat{W}_{\mathrm{i}}^{\mathrm{R}}$ is one of the tangent vectors along the geodesic curve from $\hat{\rho}_{\mathrm{i}}$ to $\hat{\rho}_{\mathrm{f}}$. Similarly, $\hat{W}_{\mathrm{f}}^{\mathrm{R}}$ is a tangent vector along the geodesic curve from $\hat{\rho}_{\mathrm{f}}$ to $\hat{\rho}_{\mathrm{i}}$.

$$\left.\frac{\mathrm{d}}{\mathrm{d}t}\right|_{t=1}\hat{\rho}(t) = -2\,|\langle\psi_{\mathrm{f}}|\psi_{\mathrm{i}}\rangle|\,\hat{W}_{\mathrm{f}}^{\mathrm{R}}. \tag{4.26}$$

Summarizing the above results, we can illustrate the operators appeared in this section as Fig. 4.1. It means that the two-state operator include the information about the initial and final state as well as the tangent vector from $\hat{\rho}_{\mathrm{i}}$ to $\hat{\rho}_{\mathrm{f}}$.

4.3 Physical interpretation of two-state operators

In this section, we consider the physical meanings of the operators $\hat{W}_{\mathrm{i}}^{\mathrm{R}}$ and $\hat{W}^{\mathrm{I}}$ introduced in Sec. 4.2.

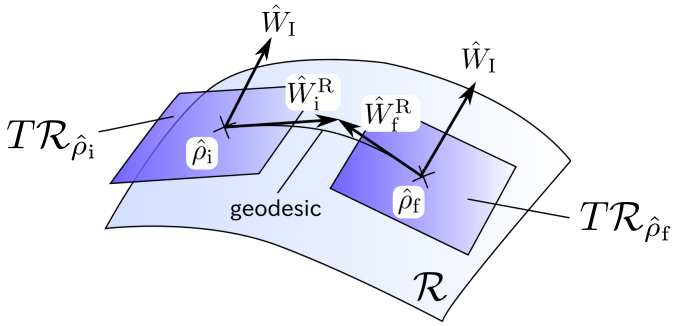

Figure 4.1: Geometry of the two-state operator. The operators $\hat{W}_{\mathrm{i}}^{\mathrm{R}}$ and $\hat{W}^{\mathrm{I}}$ are orthogonal tangent vectors with the same length at $\hat{\rho}_{\mathrm{i}}$. The operators $\hat{W}_{\mathrm{f}}^{\mathrm{R}}$ and $\hat{W}^{\mathrm{I}}$ are orthogonal tangent vectors with the same length at $\hat{\rho}_{\mathrm{f}}$. The tangent vectors $\hat{W}_{\mathrm{i}}^{\mathrm{R}}$ and $\hat{W}_{\mathrm{f}}^{\mathrm{R}}$ are oppositely directed along the geodesic curve from $\hat{\rho}_{\mathrm{i}}$ to $\hat{\rho}_{\mathrm{f}}$.

4.3.1 Real parts

In Sec. 3.4.1, we showed that the real part of the weak value is decomposed into two parts: the expectation value for the initial state and the gradient of the geometric phase. In a similar manner, we can show the relationship between the operator $\hat{W}_{\mathrm{i}}^{\mathrm{R}}$ and the geometric phase.

We assume that the state in the system is evolved according to the generator $\hat{A}$,

$$\hat{U}(\theta) = \exp(-\mathrm{i}\theta\hat{A}). \tag{4.27}$$

Let $|\psi_{\mathrm{m}}(\theta)\rangle := \hat{U}(\theta)|\psi_{\mathrm{i}}\rangle$, and then consider the geometric phase $\gamma(\theta)$ formed by the three states $|\psi_{\mathrm{i}}\rangle$, $|\psi_{\mathrm{m}}(\theta)\rangle$, and $|\psi_{\mathrm{f}}\rangle$:

$$\gamma(\theta) = \arg\langle\psi_{\mathrm{i}}|\psi_{\mathrm{f}}\rangle\langle\psi_{\mathrm{f}}|\psi_{\mathrm{m}}(\theta)\rangle\langle\psi_{\mathrm{m}}(\theta)|\psi_{\mathrm{i}}\rangle. \tag{4.28}$$

Then, we obtain the relation

$$\mathrm{tr}(\hat{W}_{\mathrm{i}}^{\mathrm{R}}\hat{A}) = -\left.\frac{\mathrm{d}}{\mathrm{d}\theta}\right|_{\theta=0}\gamma(\theta). \tag{4.29}$$

Therefore, $\hat{W}_{\mathrm{i}}^{\mathrm{R}}$ can extract the geometric phase generated by the operator $\hat{A}$.

4.3.2 Imaginary parts

The imaginary part of the weak value is related to the information obtained from the result of post-selection [50, 51].

We consider the evolution generated by $\hat{A}$ as Eq. (4.27). The success probability of post-selection is given by

$$p(\theta) = |\langle\psi_{\mathrm{f}}|\psi_{\mathrm{m}}(\theta)\rangle|^2. \tag{4.30}$$

The imaginary part of the weak value is proportional to the logarithmic derivative of the success probability

$$\mathrm{tr}(\hat{W}^{\mathrm{I}}\hat{A}) = \left.\frac{\mathrm{d}}{\mathrm{d}\theta}\right|_{\theta=0} \log p(\theta). \tag{4.31}$$

The logarithmic derivative is related to the Fisher information about the parameter θ [52]. Thus, the imaginary part of the weak value is related to the information obtained from the result of post-selection.

4.4 Bloch sphere representation of two-state operators

In this section, we describe a geometrical way to represent the two-state vector operator by using the Bloch sphere.

Assume that pre- and post-selected states are in an N-dimensional Hilbert space. We denote the two-dimensional subspace spanned by $|\psi_{\mathrm{i}}\rangle$ and $|\psi_{\mathrm{f}}\rangle$ as $\mathcal{H}_2$ and the projector onto $\mathcal{H}_2$ as $\hat{P}_2$. We can define the Pauli operators $\hat{\boldsymbol{\sigma}}$ on $\mathcal{H}_2$ by taking an appropriate basis of $\mathcal{H}_2$. By definition, the two-state operator

$$\hat{W} = \frac{|\psi_{\mathrm{i}}\rangle\langle\psi_{\mathrm{f}}|}{\langle\psi_{\mathrm{f}}|\psi_{\mathrm{i}}\rangle} \tag{4.32}$$

is an operator acting only on $\mathcal{H}_2$. Therefore, $\hat{W}$ can be decomposed by $\hat{P}_2$ and $\hat{\boldsymbol{\sigma}}$ as

$$\hat{W} = \frac{1}{2}(\hat{P}_2 + \boldsymbol{w}\cdot\hat{\boldsymbol{\sigma}}), \tag{4.33}$$

where $\boldsymbol{w}$ is a complex vector in $\mathbb{C}^3$. Let $\boldsymbol{r}_{\mathrm{i}}$ and $\boldsymbol{r}_{\mathrm{f}}$ represent the Bloch vector corresponding to $\hat{\rho}_{\mathrm{i}} = |\psi_{\mathrm{i}}\rangle\langle\psi_{\mathrm{i}}|$ and $\hat{\rho}_{\mathrm{f}} = |\psi_{\mathrm{f}}\rangle\langle\psi_{\mathrm{f}}|$, respectively, i.e.,

$$\hat{\rho}_{\mathrm{i}} = \frac{1}{2}(\hat{P}_2 + \boldsymbol{r}_{\mathrm{i}}\cdot\hat{\boldsymbol{\sigma}}), \tag{4.34}$$

$$\hat{\rho}_{\mathrm{f}} = \frac{1}{2}(\hat{P}_2 + \boldsymbol{r}_{\mathrm{f}}\cdot\hat{\boldsymbol{\sigma}}). \tag{4.35}$$

As shown in Eq. (2.56), $\hat{W}$ can also be written as

$$\hat{W} = \frac{\hat{\rho}_{\mathrm{i}}\hat{\rho}_{\mathrm{f}}}{\mathrm{tr}(\hat{\rho}_{\mathrm{f}}\hat{\rho}_{\mathrm{i}})}. \tag{4.36}$$

Substituting Eqs. (4.34) and (4.35) to this equation, we obtain [53]

$$\boldsymbol{w} = \frac{(\boldsymbol{r}_{\mathrm{i}} + \boldsymbol{r}_{\mathrm{f}}) + \mathrm{i}(\boldsymbol{r}_{\mathrm{i}}\times\boldsymbol{r}_{\mathrm{f}})}{1 + \boldsymbol{r}_{\mathrm{i}}\cdot\boldsymbol{r}_{\mathrm{f}}}. \tag{4.37}$$

We define the real and imaginary parts of $\boldsymbol{w}$ as $\boldsymbol{w}^{\mathrm{R}}$ and $\boldsymbol{w}^{\mathrm{I}}$ so that

$$\boldsymbol{w} = \boldsymbol{w}^{\mathrm{R}} + \mathrm{i}\boldsymbol{w}^{\mathrm{I}}. \tag{4.38}$$

Then $\boldsymbol{w}_{\mathrm{R}}$ and $\boldsymbol{w}_{\mathrm{I}}$ can be represented as

$$\boldsymbol{w}^{\mathrm{R}} = \frac{\boldsymbol{r}_{\mathrm{i}} + \boldsymbol{r}_{\mathrm{f}}}{1 + \boldsymbol{r}_{\mathrm{i}} \cdot \boldsymbol{r}_{\mathrm{f}}}, \tag{4.39}$$

$$\boldsymbol{w}^{\mathrm{I}} = \frac{\boldsymbol{r}_{\mathrm{i}} \times \boldsymbol{r}_{\mathrm{f}}}{1 + \boldsymbol{r}_{\mathrm{i}} \cdot \boldsymbol{r}_{\mathrm{f}}}. \tag{4.40}$$

Define two unit vectors $\boldsymbol{r} := (\boldsymbol{r}_{\mathrm{i}} + \boldsymbol{r}_{\mathrm{f}})/\left|\boldsymbol{r}_{\mathrm{i}} + \boldsymbol{r}_{\mathrm{f}}\right|$ and $\boldsymbol{q} := (\boldsymbol{r}_{\mathrm{i}} \times \boldsymbol{r}_{\mathrm{f}})/\left|\boldsymbol{r}_{\mathrm{i}} \times \boldsymbol{r}_{\mathrm{f}}\right|$, and denote the angle between $\boldsymbol{r}_{\mathrm{i}}$ and $\boldsymbol{r}_{\mathrm{f}}$ by 2θ, then

$$\boldsymbol{w}^{\mathrm{R}} = \frac{1}{\cos\theta}\boldsymbol{r}, \tag{4.41}$$

$$\boldsymbol{w}^{\mathrm{I}} = \tan\theta\, \boldsymbol{q}. \tag{4.42}$$

Define the vectors $\boldsymbol{w}_{\mathrm{i}}^{\mathrm{R}}$ and $\boldsymbol{w}_{\mathrm{f}}^{\mathrm{R}}$ related to $\hat{W}_{\mathrm{i}}^{\mathrm{R}}$ and $\hat{W}_{\mathrm{f}}^{\mathrm{R}}$ as

$$\boldsymbol{w}_{\mathrm{i}}^{\mathrm{R}} := \boldsymbol{w}^{\mathrm{R}} - \boldsymbol{r}_{\mathrm{i}}, \tag{4.43}$$

$$\boldsymbol{w}_{\mathrm{f}}^{\mathrm{R}} := \boldsymbol{w}^{\mathrm{R}} - \boldsymbol{r}_{\mathrm{f}}. \tag{4.44}$$

Then the following relation can be derived in accordance with the results shown in Sec. 4.2.

$$\boldsymbol{r}_{\mathrm{i}} \perp \boldsymbol{w}_{\mathrm{i}}^{\mathrm{R}}, \boldsymbol{r}_{\mathrm{i}} \perp \boldsymbol{w}^{\mathrm{I}}, \tag{4.45}$$

$$\boldsymbol{r}_{\mathrm{f}} \perp \boldsymbol{w}_{\mathrm{f}}^{\mathrm{R}}, \boldsymbol{r}_{\mathrm{f}} \perp \boldsymbol{w}^{\mathrm{I}}, \tag{4.46}$$

$$\boldsymbol{w}_{\mathrm{i}}^{\mathrm{R}} \perp \boldsymbol{w}^{\mathrm{I}}, \boldsymbol{w}_{\mathrm{f}}^{\mathrm{R}} \perp \boldsymbol{w}^{\mathrm{I}}, \tag{4.47}$$

$$|\boldsymbol{w}_{\mathrm{i}}^{\mathrm{R}}| = |\boldsymbol{w}_{\mathrm{f}}^{\mathrm{R}}| = |\boldsymbol{w}^{\mathrm{I}}|. \tag{4.48}$$

Summarizing the above results, the vectors $\boldsymbol{w}^{\mathrm{R}}$ and $\boldsymbol{w}^{\mathrm{I}}$ can be represented on the Bloch sphere as shown in Fig. 4.2.

4.5 Geometrical representation of weak values

In this section, we describe how weak values are derived from the Bloch sphere representation of the two-state operator.

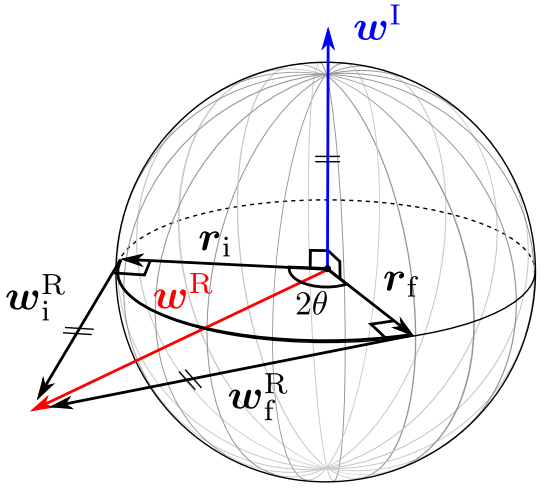

Figure 4.2: The Bloch sphere representation of the two-state operator.

4.5.1 Decomposition of weak values

Any observable $\hat{A}$ has a spectral decomposition,

$$\hat{A} = \sum_{n=1}^{N} a_n |n\rangle\langle n|. \tag{4.49}$$

Thus the weak value of $\hat{A}$ can be written in the form

$$\langle \hat{A} \rangle_{\mathrm{w}} = \sum_{n=1}^{N} a_n \langle |n\rangle\langle n| \rangle_{\mathrm{w}}. \tag{4.50}$$

We can regard $\langle |n\rangle\langle n| \rangle_{\mathrm{w}}$ as a complex probability distribution. In fact, the weak values $\langle |n\rangle\langle n| \rangle_{\mathrm{w}}$ satisfy the sum rule:

$$\sum_{n=1}^{N} \langle |n\rangle\langle n| \rangle_{\mathrm{w}} = 1, \tag{4.51}$$

which is the result of the completeness relation $\sum_{n=1}^{N} |n\rangle\langle n| = \hat{I}$. Thus the weak value of $\hat{A}$ is the weighted sum of its eigenvalues a_n with respect to the complex probability distribution $\langle |n\rangle\langle n| \rangle_{\mathrm{w}}$. Figure 4.3 illustrates this fact. The decomposition of the weak value suggests that the strangeness of the weak values attributes to that of the complex probability distribution [54].

Note that the real parts of the weak values also satisfy the sum rule:

$$\sum_{n=1}^{N} \mathrm{Re} \langle |n\rangle\langle n| \rangle_{\mathrm{w}} = 1. \tag{4.52}$$

Thus we can regard $\mathrm{Re} \langle |n\rangle\langle n| \rangle_{\mathrm{w}}$ as a quasiprobability distribution.

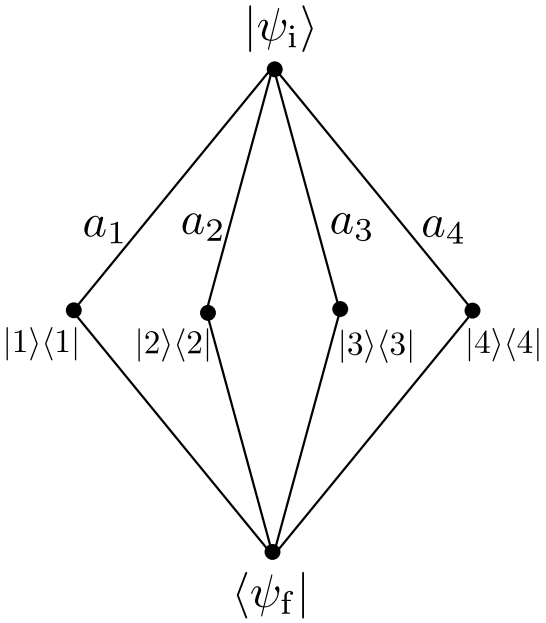

Figure 4.3: Decomposition of the weak value. The weak values of projection operators can be regarded as a complex probability distribution. The weak value $\hat{A}$ of is the weighted sum of its eigenvalues a_n with respect to the complex probability distribution $\langle|n\rangle\langle n|\rangle_{\rm w}$.

4.5.2 Geometric representation of path operators

In an N-dimensional system, we have N orthonormal basis vectors $\{|n\rangle\}$. To treat these vectors in the Bloch ball, we project these vectors onto the Hilbert space $\mathcal{H}_2$ and define the projected vectors as $\{|s_n\rangle\}$, i.e.,

$$|s_n\rangle := \hat{P}_2|n\rangle. \tag{4.53}$$

We call $|s_n\rangle\langle s_n|$ a *path operator*. From the completeness of the original basis vectors $|n\rangle$, the path operators satisfy the following relation:

$$\sum_{n=1}^{N} |s_n\rangle\langle s_n| = \hat{P}_2. \tag{4.54}$$

The set of path operators is the same as a rank-1 POVM on $\mathcal{H}_2$. The path operators can also be decomposed by using the projection operator $\hat{P}_2$ and the Pauli operators on $\mathcal{H}_2$ as

$$|s_n\rangle\langle s_n| = |\boldsymbol{s}_n|\,\hat{P}_2 + \boldsymbol{s}_n\cdot\hat{\boldsymbol{\sigma}}. \tag{4.55}$$

We call $\boldsymbol{s}_n$ a *path vector*. The condition (4.54) is equivalent to the following two condition on the path vectors $\boldsymbol{s}_n$:

$$\sum_{n=1}^{N} |\boldsymbol{s}_n| = 1, \tag{4.56}$$

$$\sum_{n=1}^{N} \boldsymbol{s}_n = \boldsymbol{0}. \tag{4.57}$$

The weak values of the projection operators $|n\rangle\langle n|$ are represented by using the path vectors as

$$\begin{aligned} \langle |n\rangle\langle n| \rangle_{\mathrm{w}} &= \langle |s_n\rangle\langle s_n| \rangle_{\mathrm{w}} \\ &= |\boldsymbol{s}_n| + \boldsymbol{s}_n \cdot \boldsymbol{w}. \end{aligned} \tag{4.58}$$

Thus the path vectors completely characterize the complex probability distribution defined by the weak values of the projection operators $|n\rangle\langle n|$.

Conversely, if N path vectors satisfying the relations (4.56) and (4.57) are given, we can choose an orthonormal basis $\{|n\rangle\}$ of an N-dimensional Hilbert space to satisfy the relation (4.58). In fact, the path vectors $\boldsymbol{s}_n$ satisfying the relations (4.56) and (4.57) have one-to-one correspondence with the path operators $|s_n\rangle\langle s_n|$ as shown in Eq. (4.55). Owing to Naimark's diliation theorem (see Appendix B.2), we can construct orthonormal basis vectors $|n\rangle$ which are projected onto $|s_n\rangle$ by $\hat{P}_2$.

4.6 Negative weak values

The complex probability distribution defined by the weak values of projection operators is used to understand quantum paradoxes relevant to pre- and post-selected ensembles. The examples of such quantum paradoxes are Hardy's paradox [5, 6] and the quantum N-box problem [7]. In such paradoxical systems, negative weak values often appear. In this section, we describe how the negative weak values are represented on the Bloch sphere.

4.6.1 The region of negative weak values

We consider the condition when the real part of the weak value of a projection operator becomes negative. From Eq. (4.58),

$$\mathrm{Re}\langle |n\rangle\langle n| \rangle_{\mathrm{w}} = |\boldsymbol{s}_n| + \boldsymbol{s}_n \cdot \boldsymbol{w}^{\mathrm{R}}, \tag{4.59}$$

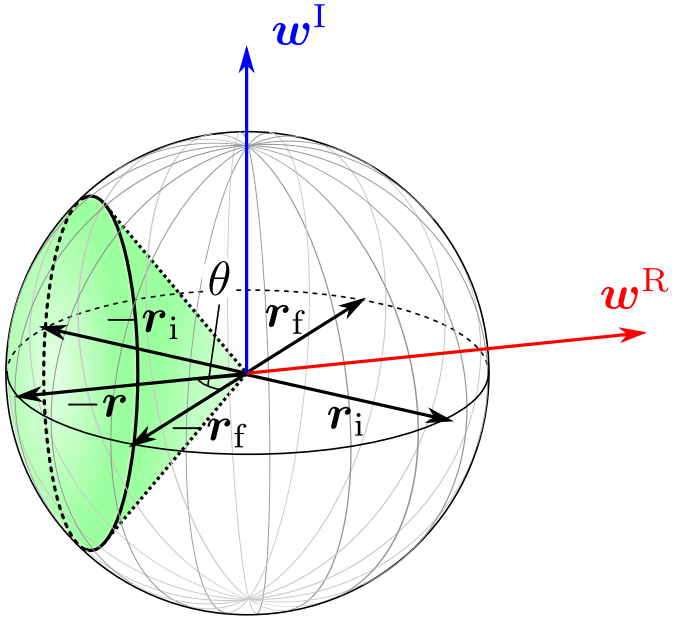

Figure 4.4: The region of negative weak values. The vectors opposite to the initial and final states, $-\boldsymbol{r}_{\mathrm{i}}$ and $-\boldsymbol{r}_{\mathrm{f}}$, are on the boundary of the negative-weak-value cone.

and the condition of the negative weak value is given by

$$|\boldsymbol{s}_n| + \boldsymbol{s}_n \cdot \boldsymbol{w}^{\mathrm{R}} < 0. \tag{4.60}$$

Using Eq. (4.41), this condition reduces to

$$\frac{\boldsymbol{s}_n}{|\boldsymbol{s}_n|} \cdot (-\boldsymbol{r}) > \cos\theta. \tag{4.61}$$

Let $0 \leq \phi \leq \pi$ denote the angle between $-\boldsymbol{r}$ and $\boldsymbol{s}_n$, the above condition is equivalent to

$$0 \leq \phi < \theta. \tag{4.62}$$

When $\boldsymbol{s}_n$ is in the circular cone with the axis $-\boldsymbol{r}$ and the aperture 2θ, the weak value $\langle |n\rangle\langle n| \rangle_{\mathrm{w}}$ becomes negative. The region of the negative weak value is shown in Fig. 4.4. The vectors $-\boldsymbol{r}_{\mathrm{i}}$ and $-\boldsymbol{r}_{\mathrm{f}}$ correspond to the opposite generatrixes of the negative-weak-value cone.

4.6.2 Three-box problem

We consider, as an example, the so-called the three-box problem [7, 8]. Assume that we have three boxes and there is one particle in any one of these boxes. The particle is assumed to be a quantum particle and the states $|1\rangle$, $|2\rangle$ and $|3\rangle$ correspond to

the case when the particle exists in the number 1, 2, and 3 box, respectively. One can pack the particle in a superposition state. The three box problem assumes that the particle was packed in an initial state $|\psi_{\rm i}\rangle$ and was found to be in a final state $|\psi_{\rm f}\rangle$. The initial and the final states are given by

$$|\psi_{\rm i}\rangle = \frac{|1\rangle + |2\rangle + |3\rangle}{\sqrt{3}}, \tag{4.63}$$

$$|\psi_{\rm f}\rangle = \frac{|1\rangle + |2\rangle - |3\rangle}{\sqrt{3}}. \tag{4.64}$$

Then, we consider the problem to guess the probability of finding the particle in one of these boxes. The quasiprobability distribution based on the weak values is given by

$$\mathrm{Re}\langle|1\rangle\langle 1|\rangle_{\rm w} = 1, \tag{4.65}$$

$$\mathrm{Re}\langle|2\rangle\langle 2|\rangle_{\rm w} = 1, \tag{4.66}$$

$$\mathrm{Re}\langle|3\rangle\langle 3|\rangle_{\rm w} = -1. \tag{4.67}$$

This means that the case of finding the particle in box 3 is more unlikely than the case with "probability"[1] 0. As a results, if we weakly measure the value of the projection operator $|3\rangle\langle 3|$, the meter of measuring device moves opposite to the ordinary direction.

We represent this situation on the Bloch sphere. The path kets $|s_n\rangle$ are given by

$$|s_1\rangle = \frac{1}{2}(|1\rangle + |2\rangle), \tag{4.68}$$

$$|s_2\rangle = \frac{1}{2}(|1\rangle + |2\rangle), \tag{4.69}$$

$$|s_3\rangle = |3\rangle. \tag{4.70}$$

Fig. 4.5 shows the configuration of the path vectors. The path vectors $\boldsymbol{s}_1$, $\boldsymbol{s}_2$, and $\boldsymbol{s}_3$ satisfy the relation:

$$\boldsymbol{s}_1 = \boldsymbol{s}_2 = \frac{1}{2}\boldsymbol{s}_3. \tag{4.71}$$

Note that the vector $\boldsymbol{s}_3$ is directed opposite to the geodesic curve connecting the initial state $\boldsymbol{r}_{\rm i}$ and the final state $\boldsymbol{r}_{\rm f}$. This means that the $\boldsymbol{s}_3$ is on a roundabout way. Thus the path $\boldsymbol{s}_3$ does not seem to be traced by the particle. This fact makes the weak value of the box $|3\rangle$ be negative. Since the weak value is determined based

[1]We used the word "probability" since the quasiprobability distribution is not a standard probability distribution.

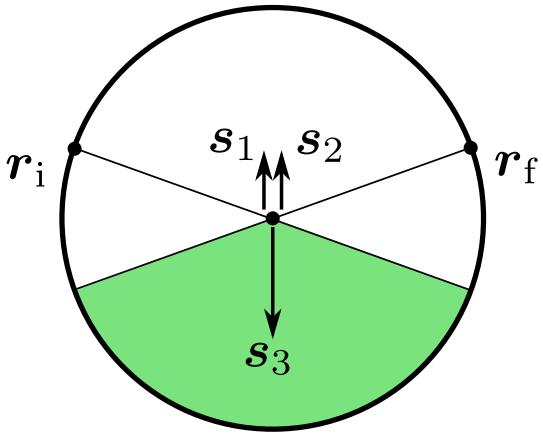

Figure 4.5: The Bloch sphere representation of three-box problem. This figure is the top view of the Bloch ball.

not only on the pre-selected state but also on the post-selected state, we have more information to guess the path traced by a particle than ordinary situations. As a results, a weak value sometimes becomes negative to show the "probability" of a rare event.

4.7 Maximizing weak value

Finally, we consider the problem to maximize the real or imaginary part of the weak value for a fixed success probability of post-selection. This problem is important to maximize the sensitivity of the weak-value amplification.

Using the spectral decomposition given in Eq. (4.50), the weak value of an observable $\hat{A}$ is written as

$$\langle \hat{A} \rangle_{\mathrm{w}} = \sum_{n=1}^{N} a_n (|\boldsymbol{s}_n| + \boldsymbol{s}_n \cdot \boldsymbol{w}). \tag{4.72}$$

Let the maximum and minimum eigenvalues of $\hat{A}$ be $a_{\max}$ and $a_{\min}$, respectively. For simplicity, we assume that $|a_{\max}| > |a_{\min}|$. We denote the path vectors corresponding to $a_{\max}$ and $a_{\min}$ as $\boldsymbol{s}_{\max}$ and $\boldsymbol{s}_{\min}$, respectively.

For a fixed success probability of post-selection, the lengths of $\boldsymbol{w}^{\mathrm{R}}$ and $\boldsymbol{w}^{\mathrm{I}}$ are also fixed. The problem is thus reduced to maximize the real or imaginary part of the right-hand side of Eq. (4.72) for given $\boldsymbol{w}^{\mathrm{R}}$ and $\boldsymbol{w}^{\mathrm{I}}$ by varying $\boldsymbol{s}_n$ under the constraints given by Eq. (4.56) and Eq. (4.57). Since $\langle \hat{A} \rangle_{\mathrm{w}}$ is a weighted sum of the value $|\boldsymbol{s}_n| + \boldsymbol{s}_n \cdot \boldsymbol{w}$, we can maximize $\mathrm{Re}\langle \hat{A} \rangle_{\mathrm{w}}$ by choosing $\boldsymbol{s}_{\max}$ to be the vector with length 1/2 along the direction of $\boldsymbol{w}^{\mathrm{R}}$ and $\boldsymbol{s}_{\min}$ to be the vector with length 1/2

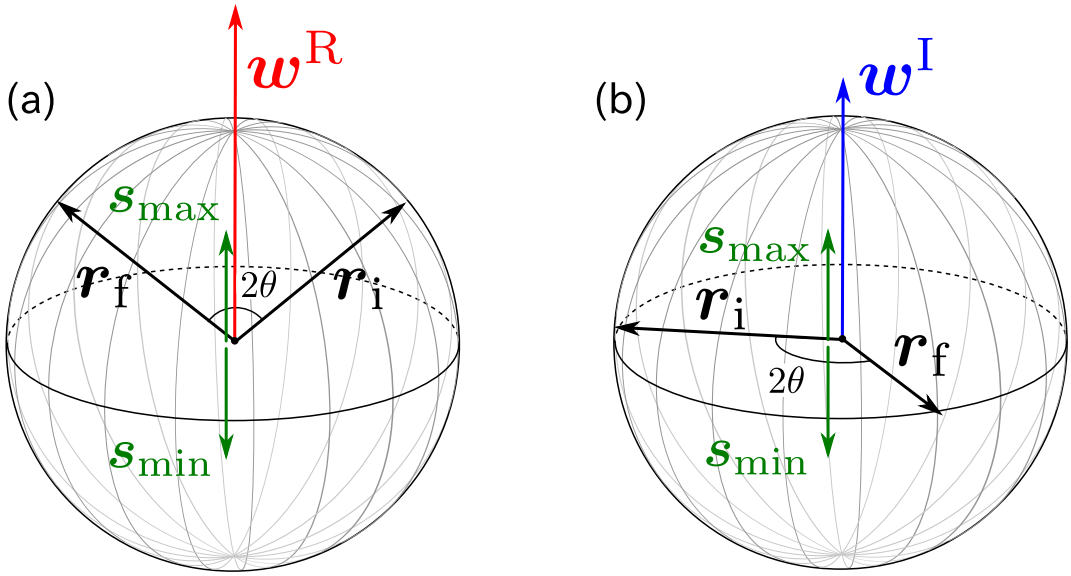

Figure 4.6: Configurations of the path vectors that maximize (a) the real part and (b) imaginary part of the weak value.

along the opposite direction of $\boldsymbol{w}^{\mathrm{R}}$. The maximization of the imaginary part can also achieved by choosing $\boldsymbol{s}_{\max}$ to be the vector with length $1/2$ along the direction of $\boldsymbol{w}^{\mathrm{I}}$ and $\boldsymbol{s}_{\min}$ to be the vector with length $1/2$ along the opposite direction of $\boldsymbol{w}^{\mathrm{I}}$

The configurations of the path vectors that maximize the real and imaginary parts of the weak value are shown in Fig 4.6. In these cases, the maximum values are calculated by Eq. (4.72) as

$$\max_{\mathcal{P}(\mathrm{f}|\mathrm{i}):\mathrm{const.}} \mathrm{Re}\langle \hat{A} \rangle_{\mathrm{w}} = \frac{a_{\max} + a_{\min}}{2} + \frac{a_{\max} - a_{\min}}{2} \left| \boldsymbol{w}^{\mathrm{R}} \right|, \tag{4.73}$$

$$\max_{\mathcal{P}(\mathrm{f}|\mathrm{i}):\mathrm{const.}} \mathrm{Im}\langle \hat{A} \rangle_{\mathrm{w}} = \frac{a_{\max} - a_{\min}}{2} \left| \boldsymbol{w}^{\mathrm{I}} \right|. \tag{4.74}$$

When we set the success probability as $\mathcal{P}(\mathrm{f}|\mathrm{i}) = \cos^2 \xi$, the lengths of the real and imaginary parts of the vector $\boldsymbol{w}$ become $\boldsymbol{w}_{\mathrm{R}} = 1/\cos\xi$ and $\boldsymbol{w}_{\mathrm{I}} = \tan\xi$. Therefore, Eq. (4.73) and Eq. (4.74) are consistent with the results given in Appendix A.2.

4.8 Summary

In this section, we have revealed the geometric properties of the two-state operators. We have also constructed the Bloch sphere representation of the two-state operators. By using the Bloch sphere representation, we have shown the region corresponding to negative "probabilities" explicitly . We found that the negative "probability"

appears when a quantum state traces the path that are opposite to the geodesic (or the shortest) path from the initial state to the final state. Finally, we showed that the strategy of maximizing the weak value can be easily understood in terms of the configuration of the path vectors.

Chapter 5

Two-state vector tomography via spin-exchange interaction

5.1 Introduction

In this chapter, we consider the weak measurements in qubit systems [55, 53, 56] and propose a method to measure the weak value of a spin component along an arbitrary direction using a single interaction. We initially use spin-exchange interaction for this purpose, but subsequently, demonstrate that a large class of interactions can be used in the same manner. The measurement of an arbitrary spin weak value enables spin-state tomography. The aim of this chapter is to establish a method of performing state tomography of pre- and post-selected ensembles by a single interaction.

5.2 Weak values in qubit systems

The state of the pre- and post-selected ensemble is fully described by the two-state operator

$$\hat{W} = \frac{|\psi_{\rm i}\rangle\langle\psi_{\rm f}|}{\langle\psi_{\rm f}|\psi_{\rm i}\rangle}. \tag{5.1}$$

The weak value of an observable $\hat{A}$ can be calculated by using $\hat{W}$ as

$$\langle\hat{A}\rangle_{\rm w} = {\rm tr}(\hat{W}\hat{A}). \tag{5.2}$$

For a qubit system, $\hat{W}$ is decomposed by the Pauli operators $\hat{\boldsymbol{\sigma}} = (\hat{\sigma}_x, \hat{\sigma}_y, \hat{\sigma}_z)^{\rm T}$ as

$$\hat{W} = \frac{1}{2}(\hat{I} + \boldsymbol{w}\cdot\hat{\boldsymbol{\sigma}}), \tag{5.3}$$

where $\hat{I}$ is the identity operator and $\boldsymbol{w}$ is a complex vector in $\mathbb{C}^3$. The vector $\boldsymbol{w}$ is known as the weak vector [57, 7]. Its components are weak values for the Pauli operators,

$$\boldsymbol{w} = \langle \hat{\boldsymbol{\sigma}} \rangle_{\mathrm{w}}. \tag{5.4}$$

We define the real and imaginary parts of weak vector $\boldsymbol{w}$ as $\boldsymbol{w}^{\mathrm{R}}$ and $\boldsymbol{w}^{\mathrm{I}}$, respectively, so that $\boldsymbol{w} = \boldsymbol{w}^{\mathrm{R}} + \mathrm{i}\boldsymbol{w}^{\mathrm{I}}$. A spin component along a unit vector $\boldsymbol{n} = (n_x, n_y, n_z)^{\mathrm{T}}$ is defined as $\hat{\sigma}_{\boldsymbol{n}} := \boldsymbol{n} \cdot \hat{\boldsymbol{\sigma}}$. The weak value for the spin component $\hat{\sigma}_{\boldsymbol{n}}$ is obtained by projecting the weak vector onto $\boldsymbol{n}$:

$$\langle \hat{\sigma}_{\boldsymbol{n}} \rangle_{\mathrm{w}} = \boldsymbol{w} \cdot \boldsymbol{n}. \tag{5.5}$$

5.3 Two-state vector tomography

We present a method to perform tomography of the weak vector $\boldsymbol{w}$ by using spin-exchange interaction. This interaction generates the partial swap between two qubits. For the case of a pre-selected only ensemble, it is understood that all information about the initial state is transferred to the probe state by the spin-exchange interaction. The spin-state tomography using spin-exchange interaction has been demonstrated experimentally [58]. We will show that the spin-exchange interaction transfers information not only about the pre-selected state but also about the post-selected state. Therefore, one can perform tomography of the two-state operator.

Assume that both of measured and probe systems are qubit systems that can be coupled with each other via the spin-exchange interaction. The Hamiltonian of the interaction is proportional to the operator

$$\hat{G} = \hat{\sigma}_x \otimes \hat{\sigma}_x + \hat{\sigma}_y \otimes \hat{\sigma}_y + \hat{\sigma}_z \otimes \hat{\sigma}_z. \tag{5.6}$$

The ensemble is measured between pre- and post-selection. The unitary evolution caused by this interaction is expressed as $U(\theta) = \exp(-\mathrm{i}\theta\hat{G})$, where θ characterizes the strength of the measurements. The conditional evolution of the probe for a given pre- and post-selected ensemble is described by the operator

$$\begin{aligned} \hat{V}(\theta) &= \langle \psi_{\mathrm{f}} | \hat{U}(\theta) | \psi_{\mathrm{i}} \rangle \\ &= \langle \psi_{\mathrm{f}} | \psi_{\mathrm{i}} \rangle (\hat{I} - \mathrm{i}\theta \hat{G}_{\mathrm{w}}) + O(\theta^2), \end{aligned} \tag{5.7}$$

where

$$\hat{G}_{\mathrm{w}} := \mathrm{tr}_{\mathrm{S}}(\hat{W}\hat{G}) = \boldsymbol{w} \cdot \hat{\boldsymbol{\sigma}} = \hat{\sigma}_{\boldsymbol{w}} \tag{5.8}$$

acts on the probe system. Here tr_{S} is the partial trace over the measured system. The operator $\hat{G}_{\mathrm{w}}$ generates the evolution of the probe states. All information about

$\boldsymbol{w}$ is stored in $\hat{G}_{\rm w}$. Denote the initial probe state as $\hat{\rho}_{\rm i}$ and the unnormalized final probe state as $\hat{\rho}_{\rm f} = \hat{V}(\theta)\hat{\rho}_{\rm i}\hat{V}(\theta)^\dagger$. Expanding $\hat{\rho}_{\rm f}$ to first order in θ, we obtain

$$\hat{\rho}_{\rm f} = |\langle\psi_{\rm f}|\psi_{\rm i}\rangle|^2 \left[\hat{\rho}_{\rm i} - {\rm i}\theta(\hat{G}_{\rm w}\hat{\rho}_{\rm i} - \hat{\rho}_{\rm i}\hat{G}_{\rm w}^\dagger)\right]. \tag{5.9}$$

Hereafter, only terms through first order are retained. Define the expectation value of a probe observable $\hat{M}$ with respect to the initial and final states as $\langle\hat{M}\rangle_{\rm i} := {\rm tr}(\hat{\rho}_{\rm i}\hat{M})/{\rm tr}\hat{\rho}_{\rm i}$ and $\langle\hat{M}\rangle_{\rm f} := {\rm tr}(\hat{\rho}_{\rm f}\hat{M})/{\rm tr}\hat{\rho}_{\rm f}$, respectively. The unnormalized expectation value of the probe observable $\hat{M}$ for the final state is

$${\rm tr}(\hat{\rho}_{\rm f}\hat{M}) = |\langle\psi_{\rm f}|\psi_{\rm i}\rangle|^2 \left(\langle\hat{M}\rangle_{\rm i} + 2\theta\,{\rm Im}\langle\hat{M}\hat{G}_{\rm w}\rangle_{\rm i}\right). \tag{5.10}$$

Define the shift operator for $\hat{M}$ as $\delta_{\rm i}\hat{M} := \hat{M} - \langle\hat{M}\rangle_{\rm i}$. The normalized readout is given by

$$\begin{aligned}\langle\delta_{\rm i}\hat{M}\rangle_{\rm f} &= 2\theta\,{\rm Im}\langle\delta_{\rm i}\hat{M}\hat{G}_{\rm w}\rangle_{\rm i} \\ &= \theta\left[\langle -{\rm i}[\hat{M}, \hat{\sigma}_{\boldsymbol{w}^{\rm R}}]\rangle_{\rm i} + \langle\{\delta_{\rm i}\hat{M}, \hat{\sigma}_{\boldsymbol{w}^{\rm I}}\}\rangle_{\rm i}\right].\end{aligned} \tag{5.11}$$

The initial probe state is represented as $\hat{\rho}_{\rm i} = (1/2)(\hat{I} + \boldsymbol{r}\cdot\hat{\boldsymbol{\sigma}})$ using the Bloch vector $\boldsymbol{r}$. Recalling the commutation and anticommutation relations: $[\hat{\sigma}_{\boldsymbol{a}}, \hat{\sigma}_{\boldsymbol{b}}] = 2{\rm i}(\boldsymbol{a}\times\boldsymbol{b})\cdot\hat{\boldsymbol{\sigma}}$ and $\{\hat{\sigma}_{\boldsymbol{a}}, \hat{\sigma}_{\boldsymbol{b}}\} = 2(\boldsymbol{a}\cdot\boldsymbol{b})\hat{I}$, the average shift of probe observable $\hat{M} = \hat{\sigma}_{\boldsymbol{n}}$ is

$$\langle\delta_{\rm i}\hat{\sigma}_{\boldsymbol{n}}\rangle_{\rm f} = 2\theta\left[\boldsymbol{w}^{\rm R}\cdot(\boldsymbol{r}\times\boldsymbol{n}) + \boldsymbol{w}^{\rm I}\cdot(\boldsymbol{n} - (\boldsymbol{n}\cdot\boldsymbol{r})\boldsymbol{r})\right]. \tag{5.12}$$

Let $\boldsymbol{w} = (w_x, w_y, w_z)^{\rm T}$. To measure w_y and w_z, we use two initial probe states $|x^+\rangle$ and $|x^-\rangle$ corresponding to $+1$ and -1 eigenstates of operator $\hat{\sigma}_x$, respectively. In these cases, the average readouts for measurements of $\hat{\sigma}_y$ and $\hat{\sigma}_z$ are

$$\langle\hat{\sigma}_y\rangle_{\rm f}^{x+} = 2\theta(w_z^{\rm R} + w_y^{\rm I}), \tag{5.13}$$
$$\langle\hat{\sigma}_y\rangle_{\rm f}^{x-} = 2\theta(-w_z^{\rm R} + w_y^{\rm I}), \tag{5.14}$$
$$\langle\hat{\sigma}_z\rangle_{\rm f}^{x+} = 2\theta(-w_y^{\rm R} + w_z^{\rm I}), \tag{5.15}$$
$$\langle\hat{\sigma}_z\rangle_{\rm f}^{x-} = 2\theta(w_y^{\rm R} + w_z^{\rm I}), \tag{5.16}$$

where the superscripts $x+$ and $x-$ represent the states $|x^+\rangle$ and $|x^-\rangle$, respectively. The evolution of the probe states generated by the real and imaginary parts of the weak values is sketched in Fig. 5.1. Adding and subtracting Eqs. (5.13)–(5.16), the y and z components of weak vector can be obtained as

$$\langle\hat{\sigma}_y\rangle_{\rm f}^{x+} - \langle\hat{\sigma}_y\rangle_{\rm f}^{x-} = 4\theta w_z^{\rm R}, \tag{5.17}$$
$$\langle\hat{\sigma}_y\rangle_{\rm f}^{x+} + \langle\hat{\sigma}_y\rangle_{\rm f}^{x-} = 4\theta w_y^{\rm I}, \tag{5.18}$$
$$\langle\hat{\sigma}_z\rangle_{\rm f}^{x+} - \langle\hat{\sigma}_z\rangle_{\rm f}^{x-} = -4\theta w_y^{\rm R}, \tag{5.19}$$
$$\langle\hat{\sigma}_z\rangle_{\rm f}^{x+} + \langle\hat{\sigma}_z\rangle_{\rm f}^{x-} = 4\theta w_z^{\rm I}. \tag{5.20}$$

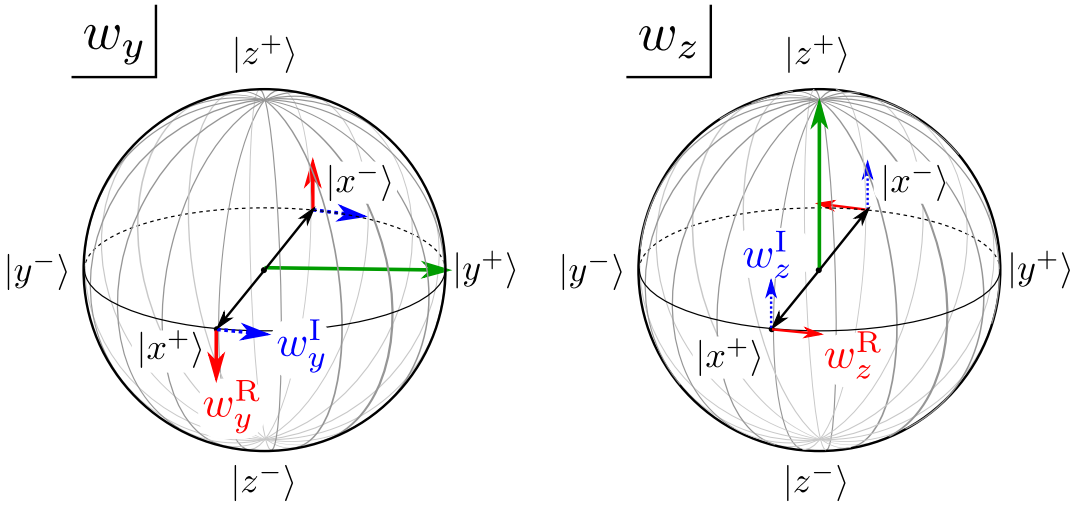

Figure 5.1: The evolution of the probe states induced by the weak values $w_y = \langle\hat{\sigma}_y\rangle_{\mathrm{w}}$ and $w_z = \langle\hat{\sigma}_z\rangle_{\mathrm{w}}$. The real part of the weak values shift the two initial states $|x^+\rangle$ and $|x^-\rangle$ in opposite directions. In contrast, the imaginary parts of the weak values shift those state in same direction. Thus we can decompose the contribution from the real and imaginary parts of the weak values by using two orthogonal states as initial probes.

The procedure used to decompose the real and imaginary parts of weak values is the same as that used to decompose the effects of optical Kerr rotation and circular dichroism in spin-state tomography [59]. The weak value of a spin component along an arbitrary direction can be extracted by using appropriate setups for the probe. For example, the value of w_x can be found by using $|y^+\rangle$ and $|y^-\rangle$ as initial probe states and measuring the observables $\hat{\sigma}_z$ and $\hat{\sigma}_x$.

Note that the measurement of the imaginary parts is simplified by using a completely mixed probe state. For such a state, or for $\boldsymbol{r} = \boldsymbol{0}$, Eq. (5.12) gives

$$\langle\hat{\sigma}_{\boldsymbol{n}}\rangle_{\mathrm{f}} = 2\theta\boldsymbol{w}^{\mathrm{I}} \cdot \boldsymbol{n}. \tag{5.21}$$

Thus, we can obtain the imaginary part of a weak value, $\mathrm{Im}\langle\sigma_{\boldsymbol{n}}\rangle_{\mathrm{w}} = \boldsymbol{w}^{\mathrm{I}} \cdot \boldsymbol{n}$, in a single experimental setup.

5.4 Optical implementation

Next we propose a simple optical setup that demonstrates the two-state vector tomography. The path and polarization of a photon serve as the measured and probe systems, respectively. The eigenstates of the generator $\hat{G}$ of the exchange

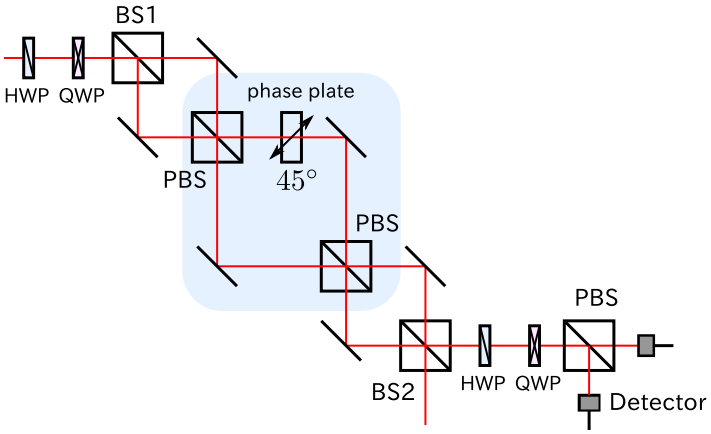

Figure 5.2: Experimental setup for two-state vector tomography. Two beam splitters (BS1 and BS2) are used for pre- and post-selection of the path. The interferometer (shaded region) composed of two polarizing beam splitters (PBSs) and phase plate realizes the exchange interaction. The two-state vector of photon path is estimated by polarization measurements. The first pair of a half-wave plate (HWP) and a quarter-wave plate (QWP) is used to prepare the initial probe state. The second pair of a HWP and a QWP is used to change the measurement basis.

interaction are the four Bell states,

$$|\beta_{ab}\rangle := \frac{|0,b\rangle + (-1)^a|1,\bar{b}\rangle}{\sqrt{2}} \quad (a,b=0,1), \tag{5.22}$$

where $\bar{b}$ is the negation of b and $|a,b\rangle$ are the computational basis states. The state $|\beta_{11}\rangle = (|0,1\rangle - |1,0\rangle)/\sqrt{2}$ belongs to eigenvalue -3 and the other three states belong to eigenvalue 1. Therefore, the exchange interaction can be implemented by shifting the phase of $|\beta_{11}\rangle$. Let $\hat{B}$ denote the unitary operator generating the Bell states from the computational basis states, i.e., $|\beta_{xy}\rangle = \hat{B}|x,y\rangle$. Define the phase shift operator as

$$\hat{O}_\theta := |0\rangle\langle 0| \otimes \hat{I} + |1\rangle\langle 1| \otimes \mathrm{e}^{\mathrm{i}\theta|1\rangle\langle 1|}, \tag{5.23}$$

such that the exchange interaction is realized up to an overall phase factor by

$$\hat{U}(\theta) = \hat{B}\hat{O}_{4\theta}\hat{B}^\dagger = \mathrm{e}^{\mathrm{i}\theta}\exp(-\mathrm{i}\theta\hat{G}). \tag{5.24}$$

Let $\hat{C}$ represent a controlled-NOT gate whose target qubit is measured qubit and let $\hat{H}$ represent an Hadamard gate. Then $\hat{B}$ can be expressed as $\hat{B} = \hat{C}(\hat{I}\otimes\hat{H})$. Therefore, we have

$$\hat{U}(\theta) = \hat{C}(\hat{I}\otimes\hat{H})\hat{O}_{4\theta}(\hat{I}\otimes\hat{H})\hat{C} = \hat{C}\hat{D}_{4\theta}\hat{C}, \tag{5.25}$$

with $\hat{D}_{4\theta} := (\hat{I} \otimes \hat{H})\hat{O}_{4\theta}(\hat{I} \otimes \hat{H})$. The operator $\hat{D}_{4\theta}$ is explicitly

$$\hat{D}_{4\theta} = |0\rangle\langle 0| \otimes \hat{I} + |1\rangle\langle 1| \otimes \mathrm{e}^{4\mathrm{i}\theta|-\rangle\langle -|}. \tag{5.26}$$

where $|-\rangle = (|0\rangle - |1\rangle)/\sqrt{2}$. In an optical setup, $\hat{C}$ can be implemented by a polarizing beam splitter (PBS) and $\hat{D}_{4\theta}$ can be implemented by inserting a phase plate with optical axis at 45° into one of the paths. Figure 5.2 shows the setup for two-state vector tomography with respect to photon path states. The first and second beam splitters (BS1 and BS2) pre-select and post-select the path states, respectively. The interferometer, composed of two PBSs and a phase plate, functions as the spin-exchange interaction. A half-wave plate (HWP) and a quarter-wave plate (QWP) before BS1 prepare the initial probe states, whereas those after BS2 change the measurement basis. To perform two-state vector tomography, we first prepare horizontally and vertically polarized photons and measure the polarization of the output photons in the diagonal/anti-diagonal polarization basis and in the left/right circular polarization basis. Adding and subtracting the results of these measurements as shown in Eqs. (5.17)–(5.20), we obtain the values of w_y and w_z. Similarly, preparing diagonally and anti-diagonally polarized photons and measuring the output polarization in the left/right circular polarization basis and the horizontal/vertical polarization basis, we can extract the value of w_x.

5.5 Generalization

We show that the form of the interaction (5.6) used in our method can be generalized. A general expression for the generator is

$$\hat{G} = \sum_{k,l\in\{x,y,z\}} g_{kl}\, \hat{\sigma}_k \otimes \hat{\sigma}_l, \tag{5.27}$$

where g_{kl} are complex numbers. We denote a matrix representing the coupling coefficients as $\boldsymbol{G} := [g_{kl}]$. For the general form of $\hat{G}$, the generator of the evolution of the probe is

$$\hat{G}_{\mathrm{w}} = \sum_{k,l\in\{x,y,z\}} g_{kl} w_k \hat{\sigma}_l = (\boldsymbol{G}^{\mathrm{T}}\boldsymbol{w}) \cdot \hat{\boldsymbol{\sigma}} = \hat{\sigma}_{\boldsymbol{G}^{\mathrm{T}}\boldsymbol{w}}. \tag{5.28}$$

Hence, we can extract vector $\boldsymbol{G}^{\mathrm{T}}\boldsymbol{w}$ in the same manner as the spin-exchange interaction. We thereby obtain $\boldsymbol{w}$ as long as $\boldsymbol{G}^{\mathrm{T}}$ is invertible.

5.6 Summary

We have developed a method to measure an arbitrary spin weak value by a spin-exchange interaction, enabling two-state vector tomography. The method can be generalized to various types of interaction. We have also proposed an optical setup to demonstrate two-state vector tomography of photon path states. Since the spin exchange interaction between particles has been demonstrated in quantum systems in two–polarization qubits [60] and spin-polarization qubits [58], our methods can be applied to various quantum systems.

Chapter 6

Weak measurements with completely mixed states

6.1 Introduction

The precision measurement is one of the primary applications of weak measurements. It is known that the weak value of an observable can be very large when the pre- and post-selected states are nearly orthogonal. Potentially large weak values hold out the possibility of "amplifying" the effect of weak interactions by appropriately designing the pre- and post-selected ensemble. The "amplification" scheme using pre- and post-selection is known as the weak-value amplification. In 2008, Hosten and Kwiat demonstrated the usefulness of the weak-value amplification by observing the spin Hall effect of light via weak measurements [15]. Inspired by this experiment, the weak-value amplification has been applied to various precision measurements including beam deflection measurements [16, 17, 18], frequency measurements [19], and measurements of the plasmonic spin Hall effect [20].

Measuring the effects of feeble interactions requires performing many runs of an experiment. The post-selection in the weak-value amplification is designed to extract only the subensemble that has a high contribution to the signal; the rest of the pre-selected ensemble is discarded. The signal of weak measurements is enhanced when post-selection succeeds, but the success probability decreases for larger enhancement factors. Consequently, weak measurements are ultimately limited by the standard quantum limit. Nevertheless, weak measurements are known to improve the signal-to-noise ratio (SNR) of the experiments that are subject to noise, as shown in Sec. 2.3.4. Whether the SNR can be improved depends on the noise characteristics. We assume that the dominant noise is proportional to N^{α}, where N denotes the total number of experimental runs and α is determined by factors

such as the noise statistics and the measurement method. For $\alpha > 1/2$, weak measurements produce a net gain in the SNR by a factor of $\mathcal{P}(\mathrm{f}|\mathrm{i})^{1/2-\alpha}$, where $\mathcal{P}(\mathrm{f}|\mathrm{i})$ is the success probability of the post-selection [17]. More detailed analyses have been given for specific noise such as noise in optical experiments [36, 61] and correlated noise [37], both of which correspond to the case $\alpha = 1$. Since practical experiments can have multiple noise sources that have different values of α, weak values should be designed to suit the individual experiments [17].

The weak value is generally a complex number. Its real and imaginary parts can be measured using the respective settings of the probe system. There are thus two possibilities when designing a weak-value experiment. Our interest is whether there are any practical difference between these two schemes when applying weak measurements to precision measurements. We show that the weak-value amplification using the imaginary parts of weak values are advantageous when the probe state for weak measurements becomes mixed.

There are some studies investigating the weak measurements with mixed probe states. Johansen [62] studied weak measurements of the real part of the weak value with mixed probe states. He theoretically showed that weak measurements with many mixed states provide the same amplification effects as pure states. Although Johansen's results are valid under first order calculation, Cho *et al.* [63] showed both theoretically and experimentally that substantial decoherence degrades the amplification effect.

In contrast to the real part of the weak value, Kedem showed that weak measurements of the imaginary part of the weak value are robust to some kinds of noise in the initial probe states [64]. This implies that a mixed, or noisy, probe state can be used for weak-value amplification. As such an experiment, interferometric phase estimation via weak measurements with white light has been proposed [65].

The first aim of this chapter is to provide a unified view of weak measurements with mixed probe states, and hence clarify the kinds of noise weak measurements can tolerate. We demonstrate the possibility of weak measurements with completely mixed probe states. It turns out that the completely mixed probe state has several advantageous properties for precision measurements. The second aim of this chapter is to experimentally demonstrate weak measurements with completely mixed probe states.

The rest of the chapter is organized as follows. In Sec. 6.2, we describe weak measurements with mixed probe states by focusing mainly on weak measurements of the imaginary pars of weak values. We also consider the robustness of the weak measurements to noise in the probe system. In Sec. 6.3, we demonstrate measurement of polarization rotation via unpolarized light, which corresponds to a weak

measurement with a completely mixed probe state. Section 6.4 summarizes the findings of the study.

6.2 Weak measurements with mixed probe states

6.2.1 Fundamentals

Weak measurements involve two quantum systems: the measured and probe systems. The measured system state is pre-selected in an initial state $|\psi_{\rm i}\rangle$ and post-selected in a final state $|\psi_{\rm f}\rangle$. The ensemble is measured between pre- and post-selections via the following unitary evolution:

$$\hat{U}(\theta) = \exp(-{\rm i}\theta \hat{A} \otimes \hat{K}), \tag{6.1}$$

where $\hat{A}$ and $\hat{K}$ are respectively observables of the measured and probe systems and θ represents the strength of measurements. The effective evolution of the probe system for the given pre- and post-selected ensemble is described by

$$\hat{V}_{\rm eff}(\theta) = \exp(-{\rm i}\theta \langle \hat{A} \rangle_{\rm w} \hat{K}) + O(\theta^2), \tag{6.2}$$

which is derived from $\hat{U}(\theta)$ as

$$\langle \psi_{\rm f}|\hat{U}(\theta)|\psi_{\rm i}\rangle = {\rm e}^{{\rm i}\arg\langle\psi_{\rm f}|\psi_{\rm i}\rangle}\sqrt{\mathcal{P}({\rm f}|{\rm i})}\hat{V}_{\rm eff}(\theta), \tag{6.3}$$

where $\mathcal{P}({\rm f}|{\rm i}) := |\langle\psi_{\rm f}|\psi_{\rm i}\rangle|^2$ represents the success probability of post-selection. Figure 6.1 shows the effective evolution of a qubit probe with $\hat{K} = \hat{Z}$, where is the Pauli Z operator. The imaginary part of the weak value $\langle \hat{A} \rangle_{\rm w}$ contributes to the non-unitary evolution and directly changes the probability distribution of $\hat{K}$, while the real part contributes to the relative phase change of the probe states.

We prepare the probe state in a mixed state $\hat{\sigma}_{\rm i}$. The final state of the probe is given by $\hat{\sigma}_{\rm f}(\theta) = \mathcal{P}({\rm f}|{\rm i})\hat{V}_{\rm eff}(\theta)\hat{\sigma}_{\rm i}\hat{V}_{\rm eff}(\theta)^\dagger$. We denote the initial and final expectation values of a probe observable $\hat{M}$ by $\langle\hat{M}\rangle_{\rm i} := {\rm tr}(\hat{\sigma}_{\rm i}\hat{M})/{\rm tr}\hat{\sigma}_{\rm i}$ and $\langle\hat{M}\rangle_{\rm f} := {\rm tr}[\hat{\sigma}_{\rm f}(\theta)\hat{M}]/{\rm tr}\hat{\sigma}_{\rm f}(\theta)$, respectively. We also define the shift operators for $\hat{M}$ as $\delta_{\rm i}\hat{M} := \hat{M} - \langle\hat{M}\rangle_{\rm i}$ and $\delta_{\rm f}\hat{M} := \hat{M} - \langle\hat{M}\rangle_{\rm f}$. The shift of the probe observable $\hat{M}$ can be derived as

$$\langle\delta_{\rm i}\hat{M}\rangle_{\rm f} = \theta\,{\rm Re}\langle\hat{A}\rangle_{\rm w}\langle -{\rm i}[\hat{M},\hat{K}]\rangle_{\rm i} + \theta\,{\rm Im}\langle\hat{A}\rangle_{\rm w}\langle\{\delta_{\rm i}\hat{M},\delta_{\rm i}\hat{K}\}\rangle_{\rm i} + O(\theta^2). \tag{6.4}$$

The factor $\langle\{\delta_{\rm i}\hat{M},\delta_{\rm i}\hat{K}\}\rangle_{\rm i}$ represents the correlation between $\hat{K}$ and $\hat{M}$ for the initial probe state. The imaginary part of the weak value affects the probe observable correlated with $\hat{K}$. Especially for $\hat{M} = \hat{K}$,

$$\langle\delta_{\rm i}\hat{K}\rangle_{\rm f} = 2\theta\,{\rm Im}\langle\hat{A}\rangle_{\rm w}\langle(\delta_{\rm i}\hat{K})^2\rangle_{\rm i} + O(\theta^2). \tag{6.5}$$

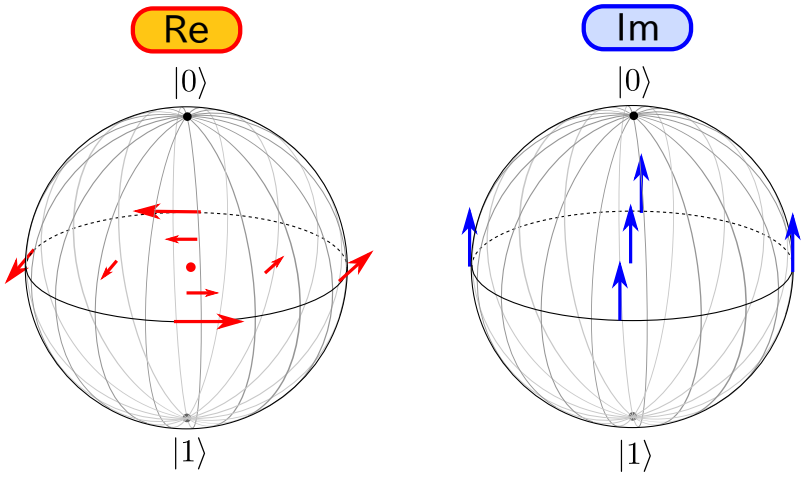

Figure 6.1: Flows of probe states induced by the real and imaginary parts of a weak value, for $\hat{K} = \hat{Z}$ and the initial probe states with $\langle \hat{Z} \rangle = 0$ (on the equatorial plane of the Bloch ball). The lengths of the arrows are proportional to the real and imaginary parts of the weak value. The real and imaginary parts of the weak value respectively contribute to unitary and non-unitary evolutions of the probe states. The unitary flow becomes smaller as the probe state becomes more mixed. In contrast, the non-unitary flow is uniform in the equatorial plane.

We can extract the contribution of only the imaginary part of the weak value by measuring $\hat{K}$. Hereafter, we treat weak measurements with $\hat{M} = \hat{K}$.

We consider the SNR of the measurement. The final variance of $\hat{K}$ is given by $\langle (\delta_{\rm f} \hat{K})^2 \rangle_{\rm f} = \langle (\delta_{\rm i} \hat{K})^2 \rangle_{\rm i} + O(\theta)$ (for details, see Appendix C.1) and the success probability of post-selection is $\mathrm{tr}\hat{\sigma}_{\rm f}(\theta) = \mathcal{P}({\rm f}|{\rm i}) + O(\theta)$. Repeating the measurement N times, the post-selection succeeds $N\mathrm{tr}\sigma_{\rm f}(\theta)$ times on average. Hence, the SNR of the measurement is derived as

$$\begin{aligned} \mathrm{SNR} &= \frac{N\mathrm{tr}\hat{\sigma}_{\rm f}(\theta) \langle \delta_{\rm i} \hat{K} \rangle_{\rm f}}{\sqrt{N\mathrm{tr}\hat{\sigma}_{\rm f}(\theta) \langle (\delta_{\rm f} \hat{K})^2 \rangle_{\rm f}}} \\ &= 2\theta \, \mathrm{Im} \langle \hat{A} \rangle_{\rm w} \sqrt{N \mathcal{P}({\rm f}|{\rm i}) \langle (\delta_{\rm i} \hat{K})^2 \rangle_{\rm i}} + O(\theta^2). \end{aligned} \tag{6.6}$$

The SNR is proportional to the standard deviation $\sqrt{\langle (\delta_{\rm i} \hat{K})^2 \rangle_{\rm i}}$ of the initial probe state; which is independent of the coherence between eigenstates $|k\rangle$ of $\hat{K}$. Therefore, the decoherence of the initial probe state does not hinder the measurement provided the standard deviation is retained. The completely mixed state can also be used as an initial probe state. Especially for a qubit probe, the completely mixed state always achieves the maximum SNR since it has the maximum standard deviation for any $\hat{K}$. This is in contrast to the real part of the weak value, which cannot

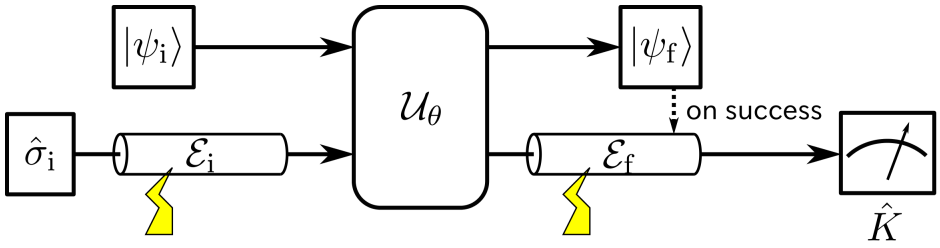

Figure 6.2: Setup for weak measurements with mixed probe states. The probe system is exposed to the noises $\mathcal{E}_\mathrm{i}$ and $\mathcal{E}_\mathrm{f}$ before and after the measurement interaction.

be measured by using the completely mixed state since $-\mathrm{i}[\hat{M}, \hat{K}]$ in Eq. (6.4) is a traceless operator.

6.2.2 Noise tolerance

We describe the noise tolerance of the weak measurements in detail. Figure 6.2 shows a schematic diagram of our setup. Assume that the probe system is exposed to the noises before and after the interaction, which are expressed by the quantum channels $\mathcal{E}_\mathrm{i}$ and $\mathcal{E}_\mathrm{f}$, respectively.

For convenience, we refer to quantum channels $\mathcal{E}$ that satisfy the following condition as phase noise: for an arbitrary eigenstate $|k\rangle$ of $\hat{K}$,

$$\mathcal{E}(|k\rangle\langle k|) = |k\rangle\langle k|. \tag{6.7}$$

This condition is satisfied if and only if the quantum channel has the Kraus representation $\{\hat{E}_n\}$ of the form (for details, see Appendix C.2)

$$\hat{E}_n = \sum_k c_n(k)|k\rangle\langle k|, \tag{6.8}$$

where $c_n(k)$ are complex numbers satisfying $\sum_n |c_n(k)|^2 = 1$. When the probe system is a two-state system and $\hat{K} = \hat{Z}$, it can be easily verified that the phase noise is simply the composition of phase-flip noise and a unitary rotation about the Z axis.

We show that if $\mathcal{E}_\mathrm{i}$ and $\mathcal{E}_\mathrm{f}$ are phase noises the results of weak measurements is unaffected by these noises. We define a map representing the measurement interaction as $\mathcal{U}_\theta(\hat{\rho}) := \hat{U}(\theta)\hat{\rho}\hat{U}(\theta)^\dagger$, where $\hat{\rho}$ is a state of the whole system. Assuming that $\mathcal{E}$ is phase noise, Eq. (6.8) indicates that $\mathcal{E}$ has the following two properties:

$$(\mathcal{I} \otimes \mathcal{E}) \circ \mathcal{U}_\theta = \mathcal{U}_\theta \circ (\mathcal{I} \otimes \mathcal{E}), \tag{6.9}$$

$$\langle k|\mathcal{E}(\hat{\sigma})|k\rangle = \langle k|\hat{\sigma}|k\rangle, \tag{6.10}$$

where $\mathcal{I}$ is the identity channel for the measured system and $\hat{\sigma}$ is an arbitrary probe state. It directly follows from Eq. (6.7) that the composition of phase noises is also a phase noise. Let $p'_{\mathrm{f}}(k)$ and $p_{\mathrm{f}}(k)$ respectively denote the final probability distributions of the weak measurement with and without noise. Then

$$\begin{aligned} p'_{\mathrm{f}}(k) &= \langle\psi_{\mathrm{f}}|\langle k|(\mathcal{I}\otimes\mathcal{E}_{\mathrm{f}})\circ\mathcal{U}_\theta\circ(\mathcal{I}\otimes\mathcal{E}_{\mathrm{i}})(|\psi_{\mathrm{i}}\rangle\langle\psi_{\mathrm{i}}|\otimes\hat{\sigma}_{\mathrm{i}})|\psi_{\mathrm{f}}\rangle|k\rangle \\ &= \langle\psi_{\mathrm{f}}|\langle k|(\mathcal{I}\otimes\mathcal{E}_{\mathrm{f}}\circ\mathcal{E}_{\mathrm{i}})\circ\mathcal{U}_\theta(|\psi_{\mathrm{i}}\rangle\langle\psi_{\mathrm{i}}|\otimes\hat{\sigma}_{\mathrm{i}})|\psi_{\mathrm{f}}\rangle|k\rangle \\ &= \langle\psi_{\mathrm{f}}|\langle k|\mathcal{U}_\theta(|\psi_{\mathrm{i}}\rangle\langle\psi_{\mathrm{i}}|\otimes\hat{\sigma}_{\mathrm{i}})|\psi_{\mathrm{f}}\rangle|k\rangle = p_{\mathrm{f}}(k). \end{aligned} \tag{6.11}$$

Hence, the results of weak measurements are unaffected by the phase noises $\mathcal{E}_{\mathrm{i}}$ and $\mathcal{E}_{\mathrm{f}}$.

In addition, using the completely mixed probe state has a further advantage in terms of noise tolerance. In fact, any noise described by a unital channel, which maps the identity operator $\hat{I}$ to itself (i.e. $\mathcal{E}_{\mathrm{i}}(\hat{I}) = \hat{I}$) cannot affect the completely mixed state. Therefore, the results of weak measurements will be insensitive to a wider class of noise before the measurement interaction.

The weak measurement of the imaginary part of the weak value seems to be more classical than that of the real part because the probe observable $\hat{K}$ commutes with the measurement interaction. Interestingly, this classicality contributes to robustness against probe noise.

6.3 Experiments

In this section, we experimentally demonstrate weak measurements with completely mixed probe states. Figure 6.3 shows the setup used for our experiments. The measured and probe systems correspond to the path and polarization of a photon, respectively. We used the unpolarized light as a completely mixed probe state, and thereby measured the path-dependent polarization rotation via weak measurements.

6.3.1 Overview

In this section, we describe the overview of the experimental setup shown in Fig 6.3. To generate the unpolarized light, we used a superluminescent diode (SLD), a Glan laser polarizer (GL), and a quartz plate. The SLD output has a sufficiently short coherence time to be depolarized by differential group delay in the quartz plate. The first beam splitter (BS1) pre-selects the path state as

$$|\psi_{\mathrm{i}}\rangle = \frac{1}{\sqrt{2}}(|0\rangle + |1\rangle), \tag{6.12}$$

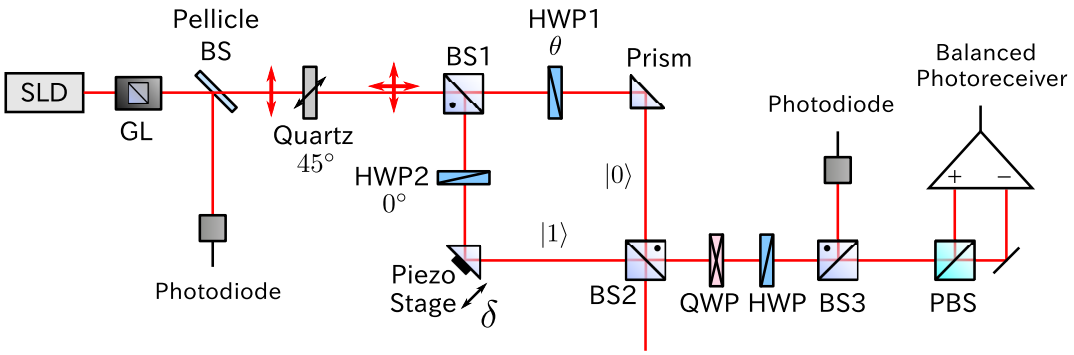

Figure 6.3: Experimental setup for weak measurements of polarization rotation with unpolarized light. The unpolarized light is produced by using a superluminescent diode (SLD), a Glan laser polarizer (GL), and a 5-mm-wide quartz plate. The SLD (QSDM-780-9, Qphotonics) has a center wavelength of 795 nm and a spectral width of 17.3 nm. The spatial mode of the SLD is filtered by a single-mode fiber. The polarization of the output light is projected onto the vertically polarized state by the GL, and then depolarized by the quartz plate. Since the differential group delay in the quartz plate is larger than the coherence time of the light, unpolarized light can be obtained by aligning the optical axis of the quartz plate at 45°. The optical power of the unpolarized light is about 1 mW. The pellicle beam splitter is inserted in between the GL and the quartz plate to monitor the optical power. The measured optical power is used to normalize the experimental results. The unpolarized light is introduced to a Mach–Zehnder interferometer. The prism in the lower path is mounted on a piezo stage. Each arm of the interferometer has a half-wave plate (HWP). The interaction strength between the path and the polarization can be varied by rotating the optical axis θ of the HWP1 in the upper path. The power and polarization of the light are measured at one of the output ports. The quarter-wave plate (QWP) and HWP are adjusted to measure the circularly polarized components of the light.

where $|0\rangle$ and $|1\rangle$ respectively represent the upper and lower path states of the Mach–Zehnder interferometer. Post-selection of the path was realized by observing one of the output ports of BS2. We can change the relative phase δ of the post-selected state $|\psi_{\rm f}\rangle$ by translating the piezo stage in the lower path:

$$|\psi_{\rm f}\rangle = \frac{1}{\sqrt{2}}(|0\rangle + {\rm e}^{{\rm i}\delta}|1\rangle). \tag{6.13}$$

The interaction between the measured and probe systems was implemented by inserting a half-wave plate (HWP) in each arm. The optical axis of the upper HWP was rotated by an angle θ. In practical applications, θ corresponds to an unknown physical parameter to be estimated. Let $\hat{U}_{\rm HWP}(\theta)$ denote the unitary operation caused by the HWP at angle θ. The unitary evolution of the whole system is then given by

$$\begin{aligned}\hat{U}(\theta) &= |0\rangle\langle 0| \otimes \hat{U}_{\rm HWP}(\theta) + |1\rangle\langle 1| \otimes \hat{U}_{\rm HWP}(0) \\ &= \hat{U}_{\rm HWP}(0)\left[|0\rangle\langle 0| \otimes \exp(2{\rm i}\theta\hat{Z}) + |1\rangle\langle 1| \otimes \hat{I}\right],\end{aligned} \tag{6.14}$$

where $\hat{Z}$ is an observable distinguishing right- and left-handed circular polarization. We can eliminate the overall polarization rotation $\hat{U}_{\rm HWP}(0)$ by adjusting the measurement basis for polarization. Therefore, we regard the unitary evolution in the Mach–Zehnder interferometer as

$$\hat{U}(\theta) = \exp\left(2{\rm i}\theta\hat{P}_0 \otimes \hat{Z}\right), \tag{6.15}$$

where we denote the projector onto the upper path state as $\hat{P}_0 := |0\rangle\langle 0|$. The weak value of the upper path operator $\hat{P}_0$ is calculated as

$${\rm Im}\langle\hat{P}_0\rangle_{\rm w} = \frac{1}{2}\tan\left(\frac{\delta}{2}\right), \tag{6.16}$$

which diverges at $\delta = \pi$. Figure 6.4 shows the imaginary part of the weak vector $\boldsymbol{w}$ and the path vector $\boldsymbol{s}_0$ corresponding to the path operator $\hat{P}_0$. The pre- and post-selected states are chosen to maximize the imaginary part of the weak value as shown in Sec. 4.7.

At the output of the interferometer, we measured the success probability of the post-selection and the circular components of the polarization. Recalling that the initial probe state is unpolarized ($\hat{\sigma}_{\rm i} = \hat{I}/2$), the expected results are given by

$${\rm tr}\hat{\sigma}_{\rm f}(\theta) = \frac{1}{2}(1 + \cos\delta\cos(2\theta)), \tag{6.17}$$

$${\rm tr}[\hat{\sigma}_{\rm f}(\theta)\hat{Z}] = -\frac{1}{2}\sin\delta\sin(2\theta). \tag{6.18}$$

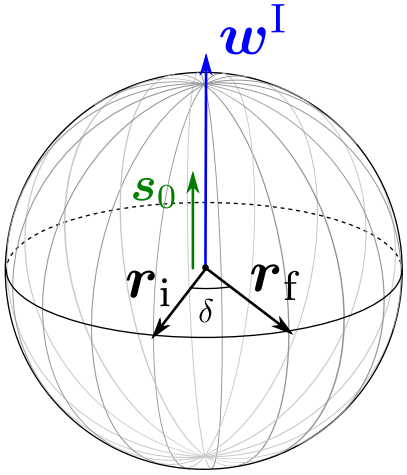

Figure 6.4: The configuration of the weak vector and the path vector.

Thus we can estimate the value of θ from the result of polarization measurements. The details of the derivation of Eqs. (6.17) and (6.18) are shown in Appendix C.3.

The imaginary part of the weak value can be extracted from Eqs. (6.17) and (6.18) since it corresponds to the normalized sensitivity to the parameter θ:

$$\mathrm{Im}\langle \hat{P}_0 \rangle = -\frac{1}{4} \frac{\mathrm{d}}{\mathrm{d}\theta}\bigg|_{\theta=0} \frac{\mathrm{tr}[\hat{\sigma}_{\mathrm{f}}(\theta)\hat{Z}]}{\mathrm{tr}\hat{\sigma}_{\mathrm{f}}(\theta)}. \tag{6.19}$$

6.3.2 Mixed state preparation

We describe the method to prepare the unpolarized light in details. To produce the unpolarized light, we use the superluminescent diode (SLD) as a photon source. This is because the SLD has a wide spectral width, and can be easily depolarized by a differential group delay. We confirmed theoretically and experimentally that the 5-mm-width quartz plate has a sufficient differential group delay to depolarize the light from the SLD.

The SLD (QSDM-780-9, Qphotonics) has a center wavelength of 795 nm and a spectral width of 17.3 nm. The spread of the frequency spectrum is calculated from the relation $f = c/\lambda$ as

$$\Delta f = \frac{c\Delta\lambda}{\lambda^2} = 8.21 \times 10^{12}\,\mathrm{Hz}. \tag{6.20}$$

Thus The coherence time of SLD is approximately $\tau_{\mathrm{c}} \simeq 1/\Delta f = 122\,\mathrm{fs}$.

We next calculate the differential group delay induced by the quartz plate. The group velocity v_{g} in a medium can be calculated by using the wavelength dependence of the refractive index as

$$v_{\mathrm{g}} = \frac{c}{n - \lambda(\partial n/\partial\lambda)}. \tag{6.21}$$

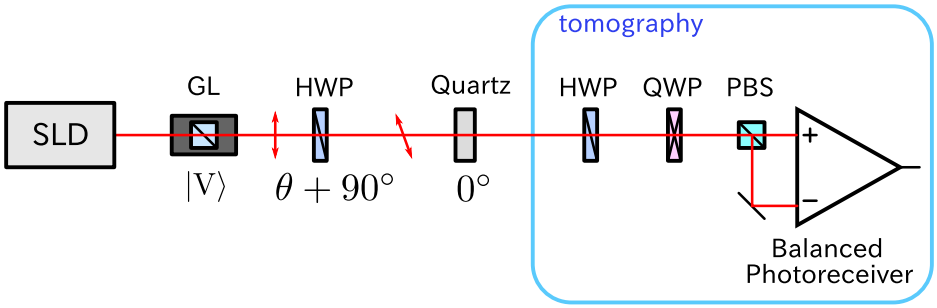

Figure 6.5: Experimental setup for polarization state tomography. The output of the SLD is projected onto the vertical polarization by Glan laser polarizer. The polarization is rotated by the HWP at an angle $\theta + 90°$. The output polarization is supposed to be linear polarization at the angle

The wavelength dependence of the refractive index is given by the Sellmeier equation [66]. By using this, the differential group delay induced by 5-mm-width quartz plate can be calculated as 158 fs. Since the group delay of 158 fs is longer than the coherence time of 122 fs, the two eigen polarization is separated temporally. This temporal separation leads to depolarization.

We also confirmed experimentally that the completely mixed state was prepared. To this purpose, we performed polarization state tomography. The experimental setup is shown in Fig. 6.5. The light is first prepared in the vertical polarization by the GL. The subsequent HWP rotates the polarization by the angle 2θ from the vertical direction. The state of polarization after the HWP is written as

$$|\psi\rangle = -\sin(2\theta)|\mathrm{H}\rangle + \cos(2\theta)|\mathrm{V}\rangle. \tag{6.22}$$

Finally, the quartz plate destroys the coherence between $|\mathrm{H}\rangle$ and $|\mathrm{V}\rangle$. The final state is expressed by the density operator,

$$\hat{\rho} = \sin^2(2\theta)|\mathrm{H}\rangle\langle\mathrm{H}| + \cos^2(2\theta)|\mathrm{V}\rangle\langle\mathrm{V}|. \tag{6.23}$$

The expected results for polarization measurements are thus

$$\langle\hat{X}\rangle = -\cos(4\theta), \tag{6.24}$$

$$\langle\hat{Y}\rangle = \langle\hat{Z}\rangle = 0. \tag{6.25}$$

We can measure the Pauli operators $\hat{X}$, $\hat{Y}$, and $\hat{Z}$ by setting the angles of HWP and QWP according to Table 6.1. The results of measurements are shown in Fig. 6.6. The experimental results agree well with the theoretical curves. The completely mixed state was obtained at $\theta = 22.5°$. At $\theta = 22.5°$, the incident

Table 6.1: The angles of HWP and QWP to measure the Pauli operators.

Measured observable	HWP angle	QWP angle
$\hat{X}$	0°	0°
$\hat{Y}$	22.5°	0°
$\hat{Z}$	0°	135°

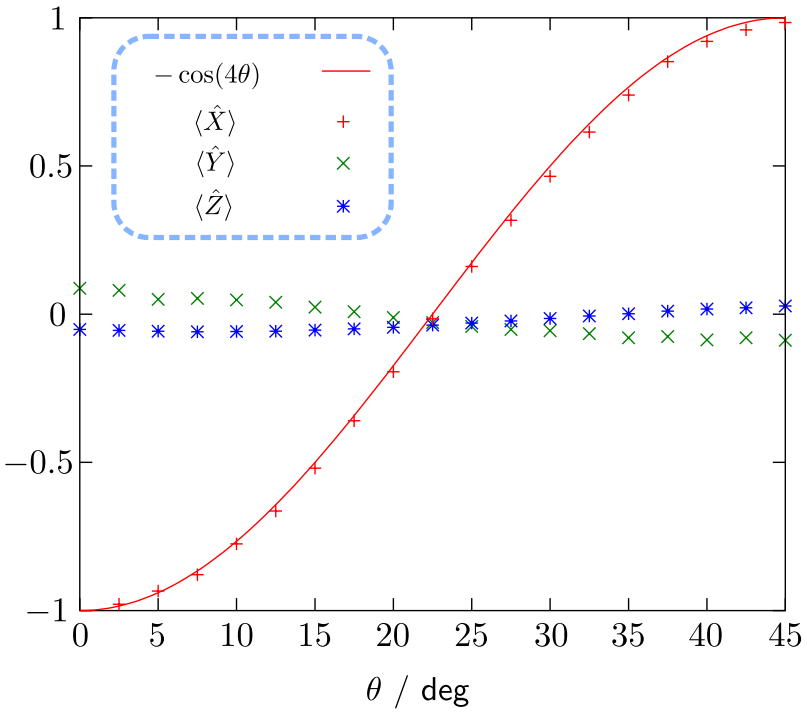

Figure 6.6: Results of the polarization measurements.

light to the quartz plate is linearly polarized at 45°. In Fig. 6.3, the quartz plate is rotated by 45° to obtain the unpolarized light, instead of preparing the linearly polarized light at 45°.

In our experiments, we used the group delay difference in a quartz plate to depolarize light. We may use a polarization maintaining fiber (PMF) for the same purpose since it also has a group delay difference. The reason why we use a quartz plate is that the pellicle beam splitter in Fig. 6.3 has different transitivity for the horizontal and vertical polarization. When we use a PMF as a depolarizer, we must insert the pellicle beam splitter before the fiber. Since the coupling efficiency of a PMF may fluctuate in time, we could not measure the optical power precisely.

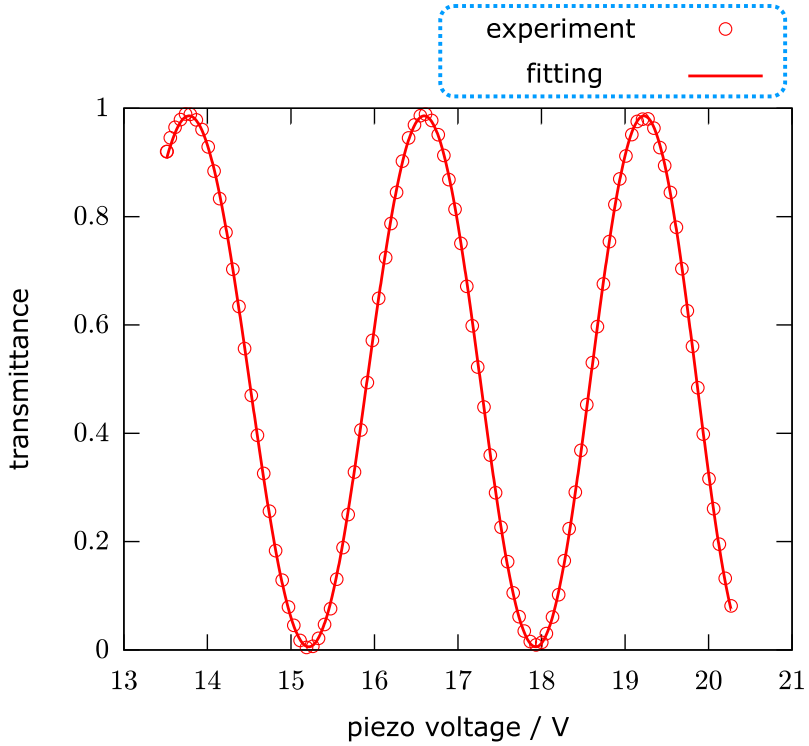

Figure 6.7: The interference in Mach–Zehnder interferometer. The vertical axis is normalized by the total optical power monitored before the interferometer. The experimental data is fitted with a sinusoidal function. Since the displacement by the piezo stage is slightly nonlinear to the applied voltage, we take into account the second order term to fit the data.

6.3.3 Measurement of the path interference

Before the main experiments, we measured interference fringes to evaluate the visibility of interference. The visibility of the interference is related to the completeness of post-selection.

When we measured interference fringes, the angle of HWP1 in Fig. 6.3 was set to $\theta = 0$. Setting the angle of HWP1 to $\theta = 0$ turns off the interaction between the path and polarization. We measured the optical power by the photodiode at the output of the interferometer as changing the voltage applied to the piezo stage.

The measured interference is shown in Fig 6.7. Fitting the results with a sinusoidal function, the visibility of the interference was found to be $\mathcal{V} = 0.989 \pm 0.001$.

6.3.4 Measurement of polarization rotation

In this section, we describe the measurements of polarization rotation with unpolarized light.

Measurement system and measurement method

We used the experimental setup as shown in Fig. 6.3. We also show the details of our control system in Fig. 6.8. The measurement procedure is as follows.

Step1. Increment the displacement of the piezo stage and fix the displacement. This procedure fixes the phase δ of the interferometer.

Step2. Rotate the HWP1. The optical power and circular components of polarization are measured via the photodiodes and the balanced photoreceiver. The angle θ is varied with 0.1° steps.

Step3. Repeat steps 1 and 2 until acquiring the data in the range $0 \leq \delta \leq 2\pi$.

Through these experiments, the displacement of the piezo stage was monitored by a strain gauge and feedback-controlled.

Measurement results

Since the phase δ of interferometer could not directly measured, we first estimated the value of δ in each measurement. Combining the output power at $\theta = 0$ for different positions of the piezo stage, we obtained interference fringes as shown in Fig. 6.9. The value of δ in each measurement was estimated by fitting these interference fringes.

The measurement results are shown in Fig. 6.10 and Fig. 6.11. We show three data with different values of δ. The theoretical curves given by Eq. (6.17) and Eq. (6.18) are depicted as solid lines in Fig. 6.10 and Fig. 6.11. The vertical error bars reflect the deviation of δ caused by the estimation error and the instability of the interferometer. The experimental results are good accordance with theoretical predictions. Figure 6.11 shows that we can estimate the angle θ of HWP1 by measuring the polarization.

6.3.5 Weak values

We can calculate the imaginary part of the weak value from the results of polarization measurements. In fact, the weak value corresponds to the normalized sensitivity

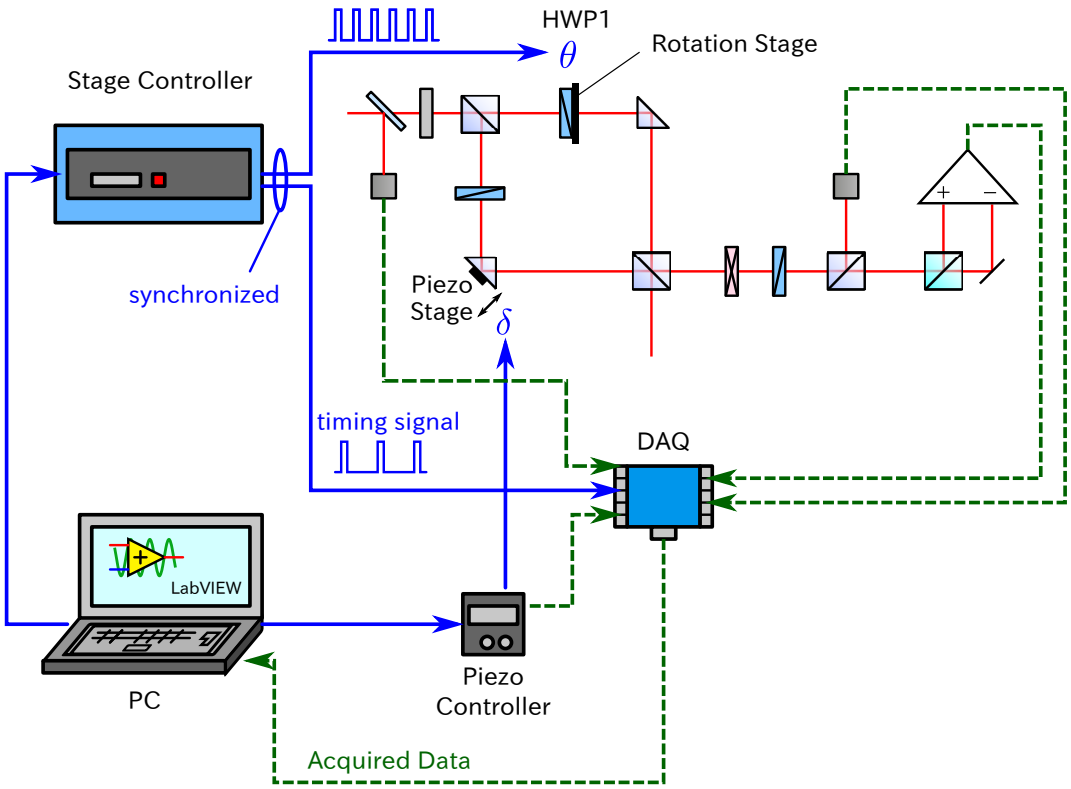

Figure 6.8: Control system. The whole devices are controlled by the personal computer (PC). The experimental date are also acquired by the same PC. The solid blue arrows represent the control signals. The dashed green arrows represent the acquired data. The phase δ of interferometer is determined by the position of the piezo stage, which is controlled via the piezo controller. The HWP1 is mounted on a rotation stage and its angle θ is controlled via the stage controller. The stage controller generates the timing signal synchronized with the rotation of the stage. This signal is sent to the data acquisition system (DAQ). The output of the two photodiodes and the balanced photoreceiver are sampled in synchronization with the timing signal.

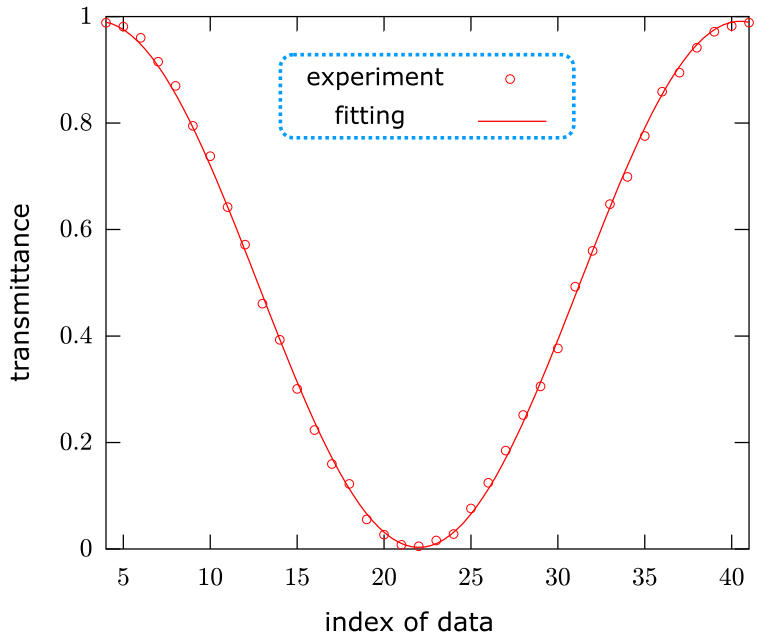

Figure 6.9: Interference fringes measured during the polarization measurements. The horizontal axis represents the indexes of data. Each index corresponds to the different displacement. By fitting the data, we estimated the values of δ.

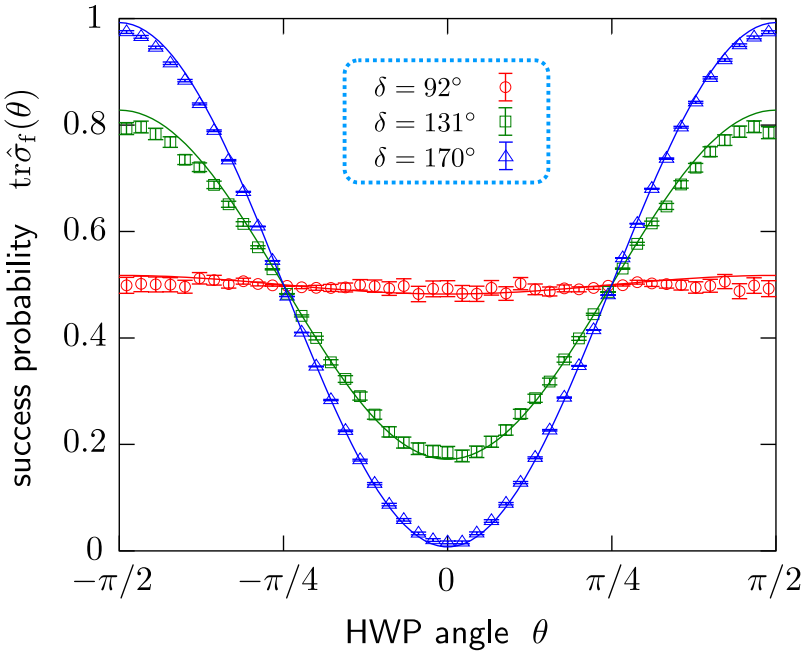

Figure 6.10: Variation of success probability as a function of the HWP angle θ. The solid lines correspond to the theoretical curves given by Eq. (6.17). The vertical error bars reflect the deviation of δ.

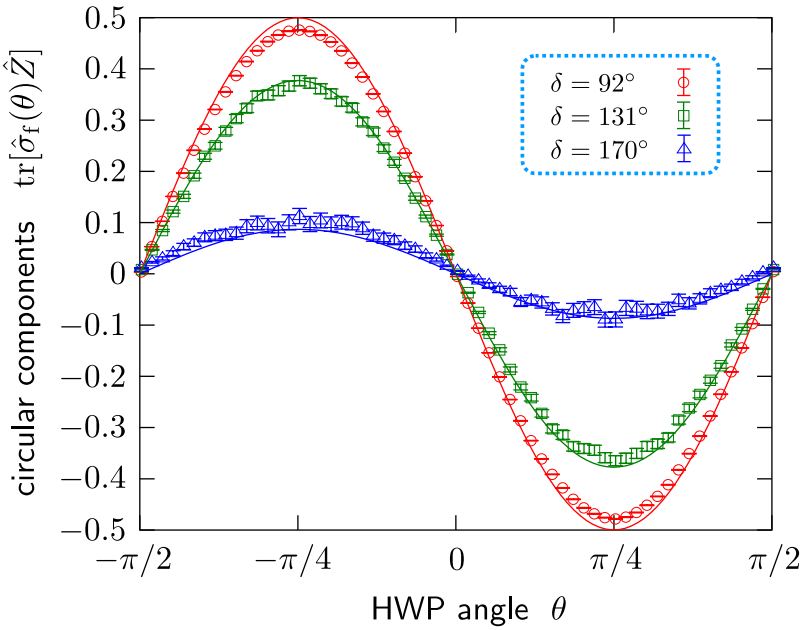

Figure 6.11: Variation of success probability as a function of the HWP angle θ. The solid lines correspond to the theoretical curves given by Eq. (6.18). The vertical error bars reflect the deviation of δ.

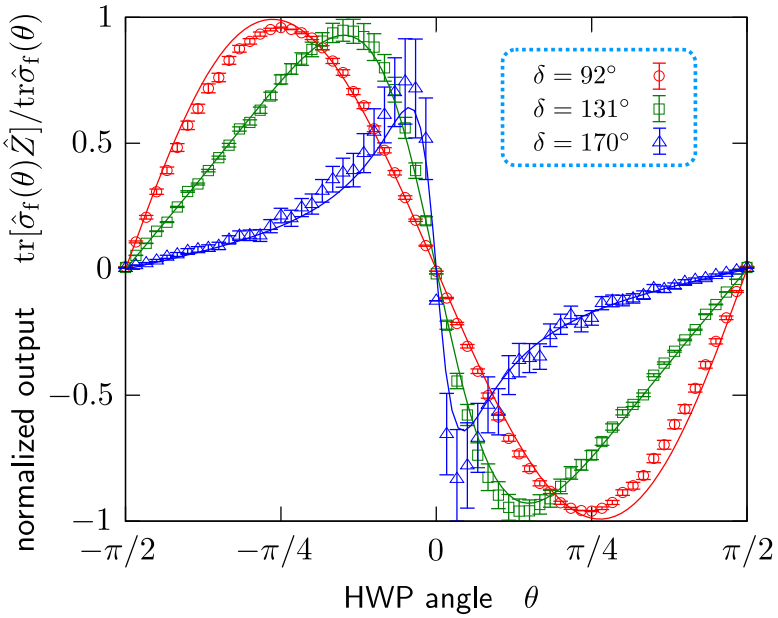

Figure 6.12: Normalized results for polarization measurements as a function of θ. The results of polarization measurements are normalized by the success probability. The solid lines correspond to the theoretical curves. The vertical error bars reflect the deviation of δ.

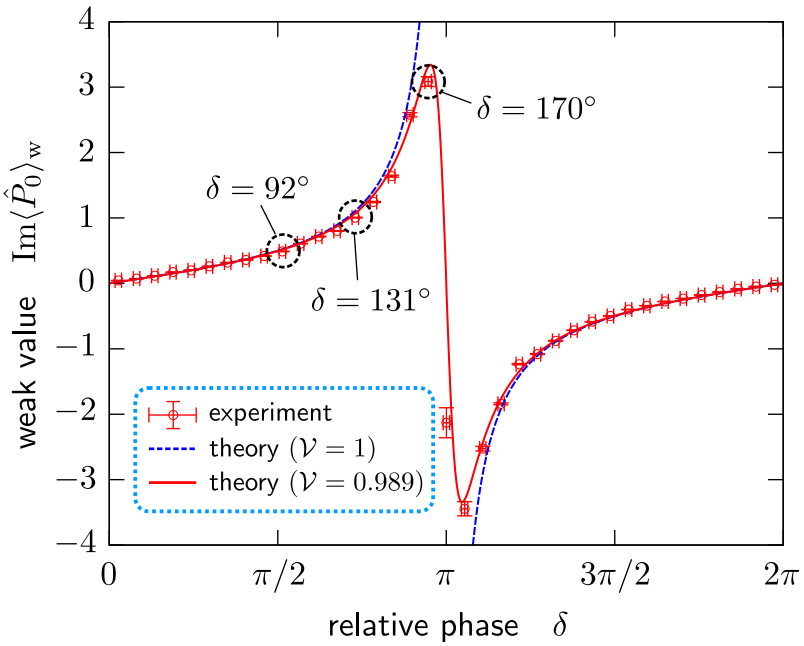

Figure 6.13: Weak values for various post-selected states. The circles represent the experimental data. The dashed blue curve and the solid red curve represent the theoretical curves for $\mathcal{V} = 1$ and $\mathcal{V} = 0.989$, respectively. The vertical error bars represent the standard deviation of the linear regression. The horizontal error bars reflect the deviation of δ.

to the parameter θ as shown in Eq. (6.19). Figure 6.12 shows the normalized results of polarization measurements. The theoretical curves take into account the incompleteness of post-selection. The theoretical curves in Fig. 6.12 are given by Eq.(C.25) of Appendix C.3.

We obtained the gradient at $\theta = 0$ by linearly fitting this normalized results of the polarization measurements in the range $-2^\circ \leq \theta \leq 2^\circ$. Note that the data were acquired at intervals of 0.1° for θ, while the data in Fig. 6.12 are plotted at intervals of 3°. We derived the weak value from the gradient at $\theta = 0$ by using Eq. (6.19). The obtained weak values are shown in Fig. 6.13.

The maximum weak value was $\mathrm{Im}\langle\hat{P}_0\rangle_\mathrm{w} = 3.08 \pm 0.07$. This is not very large because post-selection of the path state was incomplete. The actual post-selected state $\hat{\rho}_\mathrm{f}$ is expressed in terms of the visibility $\mathcal{V}$ for the case when there is no interaction ($\theta = 0$):

$$\hat{\rho}_\mathrm{f} = \mathcal{V}|\psi_\mathrm{f}\rangle\langle\psi_\mathrm{f}| + (1-\mathcal{V})\frac{\hat{I}}{2}. \tag{6.26}$$

The experimentally measured visibility was $\mathcal{V} = 0.989 \pm 0.001$. The weak value for

mixed pre- and post-selected states has been derived by Wu and Mølmer [53] as

$$\langle \hat{A} \rangle_{\mathrm{w}} = \frac{\mathrm{tr}(\hat{\rho}_{\mathrm{f}} \hat{A} \hat{\rho}_{\mathrm{i}})}{\mathrm{tr}(\hat{\rho}_{\mathrm{i}} \hat{\rho}_{\mathrm{f}})}, \tag{6.27}$$

where $\hat{\rho}_{\mathrm{i}}$ and $\hat{\rho}_{\mathrm{f}}$ denote the pre- and post-selected states, respectively. From Eq. (6.27), we can calculate the weak value for incomplete post-selection as

$$\mathrm{Im}\langle \hat{P}_0 \rangle_{\mathrm{w}} = \frac{\mathcal{V} \sin \delta}{2(1 + \mathcal{V} \cos \delta)}. \tag{6.28}$$

When $\mathcal{V} = 1$, this equation is equivalent to Eq. (6.16). The theoretical curve for the measured visibility $\mathcal{V} = 0.989$ agrees well with the experimental data, as shown in Fig. 6.13.

6.4 Summary

We have analyzed weak measurements with mixed probe states and demonstrated the advantages of weak measurements with imaginary weak values, which tolerate phase noise in the probe system. The completely mixed state was found to have some advantageous properties for precision measurements. We also experimentally demonstrated weak measurements with completely mixed probe states by measuring the polarization rotation with unpolarized light. The unpolarized light itself is insensitive to polarization rotation; however, by attaching the path degree of freedom and using a weak measurement, unpolarized light can be used to measure polarization rotation.

Weak measurements with imaginary weak values are useful for designing highly sensitive measurements with poor probe states. Weak measurements have the potential to open up new doors for measurements in practical noisy systems.

6.5 Discussion

Our results show that the completely mixes state can be used to measure the interaction strength via weak measurements of the imaginary part of the weak value. While we use a qubit system as a probe in our experiments, there are some studies about weak measurements with mixed probe states for the case where the probe is a continuous-variable system. Since the treatment of the continuous-variable probe is a little more complicated than the finite-dimensional case, we review the relevant works briefly, and then describe the relation between our studies and these works.

Johansen [62] first treated weak measurements with mixed probe states. He considered weak measurements of the real part of the weak value and showed that the wide variety of mixed probe states can be used for weak measurements. In fact, Eq. (2.74) of Chap. 2 can also be applied for mixed probe states. Rewriting Eq. (2.74),

$$\langle \delta_{\rm i}\hat{x}\rangle_{\rm f} \simeq x_0\,{\rm Re}\langle\hat{A}\rangle_{\rm w} + x_0\,{\rm Im}\langle\hat{A}\rangle_{\rm w}\frac{\langle\{\delta_{\rm i}\hat{x},\delta_{\rm i}\hat{p}\}\rangle_{\rm i}}{\hbar}. \tag{6.29}$$

Interestingly, the position shift due to the real part of the weak value in Eq. (6.29) is independent of the initial state of the probe. This fact results from the canonical commutation relation $-{\rm i}[\hat{x},\hat{p}] = \hbar$ and is particular to the continuous-variable probe. In contrast, for the case of finite-dimensional probes, the operator $-{\rm i}[\hat{M},\hat{K}]$ is always traceless, and the decoherence in the probe decreases the shift due to the real part of the weak value. Equation (6.29) indicates that as long as there are no correlation between the position and the momentum, i.e., $\langle\{\delta_{\rm i}\hat{x},\delta_{\rm i}\hat{p}\}\rangle_{\rm i} = 0$, the shift of the probe is always $x_0\,{\rm Re}\langle\hat{A}\rangle_{\rm w}$. In this sense, Johansen stated that almost an arbitrary probe state can be used for weak measurements.

Equation (6.29) apparently indicates that decoherence of the probe has no obstacle to weak measurements of the real part of weak value. Cho *et al.* [63], however, demonstrated both theoretically and experimentally that the position shift is reduced when the probe is subjected to decoherence in position. Decoherence in position disturbs the momentum of the probe. As a result, the weak-interaction condition $||\hat{A}||x_0\Delta p/\hbar \ll 1$ is violated. Thus we can no longer use Eq. (6.29) for highly mixed states. This is the reason why decoherence in position leads to the decrease of the position shift.

Decoherence in momentum was considered by Kedem [64]. It was showed that decoherence in momentum degrades the SNR for the case of weak measurements of the real part of weak value. Therefore, we cannot use highly mixed probe states for weak measurements of the real part of the weak value.

On the contrast, Kedem [64] also showed that the weak measurements of the imaginary part of the weak values can tolerate for decoherence in momentum. Our result in Sec. 6.2.2 is a generalization of Kedem's result. Our result can also be applied to the continuous-variable probe. Note that our analysis in Sec. 6.2.2 uses no approximation. Thus the weak-interaction condition is never violated under phase noise as long as initial probe state satisfies the weak-interaction condition. Therefore, we can use highly mixed probe state for weak measurements of the imaginary part of weak values.

Finally, it should be noted that there is a similar experiment to ours in the context of quantum computation. The experiment [67] demonstrated deterministic quantum computation with one clean qubit (DQC1) [68]. Since completely mixed

states are insensitive to any unitary evolution, completely mixed states themselves have no computational power. However, additional use of one pure qubit enable us to compute the trace of a unitary operator. DQC1 is known to outperform classical computation.

Similarly, in our setup, unpolarized light itself has no power to detect the polarization rotation. However, attaching the path degree of freedom as a virtually measured system, we can measure the polarization rotation by unpolarized light.

Chapter 7

Conclusion

In this thesis, we have approached the weak measurement by investigating the geometric structures related to pre- and post-selected ensembles. We also analyze the evolution of the probe state geometrically. The geometry enable us to understand how to design the pre- and post-selected ensemble in accordance with purposes. We also performed weak measurements in an optical system, to demonstrate the usefulness of weak measurements in a noisy system. In the following, we summarize the findings of each studies.

In Chapter 3, we investigate the interference effect caused by post-selection in weak measurements. We first presented an analogy between the weak measurement and the quantum eraser. Then we showed that post-selection in both experiments causes the Pancharatnam phase shift in interference patterns. We showed that the Pancharatnam phase induced by the post-selection is the origin of the anomalously large shift in weak measurements.

In Chapter 4, we investigated a geometrical representation of the two-state operator, which characterizes the state of a pre- and post-selected ensemble. We also presented the Bloch sphere representation of the two-state operator. Using this representation, we have studied the properties of the complex probability distributions defined by the weak values of projection operators. The condition for negative weak value was presented by means of geometrical description. We also presented the method to maximize the weak value in terms of the Bloch sphere representation.

In Chapter 5, we proposed a method to perform the tomography of two-state operators. We showed that we can completely determine the two-state operator by using spin-exchange interaction as a measurement interaction. The explicit procedure for reconstructing the two-state operator from the results of weak measurements was presented. We also showed that large class of interactions can be used to perform two-state vector tomography. The optical implementation of two-state

vector tomography was also proposed.

In Chapter 6, we considered weak measurements with noisy probe states. We showed that weak measurements with imaginary weak values can be performed by using completely mixed probe state. We also evaluated the effect of noise on probe system and identify which type of noise weak measurements can tolerate. We next implemented the weak measurements with completely mixed probe states in a optical system. We experimentally demonstrated that the polarization rotation by an optical element can be measured via unpolarized light using the weak measurement scheme.

Appendix A

Appendix for Chapter 2

A.1 A sufficient condition for no correlation between position and momentum

We consider when the position and momentum of a state have no correlation. The condition is given by

$$\langle\{\delta\hat{x}, \delta\hat{p}\}\rangle = 0, \tag{A.1}$$

where $\delta\hat{x} := \hat{x} - \langle x\rangle$ and $\delta\hat{p} := \hat{p} - \langle p\rangle$. We assume that $\langle\hat{x}\rangle\langle\hat{p}\rangle = 0$. Then, Eq. (A.1) turns out to be

$$\langle\{\hat{x}, \hat{p}\}\rangle = 0. \tag{A.2}$$

Let $\phi(x)$ and $\phi(p)$ be the wavefunctions in the position and momentum representations. We have

$$\begin{aligned}\langle\{\hat{x}, \hat{p}\}\rangle &= 2\,\mathrm{Re}\langle\hat{x}\hat{p}\rangle \\ &= 2\hbar\int x\,\mathrm{Im}(\phi(x)^*\phi'(x))\mathrm{d}x \qquad \text{(A.3)} \\ &= -2\hbar\int p\,\mathrm{Im}(\phi(p)^*\phi'(p))\mathrm{d}p. \qquad \text{(A.4)}\end{aligned}$$

If $\phi(x)$ or $\phi(p)$ is a real-valued function, there is no correlation between the position and momentum.

A.2 Maximizing weak value

We consider the problem to maximize the real and imaginary parts of the weak value. We first derive the state that maximize the modulus of the weak value in Sec. A.2.1. It turns out that when the modulus of the weak value is maximized, the

absolute value of the real part of the weak value is also maximized. In Sec. A.2.2, we derive the state that maximize the imaginary part of the weak value.

In Chap. 4.7, we also present a more intuitive way to maximize the real and imaginary parts of the weak value for a fixed success probability.

A.2.1 Maximizing the modulus of weak value

We consider the problem to maximize the modulus of the weak value for a fixed success probability. This problem has been considered in Ref. [54] for the case when $\hat{A}$ is a rank-1 projector. In this section, we derive the maximum weak value for a general observable $\hat{A}$.

The problem is to maximize

$$|\langle \hat{A} \rangle_{\mathrm{w}}|^2 = \frac{|\langle \psi_{\mathrm{f}}|\hat{A}|\psi_{\mathrm{i}}\rangle|^2}{|\langle \psi_{\mathrm{f}}|\psi_{\mathrm{i}}\rangle|^2} \tag{A.5}$$

under a fixed success probability. Since the weak value is gauge-invariant, we may assume that $\langle \psi_{\mathrm{f}}|\psi_{\mathrm{i}}\rangle$ is a positive real number without loss of generality. Assume $\langle \psi_{\mathrm{f}}|\psi_{\mathrm{i}}\rangle = \cos\xi$, where $0 \le \xi \le \pi/2$. The problem is reduced to maximize $|\langle \psi_{\mathrm{f}}|\hat{A}|\psi_{\mathrm{i}}\rangle|^2$ under the constraints $\langle \psi_{\mathrm{i}}|\psi_{\mathrm{i}}\rangle = 1$, $\langle \psi_{\mathrm{f}}|\psi_{\mathrm{f}}\rangle = 1$, and $\langle \psi_{\mathrm{f}}|\psi_{\mathrm{i}}\rangle = \cos\xi$. This problem can be solved by the Lagrange multiplier method. Introduce the Lagrange multipliers λ_1, λ_2, μ, and ν, then define the Lagrange function by

$$\begin{aligned} &F(|\psi_{\mathrm{i}}\rangle, |\psi_{\mathrm{f}}\rangle, \langle\psi_{\mathrm{i}}|, \langle\psi_{\mathrm{f}}|, \lambda_1, \lambda_2, \mu, \nu) \\ &\quad = |\langle \psi_{\mathrm{f}}|\hat{A}|\psi_{\mathrm{i}}\rangle|^2 - 2\lambda_1[\mathrm{Re}\langle\psi_{\mathrm{f}}|\psi_{\mathrm{i}}\rangle - \cos\xi] - 2\lambda_2\,\mathrm{Im}\langle\psi_{\mathrm{f}}|\psi_{\mathrm{i}}\rangle \\ &\qquad\qquad - \mu[\langle\psi_{\mathrm{i}}|\psi_{\mathrm{i}}\rangle - 1] - \nu[\langle\psi_{\mathrm{f}}|\psi_{\mathrm{f}}\rangle - 1]. \end{aligned} \tag{A.6}$$

Differentiating it by $\langle\psi_{\mathrm{f}}|$ and $\langle\psi_{\mathrm{i}}|$, we obtain

$$\frac{\partial F}{\partial\langle\psi_{\mathrm{f}}|} = \langle\psi_{\mathrm{i}}|\hat{A}|\psi_{\mathrm{f}}\rangle\hat{A}|\psi_{\mathrm{i}}\rangle - \lambda^*|\psi_{\mathrm{i}}\rangle - \nu|\psi_{\mathrm{f}}\rangle = 0, \tag{A.7}$$

$$\frac{\partial F}{\partial\langle\psi_{\mathrm{i}}|} = \langle\psi_{\mathrm{f}}|\hat{A}|\psi_{\mathrm{i}}\rangle\hat{A}|\psi_{\mathrm{f}}\rangle - \lambda|\psi_{\mathrm{f}}\rangle - \mu|\psi_{\mathrm{i}}\rangle = 0, \tag{A.8}$$

where $\lambda := \lambda_1 + \mathrm{i}\lambda_2$. Multiplying $\langle\psi_{\mathrm{f}}|$ to Eq. (A.7) and $\langle\psi_{\mathrm{i}}|$ to Eq. (A.8), we have

$$\nu + \lambda^*\cos\xi = \mu + \lambda\cos\xi = |\langle\psi_{\mathrm{f}}|\hat{A}|\psi_{\mathrm{i}}\rangle|^2. \tag{A.9}$$

Equation (A.9) yields that $\lambda \in \mathbb{R}$ and $\mu = \nu$. Multiplying $\langle\psi_{\mathrm{f}}|$ to Eq. (A.8), $\langle\psi_{\mathrm{f}}|\hat{A}|\psi_{\mathrm{i}}\rangle$ is found to be a real number. Thus $\langle\psi_{\mathrm{i}}|\hat{A}|\psi_{\mathrm{f}}\rangle = \langle\psi_{\mathrm{f}}|\hat{A}|\psi_{\mathrm{i}}\rangle$. Equations (A.7) and (A.8) reduce to

$$\langle\psi_{\mathrm{f}}|\hat{A}|\psi_{\mathrm{i}}\rangle\hat{A}|\psi_{\mathrm{i}}\rangle = \lambda|\psi_{\mathrm{i}}\rangle + \mu|\psi_{\mathrm{f}}\rangle, \tag{A.10}$$

$$\langle\psi_{\mathrm{f}}|\hat{A}|\psi_{\mathrm{i}}\rangle\hat{A}|\psi_{\mathrm{f}}\rangle = \mu|\psi_{\mathrm{i}}\rangle + \lambda|\psi_{\mathrm{f}}\rangle. \tag{A.11}$$

Note that $\mathcal{H}_2 := \mathrm{span}(|\psi_\mathrm{i}\rangle, |\psi_\mathrm{f}\rangle)$ is an invariant subspace of $\hat{A}$. Adding and subtracting Eqs. (A.10) and (A.11), we obtain

$$\langle\psi_\mathrm{f}|\hat{A}|\psi_\mathrm{i}\rangle\hat{A}(|\psi_\mathrm{i}\rangle + |\psi_\mathrm{f}\rangle) = (\lambda+\mu)(|\psi_\mathrm{i}\rangle + |\psi_\mathrm{f}\rangle), \tag{A.12}$$

$$\langle\psi_\mathrm{f}|\hat{A}|\psi_\mathrm{i}\rangle\hat{A}(|\psi_\mathrm{i}\rangle - |\psi_\mathrm{f}\rangle) = (\lambda-\mu)(|\psi_\mathrm{i}\rangle - |\psi_\mathrm{f}\rangle). \tag{A.13}$$

Thus $|\psi_\mathrm{i}\rangle + |\psi_\mathrm{f}\rangle$ and $|\psi_\mathrm{i}\rangle - |\psi_\mathrm{f}\rangle$ are two eigenvectors of $\hat{A}$. Let a_1 and a_2 be corresponding two eigenvalues of $\hat{A}$, we have

$$\langle\psi_\mathrm{f}|\hat{A}|\psi_\mathrm{i}\rangle a_1 = \lambda + \mu, \tag{A.14}$$

$$\langle\psi_\mathrm{f}|\hat{A}|\psi_\mathrm{i}\rangle a_2 = \lambda - \mu. \tag{A.15}$$

Then,

$$\lambda = \frac{1}{2}(a_1+a_2)\langle\psi_\mathrm{f}|\hat{A}|\psi_\mathrm{i}\rangle, \tag{A.16}$$

$$\mu = \frac{1}{2}(a_1-a_2)\langle\psi_\mathrm{f}|\hat{A}|\psi_\mathrm{i}\rangle. \tag{A.17}$$

Combining these equations with Eq. (A.9), we obtain

$$\langle\psi_\mathrm{f}|\hat{A}|\psi_\mathrm{i}\rangle = a_1\cos^2\frac{\xi}{2} - a_2\sin^2\frac{\xi}{2}. \tag{A.18}$$

Note that $\cos^2(\xi/2)$ is larger than $\sin^2(\xi/2)$ since $0 \le \xi/2 \le \pi/4$. Let a_max be the maximum eigenvalue of $\hat{A}$ and a_min be the minimum eigenvalue of $\hat{A}$; the maximum weak value is

$$\max_{\substack{\langle\psi_\mathrm{i}|\psi_\mathrm{f}\rangle=\cos\xi,\\ \langle\psi_\mathrm{i}|\psi_\mathrm{i}\rangle=\langle\psi_\mathrm{f}|\psi_\mathrm{f}\rangle=1}} |\langle\hat{A}\rangle_\mathrm{w}| = \begin{cases} \dfrac{a_\mathrm{max}\cos^2\frac{\xi}{2} - a_\mathrm{min}\sin^2\frac{\xi}{2}}{\cos\xi} & (|a_\mathrm{max}| \ge |a_\mathrm{min}|) \\ -\dfrac{a_\mathrm{min}\cos^2\frac{\xi}{2} - a_\mathrm{max}\sin^2\frac{\xi}{2}}{\cos\xi} & (|a_\mathrm{max}| < |a_\mathrm{min}|) \end{cases}. \tag{A.19}$$

Rewriting Eq. (A.19), we have

$$\max_{\substack{\langle\psi_\mathrm{i}|\psi_\mathrm{f}\rangle=\cos\xi,\\ \langle\psi_\mathrm{i}|\psi_\mathrm{i}\rangle=\langle\psi_\mathrm{f}|\psi_\mathrm{f}\rangle=1}} |\langle\hat{A}\rangle_\mathrm{w}| = \frac{1}{2}\,|a_\mathrm{max} + a_\mathrm{min}| + \frac{a_\mathrm{max} - a_\mathrm{min}}{2\cos\xi}. \tag{A.20}$$

Note that the weak value becomes a real number when its modulus is maximized. Equation (A.20) gives an inequality

$$\max_{\substack{\langle\psi_\mathrm{i}|\psi_\mathrm{f}\rangle=\cos\xi,\\ \langle\psi_\mathrm{i}|\psi_\mathrm{i}\rangle=\langle\psi_\mathrm{f}|\psi_\mathrm{f}\rangle=1}} |\langle\hat{A}\rangle_\mathrm{w}| \ge \frac{a_\mathrm{max} - a_\mathrm{min}}{2\cos\xi}. \tag{A.21}$$

Therefore, the maximum weak value scales proportional to $\mathcal{P}(\mathrm{f}|\mathrm{i})^{-1/2}$, where $\mathcal{P}(\mathrm{f}|\mathrm{i}) := |\langle\psi_\mathrm{f}|\psi_\mathrm{i}\rangle|^2 = \cos^2\xi$ is the success probability of post-selection. For the case of $a_{\max} = -a_{\min}$ (which is the case, for example, when $\hat{A}$ is the Pauli operator), the maximum weak value takes a simple form as

$$\max_{\substack{\langle\psi_\mathrm{i}|\psi_\mathrm{f}\rangle=\cos\xi,\\ \langle\psi_\mathrm{i}|\psi_\mathrm{i}\rangle=\langle\psi_\mathrm{f}|\psi_\mathrm{f}\rangle=1}} |\langle\hat{A}\rangle_\mathrm{w}| = \frac{a_{\max}}{\cos\xi} = \frac{||\hat{A}||}{\cos\xi}. \tag{A.22}$$

Next, we derive the pre- and post-selected states which maximize the modulus of the weak value. For simplicity, we assume that $|a_{\max}| \geq |a_{\min}|$. Denote the two eigenvectors of $\hat{A}$ corresponding to eigenvalues $a_{\max}$ and $a_{\min}$ as $|a_{\max}\rangle$ and $|a_{\min}\rangle$, respectively. The pre- and post-selected states achieving the maximum weak value satisfy the following two equations:

$$\frac{1}{2\cos(\xi/2)}(|\psi_\mathrm{i}\rangle + |\psi_\mathrm{f}\rangle) = \mathrm{e}^{\mathrm{i}\phi_1}|a_{\max}\rangle, \tag{A.23}$$

$$\frac{1}{2\sin(\xi/2)}(|\psi_\mathrm{i}\rangle - |\psi_\mathrm{f}\rangle) = \mathrm{e}^{\mathrm{i}\phi_2}|a_{\min}\rangle, \tag{A.24}$$

for $\phi_1, \phi_2 \in \mathbb{R}$. Thus,

$$|\psi_\mathrm{i}\rangle = \mathrm{e}^{\mathrm{i}\phi_1}\cos\frac{\xi}{2}|a_{\max}\rangle + \mathrm{e}^{\mathrm{i}\phi_2}\sin\frac{\xi}{2}|a_{\min}\rangle, \tag{A.25}$$

$$|\psi_\mathrm{f}\rangle = \mathrm{e}^{\mathrm{i}\phi_1}\cos\frac{\xi}{2}|a_{\max}\rangle - \mathrm{e}^{\mathrm{i}\phi_2}\sin\frac{\xi}{2}|a_{\min}\rangle. \tag{A.26}$$

Setting $\phi := \phi_2 - \phi_1$ and discarding overall phase factors, we obtain

$$|\psi_\mathrm{i}\rangle = \cos\frac{\xi}{2}|a_{\max}\rangle + \mathrm{e}^{\mathrm{i}\phi}\sin\frac{\xi}{2}|a_{\min}\rangle, \tag{A.27}$$

$$|\psi_\mathrm{f}\rangle = \cos\frac{\xi}{2}|a_{\max}\rangle - \mathrm{e}^{\mathrm{i}\phi}\sin\frac{\xi}{2}|a_{\min}\rangle. \tag{A.28}$$

A.2.2 Maximizing the imaginary part of weak value

We consider the problem to maximize the imaginary part of the weak value. The problem is reduced to maximize $\mathrm{Im}\langle\psi_\mathrm{f}|\hat{A}|\psi_\mathrm{i}\rangle$ under the constraints $\langle\psi_\mathrm{i}|\psi_\mathrm{i}\rangle = 1$, $\langle\psi_\mathrm{f}|\psi_\mathrm{f}\rangle = 1$, and $\langle\psi_\mathrm{f}|\psi_\mathrm{i}\rangle = \cos\xi$. The Lagrange multiplier method gives the following two equations,

$$-\mathrm{i}\hat{A}|\psi_\mathrm{i}\rangle - \lambda^*|\psi_\mathrm{i}\rangle - \nu|\psi_\mathrm{f}\rangle = 0, \tag{A.29}$$

$$\mathrm{i}\hat{A}|\psi_\mathrm{f}\rangle - \lambda|\psi_\mathrm{f}\rangle - \mu|\psi_\mathrm{i}\rangle = 0. \tag{A.30}$$

where $\lambda \in \mathbb{C}$ and $\mu, \nu \in \mathbb{R}$ are the Lagrange multipliers. Multiplying $\langle\psi_\mathrm{f}|$ to Eq. (A.29) and $\langle\psi_\mathrm{i}|$ to Eq. (A.30), we obtain

$$\mu = \nu = -\lambda^* \cos\xi - \mathrm{i}\langle\psi_\mathrm{f}|\hat{A}|\psi_\mathrm{i}\rangle. \tag{A.31}$$

Taking the real and imaginary parts of Eq. (A.31) yields

$$\mathrm{Re}\,\lambda = \frac{1}{\cos\xi}(\mathrm{Im}\langle\psi_\mathrm{f}|\hat{A}|\psi_\mathrm{i}\rangle - \mu), \tag{A.32}$$

$$\mathrm{Im}\,\lambda = \frac{\mathrm{Re}\langle\psi_\mathrm{f}|\hat{A}|\psi_\mathrm{i}\rangle}{\cos\xi}. \tag{A.33}$$

On the other hand, by multiplying $\langle\psi_\mathrm{f}|$ to Eq. (A.30) and taking the real part of the equation, we have

$$\mathrm{Re}\,\lambda = -\mu\cos\xi. \tag{A.34}$$

From Eqs. (A.32) and (A.34), we have

$$\mu = \frac{\mathrm{Im}\langle\psi_\mathrm{f}|\hat{A}|\psi_\mathrm{i}\rangle}{\sin^2\xi}, \tag{A.35}$$

$$\mathrm{Re}\,\lambda = -\frac{\cos\xi}{\sin^2\xi}\,\mathrm{Im}\langle\psi_\mathrm{f}|\hat{A}|\psi_\mathrm{i}\rangle. \tag{A.36}$$

Rewriting Eqs. (A.29) and (A.30),

$$\hat{A}|\psi_\mathrm{i}\rangle = \mathrm{i}\lambda^*|\psi_\mathrm{i}\rangle + \mathrm{i}\mu|\psi_\mathrm{f}\rangle, \tag{A.37}$$

$$\hat{A}|\psi_\mathrm{f}\rangle = -\mathrm{i}\mu|\psi_\mathrm{i}\rangle - \mathrm{i}\lambda|\psi_\mathrm{f}\rangle. \tag{A.38}$$

$\mathcal{H}_2 := \mathrm{span}(|\psi_\mathrm{i}\rangle, |\psi_\mathrm{f}\rangle)$ is found to be an invariant subspace of $\hat{A}$. Let a_1 and a_2 be two eigenvalues of $\hat{A}$. By solving the eigenvalue problem of Eqs. (A.37) and (A.38), we obtain

$$a_1 = \mathrm{Im}\,\lambda + \sqrt{\mu^2 - (\mathrm{Re}\,\lambda)^2}, \tag{A.39}$$

$$a_2 = \mathrm{Im}\,\lambda - \sqrt{\mu^2 - (\mathrm{Re}\,\lambda)^2}. \tag{A.40}$$

where we assume that $a_1 \geq a_2$. Substituting Eqs. (A.33), (A.35), and (A.36) into these equations,

$$a_1 = \frac{\mathrm{Re}\langle\psi_\mathrm{f}|\hat{A}|\psi_\mathrm{i}\rangle}{\cos\xi} + \frac{|\,\mathrm{Im}\langle\psi_\mathrm{f}|\hat{A}|\psi_\mathrm{i}\rangle|}{\sin\xi}, \tag{A.41}$$

$$a_2 = \frac{\mathrm{Re}\langle\psi_\mathrm{f}|\hat{A}|\psi_\mathrm{i}\rangle}{\cos\xi} - \frac{|\,\mathrm{Im}\langle\psi_\mathrm{f}|\hat{A}|\psi_\mathrm{i}\rangle|}{\sin\xi}. \tag{A.42}$$

Thus,

$$\mathrm{Re}\langle\psi_\mathrm{f}|\hat{A}|\psi_\mathrm{i}\rangle = \frac{a_1+a_2}{2}\cos\xi. \tag{A.43}$$

$$|\,\mathrm{Im}\langle\psi_\mathrm{f}|\hat{A}|\psi_\mathrm{i}\rangle| = \frac{a_1-a_2}{2}\sin\xi, \tag{A.44}$$

The imaginary part change its sign by replacing the initial and final states to each other. We may assume $\mathrm{Im}\langle\psi_\mathrm{f}|\hat{A}|\psi_\mathrm{i}\rangle \geq 0$. Then the weak value is

$$\mathrm{Re}\langle\hat{A}\rangle_\mathrm{w} = \frac{a_1+a_2}{2}, \tag{A.45}$$

$$\mathrm{Im}\langle\hat{A}\rangle_\mathrm{w} = \frac{a_1-a_2}{2}\tan\xi. \tag{A.46}$$

The imaginary part of weak value is maximized when $a_1 = a_\mathrm{max}$ and $a_2 = a_\mathrm{min}$,

$$\max_{\substack{\langle\psi_\mathrm{i}|\psi_\mathrm{f}\rangle=\cos\xi,\\ \langle\psi_\mathrm{i}|\psi_\mathrm{i}\rangle=\langle\psi_\mathrm{f}|\psi_\mathrm{f}\rangle=1}} \mathrm{Im}\langle\hat{A}\rangle_\mathrm{w} = \frac{a_\mathrm{max}-a_\mathrm{min}}{2}\tan\xi. \tag{A.47}$$

Next, we derive the pre- and post-selected states that maximize the imaginary part of the weak value. By calculating the eigenvectors for Eqs. (A.37) and (A.38), we have

$$\frac{1}{\sqrt{2}\sin\xi}(|\psi_\mathrm{i}\rangle - \mathrm{e}^{-\mathrm{i}\xi}|\psi_\mathrm{f}\rangle) = \mathrm{e}^{\mathrm{i}\phi_1}|a_\mathrm{max}\rangle, \tag{A.48}$$

$$\frac{1}{\sqrt{2}\sin\xi}(\mathrm{e}^{-\mathrm{i}\xi}|\psi_\mathrm{i}\rangle - |\psi_\mathrm{f}\rangle) = \mathrm{e}^{\mathrm{i}\phi_2}|a_\mathrm{min}\rangle. \tag{A.49}$$

where $\phi_1, \phi_2 \in \mathbb{R}$. Therefore,

$$|\psi_\mathrm{i}\rangle = -\frac{\mathrm{i}}{\sqrt{2}}(\mathrm{e}^{\mathrm{i}(\phi_1+\xi)}|a_\mathrm{max}\rangle - \mathrm{e}^{\mathrm{i}\phi_2}|a_\mathrm{min}\rangle), \tag{A.50}$$

$$|\psi_\mathrm{f}\rangle = -\frac{\mathrm{i}}{\sqrt{2}}(\mathrm{e}^{\mathrm{i}\phi_1}|a_\mathrm{max}\rangle - \mathrm{e}^{\mathrm{i}(\phi_2+\xi)}|a_\mathrm{min}\rangle). \tag{A.51}$$

Setting $\phi := \phi_2 - \phi_1 + \pi$ and ignoring over all phase factor, we obtain

$$|\psi_\mathrm{i}\rangle = \frac{1}{\sqrt{2}}(\mathrm{e}^{\mathrm{i}\xi}|a_\mathrm{max}\rangle + \mathrm{e}^{\mathrm{i}\phi}|a_\mathrm{min}\rangle), \tag{A.52}$$

$$|\psi_\mathrm{i}\rangle = \frac{1}{\sqrt{2}}(|a_\mathrm{max}\rangle + \mathrm{e}^{\mathrm{i}(\xi+\phi)}|a_\mathrm{min}\rangle). \tag{A.53}$$

Appendix B

Appendix for Chapter 4

B.1 Tangent space for pure state space

This section is based on the paper of Mukunda and Simon [44].

Denote a Hilbert space as $\mathcal{H}$, and the set of all normalized states in $\mathcal{H}$ as $\mathcal{N}_0$. Let $\mathcal{R}$ be the set of all pure density operators, then

$$\mathcal{R} = \{\hat{\rho} = |\psi\rangle\langle\psi| \,\big|\, |\psi\rangle \in \mathcal{N}_0\}. \tag{B.1}$$

The set $\mathcal{R}$ can also be written as

$$\mathcal{R} = \{\hat{\rho} \in \mathcal{L}(\mathcal{H}) \,|\, \hat{\rho}^\dagger = \hat{\rho},\, \hat{\rho}^2 = \hat{\rho},\, \mathrm{tr}\hat{\rho} = 1\}, \tag{B.2}$$

where $\mathcal{L}(\mathcal{H})$ is the set of all linear operators on $\mathcal{H}$.

Denote the tangent space of $\mathcal{R}$ at $\hat{\rho}$ as $T\mathcal{R}_{\hat{\rho}}$. We show that

$$T\mathcal{R}_{\hat{\rho}} = \{\hat{X} \in \mathcal{L}(\mathcal{H}) \,|\, \hat{X}^\dagger = \hat{X},\, \mathrm{tr}\hat{X} = 0,\, \{\hat{X}, \hat{\rho}\} = \hat{X}\}. \tag{B.3}$$

Consider a curve $\hat{\rho}(t)$ in $\mathcal{R}$, which satisfies $\hat{\rho}(0) = \hat{\rho}$. Any tangent vector is expressed as the derivative of a curve $\hat{\rho}(t)$. It is easy to confirm that the derivative

$$\hat{X} = \frac{\mathrm{d}}{\mathrm{d}t}\bigg|_{t=0} \hat{\rho}(t) \tag{B.4}$$

satisfies three condition in Eq. (B.3).

To show the converse, we first show that the right-hand side of Eq. (B.3) is equivalent to the set

$$\{\hat{X} = |\psi\rangle\langle\chi| + |\chi\rangle\langle\psi| \,\big|\, \langle\psi|\chi\rangle = 0, |\chi\rangle \in \mathcal{H}\}. \tag{B.5}$$

where $|\psi\rangle$ is a fixed vector satisfying $\hat{\rho} = |\psi\rangle\langle\psi|$.

Assume $\hat{X}$ satisfies the conditions in the right-hand side of Eq. (B.3). Setting $|\chi\rangle = \hat{X}|\psi\rangle$,

$$\begin{aligned}\langle\psi|\chi\rangle &= \langle\psi|\hat{X}|\psi\rangle \\ &= \langle\psi|\{\hat{X},\hat{\rho}\}|\psi\rangle \\ &= 2\langle\psi|\hat{X}|\psi\rangle \\ &= 2\langle\psi|\chi\rangle,\end{aligned} \tag{B.6}$$

and thus $\langle\psi|\chi\rangle = 0$. Rewriting $\hat{X}$ as

$$\hat{X} = |\chi\rangle\langle\psi| + |\psi\rangle\langle\chi| + \hat{C}, \tag{B.7}$$

the operator $\hat{C}$ satisfies

$$\hat{C}^\dagger = \hat{C},\ \{\hat{C},\hat{\rho}\} = \hat{C},\ \hat{C}|\psi\rangle = 0. \tag{B.8}$$

From these equations,

$$\hat{C} = \{\hat{C},\hat{\rho}\} = \hat{C}|\psi\rangle\langle\psi| + |\psi\rangle\langle\psi|\hat{C} = 0 \tag{B.9}$$

Finally, we obtain

$$\hat{X} = |\chi\rangle\langle\psi| + |\psi\rangle\langle\chi|. \tag{B.10}$$

It can be easily checked that $\hat{X}$ satisfying the conditions in Eq.(B.5) also satisfies the conditions in the right-hand side of Eq.(B.3)

Finally, we show that any operator $\hat{X}$ satisfying the conditions in Eq.(B.5) is an element of $T\mathcal{R}_{\hat{\rho}}$. For given $\hat{X} = |\psi\rangle\langle\chi| + |\chi\rangle\langle\psi|$, define a curve

$$\hat{\rho}(t) = |\psi(t)\rangle\langle\psi(t)|, \tag{B.11}$$

$$|\psi(t)\rangle = \cos(t)|\psi\rangle + \sin(t)|\chi\rangle. \tag{B.12}$$

Then,

$$\left.\frac{\mathrm{d}}{\mathrm{d}t}\right|_{t=0} \hat{\rho}(t) = |\chi\rangle\langle\psi| + |\psi\rangle\langle\chi| = \hat{X}. \tag{B.13}$$

Thus $\hat{X} \in T\mathcal{R}_{\hat{\rho}}$.

B.2 Naimark's dilation theorem

In this section, we describe the finite-dimensional version of Naimark's dilation theorem [69].

Theorem B.2.1. (**Naimark's dilation theorem**) *Let $\mathcal{H}$ be an M-dimensional Hilbert space, and positive operators $\{\hat{E}_n\}_{n=1}^N$ satisfy*

$$\sum_{n=1}^{N} \hat{E}_n = \hat{I}_M, \tag{B.14}$$

where $\hat{1}_M$ is the identity operator on $\mathcal{H}$. Then there exists an N'-dimensional extended Hilbert space $\tilde{\mathcal{H}}$ and orthogonal projection operators $\{\hat{F}_n\}_{n=1}^N$ such that

$$\hat{E}_n = \hat{P}\hat{F}_n\hat{P}, \tag{B.15}$$

where $\hat{P}$ is projector from $\tilde{\mathcal{H}}$ onto $\mathcal{H}$. Let r_n be the ranks of the operators $\hat{E}_n$. We can construct the extended Hilbert space $\tilde{\mathcal{H}}$ such that its dimension N' satisfies

$$N' = \sum_{n=1}^{N} r_n. \tag{B.16}$$

If all the operators $\hat{E}_n$ are of rank-1, the dimension N' of the extended Hilbert space coincides with the number of operators N.

The following proof is based on the proof given by Peres [70, 71]. There are similar proofs given by Preskill [72] and Chen [73].

Proof. Any positive positive $\hat{E}_n$ can be written as the form

$$\hat{E}_n = \sum_{\mu=1}^{r_n} |s_{n,\mu}\rangle\langle s_{n,\mu}|, \tag{B.17}$$

where $|s_{n,\mu}\rangle$ are orthogonal to each other, but not necessarily normalized. Therefore, without loss of generality we may assume that all $\hat{E}_n$ are of rank 1, that is

$$\hat{E}_n = |s_n\rangle\langle s_n|. \tag{B.18}$$

Then, the number of the positive operators $\hat{E}_n$ becomes N'. The completeness relation is written as

$$\sum_{n=1}^{N'} |s_n\rangle\langle s_n| = \hat{I}_M. \tag{B.19}$$

We introduce an orthonormal basis $\{|e_m\rangle\}_{m=1}^M$ of $\mathcal{H}_M$, then

$$|s_n\rangle = \sum_{m=1}^{M} s_{m,n}|e_m\rangle. \tag{B.20}$$

We can extend the Hilbert space $\mathcal{H}$ to $\tilde{\mathcal{H}}$ by adding the $N'-M$-dimensional Hilbert space $\mathcal{H}^\perp$ so that $\tilde{\mathcal{H}} = \mathcal{H} \oplus \mathcal{H}^\perp$. The problem is reduced to find the vectors $|t_n\rangle \in \mathcal{H}^\perp$ such that the vectors

$$|u_n\rangle := |s_n\rangle + |t_n\rangle \tag{B.21}$$

form an orthonormal basis of $\tilde{\mathcal{H}}$, i.e.,

$$\langle u_m | u_n \rangle = \delta_{mn}. \tag{B.22}$$

Denote an orthonormal basis of $\mathcal{H}^\perp$ as $\{|e_m\rangle\}_{m=M+1}^{N'}$. The vectors $|t_n\rangle$ can be written as

$$|t_n\rangle = \sum_{m=M+1}^{N'} t_{m,n} |e_m\rangle. \tag{B.23}$$

What to prove is that we can choose $\{t_{m,n}\}$ such that

$$\begin{aligned} \hat{U} &:= \begin{pmatrix} |s_1\rangle & \cdots & |s_{N'}\rangle \\ |t_1\rangle & \cdots & |t_{N'}\rangle \end{pmatrix} \\ &= \begin{pmatrix} s_{1,1} & \cdots & s_{1,N'} \\ \vdots & & \vdots \\ s_{M,1} & \cdots & s_{M,N'} \\ t_{M+1,1} & \cdots & t_{M+1,N'} \\ \vdots & & \vdots \\ t_{N',1} & \cdots & t_{N',N'} \end{pmatrix} \end{aligned} \tag{B.24}$$

becomes unitary. From the completeness relation (A.19), we have

$$\sum_{n=1}^{N'} s_{k,n} s_{l,n}^* = \delta_{kl} \tag{B.25}$$

This means that the upper M row vectors in Eq. (B.24) are orthogonal to each other. We can thus choose $\{t_{mn}\}$ such that $\hat{U}$ becomes unitary by the Gram-Schumidt orthonormalization. □

The above construction has a freedom of the choice of $|t_n\rangle$. This freedom is represented by a unitary operation $\hat{V}_\perp$ on $\mathcal{H}^\perp$. The operation $\hat{1}_M \oplus \hat{V}_\perp$ on $\{|u_n\rangle\}$ leads another orthonormalization of $\{|s_n\rangle\}$.

Appendix C

Appendix for Chapter 6

C.1 General formula for the cumulant

We describe a general formula for calculating the shift of the cumulant of $\hat{K}$ in weak measurements. We introduce the cumulant generating function

$$\Phi(s) := \log\langle \mathrm{e}^{s\hat{K}} \rangle = \log \frac{\mathrm{tr}(\hat{\sigma}\mathrm{e}^{s\hat{K}})}{\mathrm{tr}\hat{\sigma}}, \tag{C.1}$$

for the probe state $\hat{\sigma}$. The nth-order cumulant $\langle \hat{K}^n \rangle^{\mathrm{c}}$ is calculated from $\Phi(s)$ as

$$\langle \hat{K}^n \rangle^{\mathrm{c}} = \left. \frac{\mathrm{d}^n \Phi(s)}{\mathrm{d}s^n} \right|_{s=0}. \tag{C.2}$$

A straightforward calculation gives the relationship between the cumulant generating functions $\Phi_{\mathrm{i}}(s)$ and $\Phi_{\mathrm{f}}(s)$ for the initial state $\hat{\sigma}_{\mathrm{i}}$ and the final state $\hat{\sigma}_{\mathrm{f}}$:

$$\Phi_{\mathrm{f}}(s) = \Phi_{\mathrm{i}}(s + 2\theta \,\mathrm{Im}\langle \hat{A} \rangle_{\mathrm{w}}) - 2\theta \,\mathrm{Im}\langle \hat{A} \rangle_{\mathrm{w}} \langle \hat{K} \rangle_{\mathrm{i}} + O(\theta^2). \tag{C.3}$$

This relation gives the general formula for calculating the cumulant for the final state:

$$\begin{aligned}
\langle \hat{K}^n \rangle_{\mathrm{f}}^{\mathrm{c}} &= \left. \frac{\mathrm{d}^n \Phi_{\mathrm{f}}(s)}{\mathrm{d}s^n} \right|_{s=0} \\
&= \left. \frac{\mathrm{d}^n \Phi_{\mathrm{i}}(s + 2\theta \,\mathrm{Im}\langle \hat{A} \rangle_{\mathrm{w}})}{\mathrm{d}s^n} \right|_{s=0} + O(\theta^2) \\
&= \left. \frac{\mathrm{d}^n \Phi_{\mathrm{i}}(s)}{\mathrm{d}s^n} \right|_{s=0} + 2\theta \,\mathrm{Im}\langle \hat{A} \rangle_{\mathrm{w}} \left. \frac{\mathrm{d}^{n+1} \Phi_{\mathrm{i}}(s)}{\mathrm{d}s^{n+1}} \right|_{s=0} + O(\theta^2) \\
&= \langle \hat{K}^n \rangle_{\mathrm{i}}^{\mathrm{c}} + 2\theta \,\mathrm{Im}\langle \hat{A} \rangle_{\mathrm{w}} \langle \hat{K}^{n+1} \rangle_{\mathrm{i}}^{\mathrm{c}} + O(\theta^2).
\end{aligned} \tag{C.4}$$

The case of $n = 1$ corresponds to Eq. (6.5), and the case of $n = 2$ gives the change in variance:

$$\langle \delta_{\mathrm{f}} \hat{K}^2 \rangle_{\mathrm{f}} = \langle \delta_{\mathrm{i}} \hat{K}^2 \rangle_{\mathrm{i}} + 2\theta \,\mathrm{Im}\langle \hat{A} \rangle_{\mathrm{w}} \langle \hat{K}^3 \rangle_{\mathrm{i}}^{\mathrm{c}} + O(\theta^2). \tag{C.5}$$

C.2 Phase noises

Assume quantum channels satisfy the condition $\mathcal{E}(|k\rangle\langle k|) = |k\rangle\langle k|$ for all k. We referred to this type of quantum channels as phase noise. In this section, We derive the condition imposed on the Kraus representation of phase noise.

Denote the Kraus representation of phase noise $\mathcal{E}$ as $\{\hat{E}_n\}$. The condition of being phase noise is rewritten as

$$\sum_n \hat{E}_n|k\rangle\langle k|\hat{E}_n^\dagger = |k\rangle\langle k|. \tag{C.6}$$

Multipling $\langle k'|$ and $|k'\rangle$ from left and right, we have

$$\sum_n \left|\langle k'|\hat{E}_n|k\rangle\right|^2 = \delta_{kk'}. \tag{C.7}$$

For $k \neq k'$ and all n,

$$\langle k'|\hat{E}_n|k\rangle = 0. \tag{C.8}$$

Therefore $\hat{E}_n$ must be

$$\hat{E}_n = \sum_k c_n(k)|k\rangle\langle k|. \tag{C.9}$$

Setting $k' = k$ in Eq. (C.7) gives

$$\sum_n |c_n(k)|^2 = 1. \tag{C.10}$$

Conversely, if the quantum channel $\mathcal{E}$ has the Kraus representation $\{\hat{E}_n\}$ satisfying Eq. (C.9) and (C.10), then Eq. (C.6) is satisfied.

We finally show that when the system is a two-state system and $\hat{K} = \hat{Z}$, the phase noises is simply the composition of a phase-flip noise and a unitary rotation around Z axis. If $\mathcal{E}$ is phase noise,

$$\mathcal{E}(|0\rangle\langle 1|) = \sum_n c_n(0)c_n(1)^*|0\rangle\langle 1|. \tag{C.11}$$

Using the Cauchy-Schwarz inequality, we have

$$\left|\sum_n c_n(0)c_n(1)^*\right|^2 \leq \left(\sum_n |c_n(0)|^2\right)\left(\sum_n |c_n(1)|^2\right) = 1. \tag{C.12}$$

Define p and θ such that $(1-2p)\mathrm{e}^{\mathrm{i}\theta} = \sum_n c_n(0)c_n(1)^*$. Then $\mathcal{E}$ is expressed as the composition of the phase-flip channel with rate p and the unitary operation $\mathrm{e}^{\mathrm{i}\theta\hat{Z}/2}$

C.3 Calculation of the measurement results

We first derive Eqs. (6.17) and (6.18). Then we also present the results taking into account the incompleteness of post-selection.

We define an unnormalized effective evolution operator $\hat{V}(\theta, \delta)$ as

$$\hat{V}(\theta, \delta) = \langle \psi_{\rm f}(\delta) | \hat{U}(\theta) | \psi_{\rm i} \rangle, \tag{C.13}$$

where

$$|\psi_{\rm i}\rangle = \frac{1}{\sqrt{2}}(|0\rangle + |1\rangle), \tag{C.14}$$

$$|\psi_{\rm f}(\delta)\rangle = \frac{1}{\sqrt{2}}(|0\rangle + {\rm e}^{{\rm i}\delta}|1\rangle), \tag{C.15}$$

$$\hat{U}(\theta) = \exp(2\theta \hat{P}_0 \otimes \hat{Z}). \tag{C.16}$$

Note that the relative phase δ of two paths is explicitly represented as a parameter in Eq. (C.13).

The operator $\hat{V}(\theta, \delta)$ is explicitly

$$\hat{V}(\theta, \delta) = \frac{1}{2}\left[({\rm e}^{-{\rm i}\delta} + \cos(2\theta))\hat{I} + {\rm i}\sin(2\theta)\hat{Z}\right]. \tag{C.17}$$

Since the initial state is $\hat{\sigma}_{\rm i} = \hat{I}/2$, the final state of the probe is

$$\begin{aligned} \hat{\sigma}_{\rm f}(\theta, \delta) &= \hat{V}(\theta, \delta)\hat{\sigma}_{\rm i}\hat{V}(\theta, \delta)^\dagger \\ &= \frac{1}{2}\hat{V}(\theta, \delta)\hat{V}(\theta, \delta)^\dagger \\ &= \frac{1}{4}\left[(1 + \cos\delta\cos(2\theta))\hat{I} - \sin\delta\sin(2\theta)\hat{Z}\right]. \end{aligned} \tag{C.18}$$

Therefore,

$${\rm tr}\hat{\sigma}_{\rm f}(\theta, \delta) = \frac{1}{2}(1 + \cos\delta\cos(2\theta)), \tag{C.19}$$

$${\rm tr}[\hat{\sigma}_{\rm f}(\theta, \delta)\hat{Z}] = -\frac{1}{2}\sin\delta\cos(2\theta). \tag{C.20}$$

These equations are the same as Eqs. (6.17) and (6.18).

Next, we consider the case of incomplete post-selection. The post-selected state can be expressed by using the visibility $\mathcal{V}$ of interference as

$$\begin{aligned} \hat{\rho}_{\rm f}(\delta) &= \mathcal{V}|\psi_{\rm f}(\delta)\rangle\langle\psi_{\rm f}(\delta)| + (1 - \mathcal{V})\frac{\hat{I}}{2} \\ &= \frac{1 + \mathcal{V}}{2}|\psi_{\rm f}(\delta)\rangle\langle\psi_{\rm f}(\delta)| + \frac{1 - \mathcal{V}}{2}|\psi_{\rm f}(\pi + \delta)\rangle\langle\psi_{\rm f}(\pi + \delta)|. \end{aligned} \tag{C.21}$$

The post-selected state is thus the mixture of $|\psi_{\rm f}(\delta)\rangle$ and $|\psi_{\rm f}(\pi+\delta)\rangle$ with probability $(1+\mathcal{V})/2$ and $(1-\mathcal{V})/2$, respectively. The final state $\hat{\sigma}'_{\rm f}(\theta,\delta)$ of the probe is

$$\begin{aligned}\hat{\sigma}'_{\rm f}(\theta,\delta) &= \frac{1+\mathcal{V}}{2}\hat{\sigma}_{\rm f}(\theta,\delta)+\frac{1-\mathcal{V}}{2}\hat{\sigma}_{\rm f}(\theta,\pi+\delta)\\ &= \frac{1}{4}\left[(1+\mathcal{V}\cos\delta\cos(2\theta))\hat{I}-\mathcal{V}\sin\delta\sin(2\theta)\hat{Z}\right]. \end{aligned} \tag{C.22}$$

Hence,

$$\mathrm{tr}\hat{\sigma}'_{\rm f}(\theta,\delta) = \frac{1}{2}(1+\mathcal{V}\cos\delta\cos(2\theta)), \tag{C.23}$$

$$\mathrm{tr}[\hat{\sigma}'_{\rm f}(\theta,\delta)\hat{Z}] = -\frac{1}{2}\mathcal{V}\sin\delta\sin(2\theta). \tag{C.24}$$

The normalized readout of circular components is

$$\frac{\mathrm{tr}[\hat{\sigma}'_{\rm f}(\theta,\delta)\hat{Z}]}{\mathrm{tr}\hat{\sigma}'_{\rm f}(\theta,\delta)} = -\frac{\mathcal{V}\sin\delta\sin(2\theta)}{1+\mathcal{V}\cos\delta\cos(2\theta)}. \tag{C.25}$$

Differentiating this equation, we obtain the weak value of $\hat{P}_0$ for incomplete post-selection as

$$\begin{aligned}\mathrm{Im}\langle\hat{P}_0\rangle_{\rm w} &= -\frac{1}{4}\left.\frac{\mathrm{d}}{\mathrm{d}\theta}\right|_{\theta=0}\frac{\mathrm{tr}[\hat{\sigma}'_{\rm f}(\theta,\delta)\hat{Z}]}{\mathrm{tr}\hat{\sigma}'_{\rm f}(\theta,\delta)}\\ &= \frac{\mathcal{V}\sin\delta}{2(1+\mathcal{V}\cos\delta)}, \end{aligned} \tag{C.26}$$

which coincides with Eq. (6.28).

Acknowledgments

I would like to offer my special thanks to my supervisor Professor Masao Kitano for his warm encouragement of my study. I have learned a lot of things from his intuition and way of thinking about physics.

I would like to thank Professor Katsuji Yamamoto and Professor Takashi Hikihara for helpful discussion and valuable comments.

I wish to thank Associate Professor Kazuhiko Sugiyama for his advice and encouragement. He gave me lots of technical advice about my experiments. I would like to express my gratitude to Assistant Professor Toshihiro Nakanishi for his gentle guidance. He always supported me and gave helpful advice.

During my course of study, I am indebted to many people, especially members of the Kitano laboratory. First of all, my special thanks go to Dr. Hirokazu Kobayashi. He kindly taught me the basics of quantum optics and optical experiments during my first few years in graduate school. Without his teaching and encouragement, I would not complete my study. I would like to thank Dr. Yasuhiro Tamayama for his support and advice. His attitude toward research has taught me many things. I thank Yosuke Nakata for daily discussions and valuable comments. I enjoyed the conversations with him very much. I have leaned much about the geometry of physics from him. I thank Kazuhisa Ogawa and Ken Hamada for helpful comments on my study. I would like to thank all other members of the Kitano laboratory. I am particularly grateful for the official assistance given by Keiko Yamada and Hisako Sekiguchi.

Finally, I wish to thank my parents, my brother, and my sister for their support and encouragement.

References

[1] Y. Aharonov, P. G. Bergmann, and J. L. Lebowitz, Phys. Rev. **134**, B1410 (1964).

[2] B. Reznik and Y. Aharonov, Phys. Rev. A **52**, 2538 (1995).

[3] Y. Aharonov and L. Vaidman, Lect. Notes Phys. **734**, 399 (2007).

[4] Y. Aharonov, D. Z. Albert, and L. Vaidman, Phys. Rev. Lett. **60**, 1351 (1988).

[5] L. Hardy, Phys. Rev. Lett. **68**, 2981 (1992).

[6] Y. Aharonov, A. Botero, S. Popescu, B. Reznik, and J. Tollaksen, Phys. Lett. A **301**, 130 (2002).

[7] Y. Aharonov and L. Vaidman, J. Phys. A **24**, 2315 (1991).

[8] K. Resch, J. Lundeen, and A. Steinberg, Phys. Lett. A **324**, 125 (2004).

[9] J. Lundeen and A. Steinberg, Phys. Rev. Lett. **102**, 020404 (2009).

[10] K. Yokota, T. Yamamoto, M. Koashi, and N. Imoto, New J. Phys. **11**, 033011 (2009).

[11] N. Williams and A. Jordan, Phys. Rev. Lett. **100**, 026804 (2008).

[12] A. Palacios-Laloy, F. Mallet, F. Nguyen, P. Bertet, D. Vion, D. Esteve, and A. N. Korotkov, Nature Phys. **6**, 442 (2010).

[13] M. E. Goggin, M. P. Almeida, M. Barbieri, B. P. Lanyon, J. L. O'Brien, A. G. White, and G. J. Pryde, Proc. Natl. Acad. Sci. USA **108**, 1256 (2011).

[14] K. Yokota and N. Imoto, New J. Phys. **14**, 083021 (2012).

[15] O. Hosten and P. Kwiat, Science **319**, 787 (2008).

[16] P. B. Dixon, D. J. Starling, A. N. Jordan, and J. C. Howell, Phys. Rev. Lett. **102**, 173601 (2009).

[17] J. M. Hogan, J. Hammer, S.-W. Chiow, S. Dickerson, D. M. S. Johnson, T. Kovachy, A. Sugarbaker, and M. A. Kasevich, Opt. Lett. **36**, 1698 (2011).

[18] M. D. Turner, C. A. Hagedorn, S. Schlamminger, and J. H. Gundlach, Opt. Lett. **36**, 1479 (2011).

[19] D. J. Starling, P. B. Dixon, A. N. Jordan, and J. C. Howell, Phys. Rev. A **82**, 063822 (2010).

[20] Y. Gorodetski, K. Y. Bliokh, B. Stein, C. Genet, N. Shitrit, V. Kleiner, E. Hasman, and T. W. Ebbesen, Phys. Rev. Lett. **109**, 013901 (2012).

[21] M. Pfeifer and P. Fischer, Opt. Express **19**, 16508 (2011).

[22] A. D. Parks and S. E. Spence, Appl. Opt. **51**, 3364 (2012).

[23] P. Egan and J. A. Stone, Opt. Lett. **37**, 4991 (2012).

[24] J. S. Lundeen, B. Sutherland, A. Patel, C. Stewart, and C. Bamber, Nature **474**, 188 (2011).

[25] S. Kocsis, B. Braverman, S. Ravets, M. J. Stevens, R. P. Mirin, L. K. Shalm, and A. M. Steinberg, Science **332**, 1170 (2011).

[26] L. Rozema, A. Darabi, D. Mahler, A. Hayat, Y. Soudagar, and A. Steinberg, Phys. Rev. Lett. **109**, 100404 (2012).

[27] M. A. Nielsen and I. L. Chuang, *Quantum Computation and Quantum Information* (Cambridge University Press, 2000).

[28] M.-D. Choi, Linear Alg. Appl. **10**, 285 (1975).

[29] K. Kraus, *States, Effects, and Operations Fundamental Notions of Quantum Theory* (Springer Berlin, 1983).

[30] J. von Neumann, *Mathematical Foundations of Quantum Mechanics* (Princeton University Press, 1996).

[31] Y. Shikano and A. Hosoya, J. Phys. A **43**, 025304 (2010).

[32] S. Massar and S. Popescu, Phys. Rev. A **84**, 052106 (2011).

[33] R. Jozsa, Phys. Rev. A **76**, 044103 (2007).

[34] S. Wu and Y. Li, Phys. Rev. A **83**, 052106 (2011).

[35] I. Duck, P. Stevenson, and E. Sudarshan, Phys. Rev. D **40**, 2112 (1989).

[36] D. J. Starling, P. B. Dixon, A. N. Jordan, and J. C. Howell, Phys. Rev. A **80**, 041803 (2009).

[37] A. Feizpour, X. Xing, and A. M. Steinberg, Phys. Rev. Lett. **107**, 133603 (2011).

[38] I. Chuang and Y. Yamamoto, Phys. Rev. A **52**, 3489 (1995).

[39] M. Scully and K. Drühl, Phys. Rev. A **25**, 2208 (1982).

[40] M. V. Berry, Proc. R. Soc. London, Ser. A **392**, 45 (1984).

[41] S. Pancharatnam, Proc. Ind. Acad. Sci. A **44**, 247 (1956).

[42] B.-G. Englert, Phys. Rev. Lett. **77**, 2154 (1996).

[43] M. V. Berry, J. Mod. Opt. **34**, 1401 (1987).

[44] N. Mukunda and R. Simon, Ann. Phys. **228**, 205 (1993).

[45] H. Schmitzer, S. Klein, and W. Dultz, Phys. Rev. Lett. **71**, 1530 (1993).

[46] Q. Li, L. Gong, Y. Gao, and Y. Chen, Opt. Commun. **169**, 17 (1999).

[47] R. Bhandari, Phys. Lett. A **157**, 221 (1991).

[48] M. Kitano, T. Nakanishi, and K. Sugiyama, IEEE J. Sel. Top. Quantum Electron. **9**, 43 (2003).

[49] A. D. Parks, D. W. Cullin, and D. C. Stoudt, Proc. R. Soc. London, Ser. A **454**, 2997 (1998).

[50] H. Hofmann, Phys. Rev. A **83**, 022106 (2011).

[51] J. Dressel and A. Jordan, Phys. Rev. A **85**, 012107 (2012).

[52] S. Amari and H. Nagaoka, *Methods of Information Geometry* (American Mathematical Society, 2000).

[53] S. Wu and K. Mølmer, Phys. Lett. A **374**, 34 (2009).

[54] A. Hosoya and Y. Shikano, J. Phys. A **43**, 385307 (2010).

[55] T. Brun, L. Diósi, and W. Strunz, Phys. Rev. A **77**, 032101 (2008).

[56] Y. Shikano and S. Tanaka, EPL **96**, 40002 (2011).

[57] Y. Aharonov and L. Vaidman, Phys. Rev. A **41**, 11 (1990).

[58] H. Kosaka, T. Inagaki, Y. Rikitake, H. Imamura, Y. Mitsumori, and K. Edamatsu, Nature **457**, 702 (2009).

[59] T. Inagaki, H. Kosaka, Y. Rikitake, H. Imamura, Y. Mitsumori, and K. Edamatsu, Japanese J. Appl. Phys. **49**, 04DJ09 (2010).

[60] A. Černoch, J. Soubusta, L. Bartšková, M. Dušek, and J. Fiurášek, Phys. Rev. Lett. **100**, 180501 (2008).

[61] H. Kobayashi, Y. Ikeda, S. Tamate, T. Nakanishi, and M. Kitano, Phys. Rev. A **83**, 063808 (2011).

[62] L. Johansen, Phys. Rev. Lett. **93**, 120402 (2004).

[63] Y.-W. Cho, H.-T. Lim, Y.-S. Ra, and Y.-H. Kim, New J. Phys. **12**, 023036 (2010).

[64] Y. Kedem, Phys. Rev. A **85**, 060102 (2012).

[65] C.-F. Li, X.-Y. Xu, J.-S. Tang, J.-S. Xu, and G.-C. Guo, Phys. Rev. A **83**, 044102 (2011).

[66] G. Ghosh, Opt. Commun. **163**, 95 (1999).

[67] B. P. Lanyon, M. Barbieri, M. P. Almeida, and A. G. White, Phys. Rev. Lett. **101**, 200501 (2008).

[68] E. Knill and R. Laflamme, Phys. Rev. Lett. **81**, 5672 (1998).

[69] A. Holevo, *Probabilistic and Statistical Aspects of Quantum Theory* (Edizioni della Normale, Pisa, 2011).

[70] A. Peres, Found. Phys. **20**, 1441 (1990).

[71] A. Peres, *Quantum Theory: Concepts and Methods* (Springer, 1995).

[72] J. Preskill, *Quantum Information and Computation: Lecture Notes for Physics 229.*

[73] P.-X. Chen, J. Bergou, S.-Y. Zhu, and G.-C. Guo, Phys. Rev. A **76**, 060303 (2007).

List of publications

Journal papers

1. S. Tamate, H. Kobayashi, T. Nakanishi, K. Sugiyama, and M. Kitano, "Geometrical aspects of weak measurements and quantum erasers," New J. Phys. **11**, 093025 (2009).
2. H. Kobayashi, S. Tamate, T. Nakanishi, K. Sugiyama, and M. Kitano, "Direct observation of geometric phases using a three-pinhole interferometer," Phys. Rev. A **81**, 012104 (2010).
3. H. Kobayashi, S. Tamate, T. Nakanishi, K. Sugiyama, and M. Kitano, "Observation of Geometric Phases in Quantum Erasers," J. Phys. Soc. Jpn. **80**, 034401 (2011).
4. H. Kobayashi, Y. Ikeda, S. Tamate, T. Nakanishi, and M. Kitano, "Nonlinear behavior of geometric phases induced by photon pairs," Phys. Rev. A **83**, 063808 (2011).
5. S. Tamate, K. Ogawa, and M. Kitano, "Bloch-sphere representation of three-vertex geometric phases," Phys. Rev. A **84**, 052114 (2011).
6. S. Tamate, T. Nakanishi, and M. Kitano, "Weak measurements with completely mixed probe states," (submitted), arXiv:quant-ph/1211.4292 (2012).
7. S. Tamate and M. Kitano, "Two-state Vector Tomography via Spin-Exchange Interaction," (in preparation).

International conferences

1. H. Kobayashi, S. Tamate, T. Nakanishi, K. Sugiyama, and M. Kitano, "Geometrical aspects of weak measurements and quantum erasers," ONR workshop "Entanglement Beyond the Optical Regime," California, U.S.A, Feb. (2009).
2. S. Tamate, H. Kobayashi, T. Nakanishi, K. Sugiyama, and M. Kitano, "Geometric phase in quantum eraser and weak measurement," The 10th Interna-

tional Conference on Quantum Communication, Measurement and Computing, The University of Queensland, Australia, Jul. (2010); AIP Conference Proceedings **1363**, 377 (2011).

3. H. Kobayashi, S. Tamate, T. Nakanishi, K. Sugiyama, and M. Kitano, "Direct observation of geometric phases without state evolution," The 10th International Conference on Quantum Communication, Measurement and Computing, The University of Queensland, Australia, Jul. (2010); AIP Conference Proceedings **1363**, 373 (2011).
4. S. Tamate, H. Kobayashi, T. Nakanishi, K. Sugiyama, and M. Kitano, "Geometric phase and quantum interference in weak measurements," CREST 2010 International Symposium on Physics of Quantum Technology, Tokyo, Japan, Apr. (2010).
5. H. Kobayashi, S. Tamate, T. Nakanishi, K. Sugiyama, and M. Kitano, "Direct observation of geometric phases using a three-pinhole interferometer," CREST 2010 International Symposium on Physics of Quantum Technology, Tokyo, Japan, Apr. (2010).
6. S. Tamate, K. Ogawa, and M. Kitano, "Bloch-sphere representation of three-vertex geometric phases," Global COE 5th International Symposium on Phtonics and Electronics Science and Engineering, Kyoto, Japan, Mar. (2012).

Domestic conferences

1. S. Tamate, H. Kobayashi, T. Nakanishi, K. Sugiyama, and M. Kitano, "Geometrical aspects of weak measurements and quantum erasers," The 20th Quantum Information Technology Symposium, Hiroshima, May (2009).
2. S. Tamate, H. Kobayashi, T. Nakanishi, K. Sugiyama, and M. Kitano, "Geometrical aspects of weak measurements and quantum erasers," Fall Meeting of the Physical Society of Japan, Kumamoto, Sep. (2009).
3. H. Kobayashi, S. Tamate, T. Nakanishi, K. Sugiyama, and M. Kitano, "Direct observation of geometric phases using a three-pinhole interferometer," Annual Meeting of the Physical Society of Japan, Okayama, Mar. (2010).
4. Y. Ikeda, H. Kobayashi, S. Tamate, T. Nakanishi, K. Sugiyama, and M. Kitano, "Observation of geometric phase for photon pairs," Fall Meeting of the Physical Society of Japan, Osaka, Sep. (2010).
5. K. Ogawa, S. Tamate, H. Kobayashi, and M. Kitano, "Geometric phases in three-state quantum systems," The 24th Quantum Information Technology Symposium, Tokyo, May (2011).

6. S. Tamate, "Geometric picture for weak measurements," Atomic, Molecular, and Optical Science Workshop, Tokyo, Jun. (2011).
7. S. Tamate and M. Kitano, "Geoemtric picture of weak measurements on the Bloch sphere," Fall Meeting of the Physical Society of Japan, Toyama, Sep. (2011).
8. K. Ogawa, S. Tamate, H. Kobayashi, M. Kitano, "Majorana representation of geometric phases," Fall Meeting of the Physical Society of Japan, Toyama, Sep. (2011).
9. S. Tamate, "Bloch sphere representation of geometric phases in N-dimensional quantum systems," Photon Frontier Network Symposium, Nagoya, Nov. (2011).
10. S. Tamate, T. Nakanishi, and M. Kitano, "Weak measurements of polarization rotation via mixed probe states," Fall Meeting of the Physical Society of Japan, Yokohama, Sep. (2012).
11. K. Ogawa, S. Tamate, H. Kobayashi, and M. Kitano, "Observation of geometric phases in three-state quantum system," Fall Meeting of the Physical Society of Japan, Yokohama, Sep. (2012).